

UNIVERSITY OF OKLAHOMA

GRADUATE COLLEGE

MECHANISTIC UNDERSTANDING OF CATALYTIC UPGRADING REACTIONS

OF BIOMASS-DERIVED C₂ OXYGENATES

A DISSERTATION

SUBMITTED TO THE GRADUATE FACULTY

in partial fulfillment of the requirements for the

Degree of

DOCTOR OF PHILOSOPHY

By

TU NGUYET PHAM

Norman, Oklahoma

2014

MECHANISTIC UNDERSTANDING OF CATALYTIC UPGRADING REACTIONS
OF BIOMASS-DERIVED C2 OXYGENATES

A DISSERTATION APPROVED FOR THE
SCHOOL OF CHEMICAL, BIOLOGICAL AND MATERIALS ENGINEERING

BY

Dr. Daniel E. Resasco, Chair

Dr. Steven P. Crossley

Dr. Friederike C. Jentoft

Dr. Lance L. Lobban

Dr. Daniel T. Glatzhofer

© Copyright by TU NGUYET PHAM 2014
All Rights Reserved.

To my loving family

Acknowledgements

I am thankful to many wonderful people, who have not only made this dissertation possible but also made my graduate student life so enjoyable that I will treasure forever.

First and foremost, I would like to express my deepest gratitude to my advisor and mentor, Professor Daniel E. Resasco. It has been a privilege and honor for me to be a part of his group, and to experience his in-depth knowledge and endless passion in research. He introduced and showed me the beauty of catalysis world and taught me to love research. I am grateful for his faith in my ability, which has lifted up my confidence and helped me to become who I am today. His guidance, understanding, encouragement and support made these five years very memorable and enjoyable for me and it is honestly difficult to leave it all behind.

I also owe much gratitude to Dr. Tawan Sooknoi for his invaluable discussion and instruction. He has demonstrated to me the tremendous power of applying fundamental organic chemistry in understanding a catalysis system. My special appreciation also goes to Dr. Steven Crossley and Dr. Jimmy Faria, whose instruction, help, enthusiasm and encouragement was invaluable not only for my research projects but also for my career development.

I am grateful to Dr. Friederike Jentoft, Dr. Lance Lobban and Dr. Richard Mallinson for their helpful criticism and enlightening discussion in the group meeting. I would like to thank Dr. Daniel T. Glatzhofer for being my committee member.

I greatly appreciate Dr. Rolf Jentoft and James Miles for their tremendous help with instruments and reactors. The department staff, Vernita, Terry, Donna, Wanda, and

Kelly have been helping me with purchasing and paperwork, which has ensured smooth progress of my research.

I would especially like to thank all current and past group members, whom I have had the pleasure to interact and collaborate with. I appreciate the help, support and enjoyable friendship of Paula, Kyu, Veronica, Pilar, Amalia, Air, Mohannad, Santiago, Lu, Anh, Yen, Hai, Taiwo, Ali, Yi, Onn, Bokie, Lei, Abhishek, Miguel, Felipe, Daniel, Malli, Zheng, Shaolong, Tan, Nick, Ayut, Wesley, Karl, and Joseph.

I am thankful to have wonderful friends, Phuong, Bao-Yen, Linh, Ha, Dzung, Nhung, Andrea, Cristian, Camille and Gap for becoming my second family here. I am truly grateful to Dachuan, for his love, care and wonderful sense of humor.

Words cannot express my gratefulness to my amazing and incredible family. I am lucky and blessed to have their unconditional and endless love, understanding and support in my life. Without them, I would never have gotten where I am today.

Finally, I would like to acknowledge the financial supports for this work from Department of Energy, Abengoa Research and National Science Foundation.

Table of Contents

<i>Acknowledgements</i>	iv
<i>List of Tables</i>	x
<i>List of Figures</i>	xii
<i>Abstract</i>	xvii
A. General Introduction and Research Direction	1
A.1. Energy Outlook.....	1
<i>References</i>	4
A.2. Research Direction	5
B. Catalytic Upgrading of Acetic Acid - Derived Biomass by Ketonization	7
B.1. Biomass Conversion Processes to Liquid Fuel.....	7
<i>References</i>	15
B.2. Literature Review on Ketonization.....	17
B.2.1. Ketonization Mechanism	17
B.2.1.1. Ketene Mechanism	26
B.2.1.2. β -ketoacid Intermediate	31
B.2.1.3. Other Mechanisms	34
B.2.2. Ketonization Catalysts	37
B.2.2.1. Interaction of Carboxylic Acids with Oxide Surfaces	39
B.2.2.2. Acid-base Properties	43
B.2.2.3. Redox Properties.....	45
B.2.2.4. Effect of Dopants and Catalyst Pretreatments	46
<i>References</i>	52

B.3. Research Objectives.....	57
B.4. Ketonization of Acetic Acid over Ru/TiO ₂ /Carbon Catalysts in the Aqueous Phase	58
B.4.1. Introduction.....	58
B.4.2. Experimental Techniques	60
B.4.2.1. Catalyst Preparation	60
B.4.2.2 Catalyst Characterization	61
B.4.2.3. Reaction Studies	62
B.4.3. Results.....	63
B.4.3.1 Catalyst Characterization Results	63
B.4.3.2 Catalytic performance of TiO ₂ /C and Ru/TiO ₂ /C catalysts	72
B.4.4. Conclusion	79
<i>References</i>	81
B.5. Reaction Kinetics and Mechanism of Ketonization of Aliphatic Carboxylic Acids with Different Carbon Chain Lengths over Ru/TiO ₂ Catalyst	85
B.5.1. Introduction.....	85
B.5.2. Experimental	86
B.5.2.1. Catalyst Synthesis	86
B.5.2.2. Catalyst Characterization	87
B.5.2.3. Kinetic Measurements	87
B.5.3. Results.....	88
B.5.3.1. Catalyst Characterization	88
B.5.3.2. Catalytic Activity Measurements.....	89

B.5.3.2.1. Removal of transport and thermodynamic limitations in kinetic measurements	89
B.5.3.2.2. Ketonization products from the various acids	92
B.5.3.2.3. Kinetics results. Differential reactor analysis	93
B.5.3.2.4. Reaction rate data and kinetic fitting. Integral reactor analysis.....	94
B.5.4. Discussion	110
B.5.4.1. Nature of Catalyst Active Sites.....	110
B.5.4.2. Nature of the Adsorbed Species under Reaction Conditions.....	112
B.5.4.3. Nature of the Transition State.....	113
B.5.5. Summary	119
<i>References</i>	121
B.6. General Conclusions and Recommendations for Ketonization	124
C. Catalytic Conversion of Bio-Ethanol to 1,3-Butadiene	128
C.1. Motivation.....	128
C.2. Experimental.....	132
C.2.1. Catalyst Preparation	132
C.2.2. Catalyst Characterization.....	133
C.2.3. Catalytic Activity Measurements.....	135
C.3. Results.....	136
C.3.1. Catalyst Characterization.....	136
C.3.2. Reaction Network of Ethanol and Acetaldehyde.....	144
C.3.3. Reaction Data.....	146
C.4. Discussion.....	152

C.4.1. Structural Characteristics and Properties of B-MgO catalysts prepared by combustion method	152
C.4.2. Compositional Effects on the Catalytic Activity.	154
C.5. Conclusion and Recommendations for Ethanol Conversion	156
<i>References</i>	157

List of Tables

<i>Table 1. Molar composition of effluent flow in the reaction of 1:1 molar ratio of propanoic acid with carboxylic acid at 375°C using CeO₂-Mn₂O₃ (Mn: 60 mol%)[28]22</i>	
<i>Table 2. Distribution of labeled and unlabeled ketones products in the reaction of CH₃¹³COOH and (CH₃)₃COOH over TiO₂ catalyst at 350°C [5].....</i>	29
<i>Table 3. Activity of 10 wt% MO_x/SiO₂ catalysts in ketonization of acetic acid [39]</i>	38
<i>Table 4. BET surface area and pore volumes of the synthesized catalysts</i>	64
<i>Table 5. Surface composition of TiO₂/C and Ru/TiO₂/C catalysts as determined by XPS characterization.....</i>	70
<i>Table 6. Catalytic activity of 5%Ru/C, TiO₂/C, Ru/TiO₂/C, TiO₂ P25 and 5% Ru/TiO₂ catalysts for the reactions at 180°C in 5 hours in water phase.....</i>	74
<i>Table 7. Thermodynamic equilibrium constants and conversion values of acetic acid ketonization at different temperatures.....</i>	92
<i>Table 8. Optimized kinetic and thermodynamic parameters for the ketonization of acetic acid obtained from fitting the experimental data with the Langmuir-Hinshelwood model</i>	103
<i>Table 9. Optimized kinetic and thermodynamic parameter values for the ketonization of propionic acid obtained from fitting the experimental data with the Langmuir-Hinshelwood kinetic model.....</i>	103
<i>Table 10. Optimized kinetic and thermodynamic parameter values for the ketonization butyric acid obtained from fitting the experimental data with the Langmuir-Hinshelwood kinetic model.....</i>	104

<i>Table 11. Measured rate obtained at 275°C and after 30 minute time on stream using different pre-treated Ru/TiO₂</i>	109
<i>Table 12. Activation enthalpies and entropies for ketonization of acetic, propionic and butyric acid over Ru/TiO₂ catalyst</i>	116
<i>Table 13. BET surface area, pore volume and pore diameter of MgO, B₂O₃ and mixed c-B-MgO prepared by combustion method</i>	136
<i>Table 14. Basic site density of of MgO, B₂O₃ and mixed B-MgO prepared by combustion method obtained from CO₂-TPD analysis</i>	140
<i>Table 15. Product yields for conversion of ethanol and acetaldehyde over MgO, physical mixture of B₂O₃ and MgO, and impregnation 2 wt% of B₂O₃/MgO. Reaction condition: T = 250°C, P= 300 psi N₂, t = 4 hours, catalyst mass: 200 mg, 20 mL ethanol, 2 mL acetaldehyde</i>	146
<i>Table 16. Product yields for conversion of ethanol and acetaldehyde over c-B-MgO prepared by combustion method with different loadings of Boron. Reaction condition:</i>	148
<i>Table 17. Product yields for conversion of ethanol and acetaldehyde over c-B-MgO prepared by combustion method with 7.5 wt% of Boron. Reaction condition:</i>	149

List of Figures

<i>Figure 1. World total energy consumption 1990-2040 (quadrillion BTU)</i>	<i>1</i>
<i>Figure 2. Process Concept: Liquid phase catalytic cascade connected to a multi-stage pyrolysis for biofuel production and upgrading.....</i>	<i>8</i>
<i>Figure 3. Ketonization mechanism of adipic acid proposed.....</i>	<i>21</i>
<i>Figure 4. Conversion and product selectivity for ketonization of a mix of valeric and pivalic acid (1:1 molar ratio) [29].....</i>	<i>23</i>
<i>Figure 5. Dianion acetate species on the surface of ZrO₂ [32]</i>	<i>24</i>
<i>Figure 6. Ketene-based mechanism of acetic acid ketonization</i>	<i>27</i>
<i>Figure 7. Decarboxylation mechanism of β-ketoacid</i>	<i>31</i>
<i>Figure 8. Proposed β- ketoacid based mechanism for vapor phase ketonization of carboxylic acid over CeO₂-Mn₂O₃ catalyst [28].....</i>	<i>32</i>
<i>Figure 9. Proposed mechanism for carboxylic acid ketonization over ZrO₂ catalyst via β- ketoacid formed by an acyl and an enolized carboxylate on the surface [29]</i>	<i>33</i>
<i>Figure 10. Proposed mechanism for ketonization of carboxylic acid over TiO₂ catalyst by Ponec et al. [6]</i>	<i>35</i>
<i>Figure 11. Proposed decomposition pathways of acid anhydride [38]</i>	<i>36</i>
<i>Figure 12. Possible ketone formation mechanism from acid anhydride</i>	<i>37</i>
<i>Figure 13. Different adsorption configuration of carboxylates on catalyst surfaces</i>	<i>40</i>
<i>Figure 14. XRD patterns of commercial TiO₂ powder P25, TiO₂/C, and Ru/TiO₂/C</i>	<i>64</i>
<i>Figure 15. TEM images of a) activated carbon support; b) TiO₂/C; and c) Ru/TiO₂/C</i>	<i>65</i>
<i>Figure 16. High Resolution TEM images of TiO₂/C; and Ru/TiO₂/C</i>	<i>66</i>

<i>Figure 17. TPR profiles of (a) 5%Ru/C; (b) TiO₂/C; and (c) Ru/TiO₂/C.....</i>	<i>67</i>
<i>Figure 18. Ti 2p XPS spectra of (a) TiO₂/C (as-synthesized) ; (b) Ru/TiO₂/C (as-synthesized); (c) Ru/TiO₂/C (ex-situ reduced at 500oC in H2 before XPS experiment); and (d) normalized Ti 2p1/2 peak for the three samples.....</i>	<i>69</i>
<i>Figure 19. EPR spectra of as synthesized and reduced Ru/TiO₂/C catalysts</i>	<i>72</i>
<i>Figure 20. Proposed mechanism for liquid phase ketonization of carboxylic acid over TiO₂ catalyst</i>	<i>77</i>
<i>Figure 21. Catalytic activity of TiO₂/C, Ru/TiO₂ P25 and Ru/TiO₂/C catalysts for the reactions at 180° C in 5 h in three different solvents: water, n-hexane and N-methyl pyrrolidone. All the catalysts was pre-reduced before the reaction</i>	<i>78</i>
<i>Figure 22. X-ray Diffractogram (XRD) of Ru/TiO₂ and bare TiO₂ P25</i>	<i>89</i>
<i>Figure 23. . Effect of carrier gas velocity and catalyst particle sizes on ketonization rate at 275° C on pre-reduced Ru/TiO₂</i>	<i>90</i>
<i>Figure 24. Proposed early and late transition state (TS) structures for ketonization of carboxylic acids</i>	<i>95</i>
<i>Figure 25. Parity plot comparison of experimental data (points) obtained with differential reactor model with the fitted data from Langmuir Hinshelwood model (line).</i>	<i>97</i>
<i>Figure 26. Partial pressures of acetic acid and acetone as a function of W/F at 30 minutes time on stream on Ru/TiO₂ at 275 (a), 280 (b) and 285° C (c). Catalysts were pre-reduced in H₂ stream at 400° C in 1 hour. The points are experimental data and the lines are fitted data from the Langmuir-Hinshelwood fitting model</i>	<i>99</i>

<i>Figure 27. Partial pressures of propionic acid and 3-pentanone as a function of W/F at 30 minutes time on stream on Ru/TiO₂ at 290, 300, and 310°C. Catalysts were pre-reduced in H₂ stream at 400°C in 1 hour. The points are experimental data and the lines are fitted data from the Langmuir-Hinshelwood fitting model</i>	100
<i>Figure 28. Partial pressures of butyric acid and 4-heptanone as a function of W/F at 30 minutes time on stream on Ru/TiO₂ at 315, 325, and 335°C. Catalysts were pre-reduced in H₂ stream at 400°C in 1 hour. The points are experimental data and the lines are fitted data from the Langmuir-Hinshelwood fitting model.....</i>	102
<i>Figure 29. Adsorption enthalpies and entropies as function of carbon chain length of acid and ketones over Ru/TiO₂ catalyst.....</i>	105
<i>Figure 30. Surface fraction coverage of acid, ketone, water and CO₂ as a function of conversion over Ru/TiO₂ catalyst.....</i>	107
<i>Figure 31. Natural log of kinetic rate constant (k) as a function of inverse reaction temperature.....</i>	108
<i>Figure 32. Ketonization activation energies as a function of carbon chain length. Error bars indicate 95% confidence interval</i>	108
<i>Figure 33. Compensation plots for ketonization of acetic, propionic and butyric acids over Ru/TiO₂ catalyst. Error bars indicate 95% confidence interval.....</i>	117
<i>Figure 34. Reaction pathway to convert ethanol to butadiene</i>	129
<i>Figure 35. Base catalyzed mechanism for the aldol condensation of acetaldehyde followed by dehydration</i>	130
<i>Figure 36. Meerwein-Ponndorf-Verley (MPV) reaction mechanism of acetaldehyde and ethanol</i>	131

<i>Figure 37. X-ray diffractograms of MgO, B₂O₃ and mixed B-MgO prepared by combustion method.....</i>	<i>137</i>
<i>Figure 38. Effect of Boron loading on the XRD intensity of different MgO planes</i>	<i>138</i>
<i>Figure 39. CO₂- TPD MS characterization of MgO, B₂O₃ and mixed B-MgO prepared by combustion method</i>	<i>139</i>
<i>Figure 40. O 1s (top) and B 1s (bottom) X-ray photoelectron spectroscopy data of MgO, B₂O₃ and mixed B-MgO prepared by combustion method.....</i>	<i>141</i>
<i>Figure 41. ¹¹B-NMR characterization of B₂O₃ and mixed B-MgO prepared by combustion method.....</i>	<i>142</i>
<i>Figure 42. SEM images of MgO, B₂O₃ and mixed B-MgO with 7.5% weight loading of Boron prepared by combustion method</i>	<i>143</i>
<i>Figure 43. TEM-EDS images of mixed B-MgO with 7.5% weight loading of Boron prepared by combustion method</i>	<i>144</i>
<i>Figure 44. Reaction network for ethanol and acetaldehyde conversion in the presence of MgO, B₂O₃ or combination of B₂O₃ and MgO catalysts prepared by physical mixture, combustion or impregnation method.....</i>	<i>145</i>
<i>Figure 45. Product yield ratios obtained over the conversion of ethanol and acetaldehyde over MgO, physical mixture of B₂O₃ and MgO, and impregnation 2 wt% of B₂O₃/MgO. Reaction condition: T = 250°C, P= 300 psi N₂, t = 4 hours, catalyst mass: 200 mg, 20 mL ethanol, 2 mL acetaldehyde.....</i>	<i>147</i>
<i>Figure 46. Product yields for conversion of ethanol and acetaldehyde over fresh and recycled c-B-MgO prepared by combustion method with 7.5 wt% of Boron. Reaction</i>	

condition: T = 250°C, P= 300 psi N₂, t = 3 hours, catalyst mass: 200 mg, 20 mL ethanol, 2 mL acetaldehyde 150

Figure 47. Comparison of product selectivity for conversion of ethanol and acetaldehyde over c-B-MgO prepared by combustion method with 7.5 wt% of Boron using different ethanol: acetaldehyde feed ratios. Reaction condition: T = 250°C, P= 300 psi N₂, t = 3 hours, catalyst mass: 200 mg 151

Figure 48. Product yields of butanal and butanol for the conversion of crotonaldehyde over c-B-MgO prepared by combustion method with 7.5 wt% of Boron using H₂, isopropanol and 1-propanol as the hydrogenation agent. 152

Abstract

Lignocellulosic biomass, being the promising renewable source of carbon, has a great potential to serve as a sustainable platform for the production of fuels and chemicals. The conversion of lignocellulose to fuels and chemicals requires the effective utilization of small light oxygenates, in particular, C₂ as the major compounds derived from hemicellulose portion. In this study, catalytic processes for the conversion of biomass to fuels and chemicals were developed and investigated through two important C₂ platform molecules, acetic acid and ethanol.

In the first part, catalytic processing of acetic acid as a common product formed in biomass pyrolysis was studied. Ketonization is an ideal reaction for upgrading of this compound as it removes acidity and oxygen as well as creates C-C bonds that enlarge carbon backbones and maximize carbon yields in the fuel range. In this study, we have developed a new catalyst, Ru/TiO₂ that shows high activity and selectivity for ketonization of acetic acid in both vapor and liquid (organic and aqueous) phase. A rigorous kinetics study using carboxylic acids of varying carbon chain length, i.e., acetic, propionic, and butyric acid have been conducted over this catalyst. A thorough analysis built upon a Langmuir Hinshelwood (LH) model and transition state theory (TST) shows that the reaction follows a second-order expression with respect to carboxylic acids. The heat of adsorption was found very similar for the three acids, in spite of their different chain lengths, and significantly higher than those of the ketonization products, i.e. ketone, water and CO₂. The change in adsorption entropy of the acids (in absolute value) with respect to the gas phase was found to decrease with increasing chain length. These results are consistent with a strongly adsorbed bidentate

configuration, in which the main interaction with the surface is via the carboxylic group while the alkyl group moves rather freely. Activation energy derived from the LH model as well as activation enthalpy and entropy derived from TST provided insight into the reaction intermediates. Both of the latter two parameters were found to increase with increasing carbon chain length of the acids. This compensation effect can be interpreted in terms of the nature of the transition state. It is concluded that ketonization proceeds through a β -ketoacid intermediate with an early transition state, in which the C-C bond forms.

In the second part, catalytic conversion of bio-ethanol as an economically attractive feedstock to a valuable chemical, i.e. 1,3-butadiene, was investigated. This study provides a method to optimize the key intermediate step in butadiene production process from ethanol, which is the conversion of acetaldehyde and ethanol to crotonaldehyde and crotyl alcohol. This process requires an appropriate balance of acid and basic sites on the catalyst surface to maximize the yields of the crotonaldehyde and crotyl alcohol. By tailoring the molar ratio of the MgO and B₂O₃ during catalyst preparation through a combustion method, we developed a new B-MgO material, which has excellent catalytic properties with high selectivity of up to 75% for crotonaldehyde and crotyl alcohol. A thorough characterization of the catalysts suggests that the incorporation of Boron into MgO structure during the synthesis effectively modifies the properties and structure of MgO, creating well-balanced Lewis acid and basic sites and enhancing the catalytic performance.

A. General Introduction and Research Direction

A.1. Energy Outlook

World energy consumption is projected to increase from 524 quadrillion BTU in 2010 to 630 quadrillion BTU in 2020 and 820 quadrillion BTU in 2040, a 56 percent increase over a 30-year period, as indicated in Figure 1 [1]. Expanding population and rapid economic growth, especially in the developing countries outside the organization for economic cooperation and development (non-OECD), such as China and Brazil, are the key drivers behind this growing demand. Liquid fossil fuel remains as the dominant source of energy in the world, especially in the transportation sector. The worldwide consumption of liquid fuels will increase from 87 million barrels per day in 2010 to 97 million barrels per day in 2020 and 115 million barrels per day in 2040. The liquid fossil fuels consumption in the United States is expected to slowly increase from the 20 million barrels consumed per day in 2008 to 22 million barrels per day by 2035 [2].

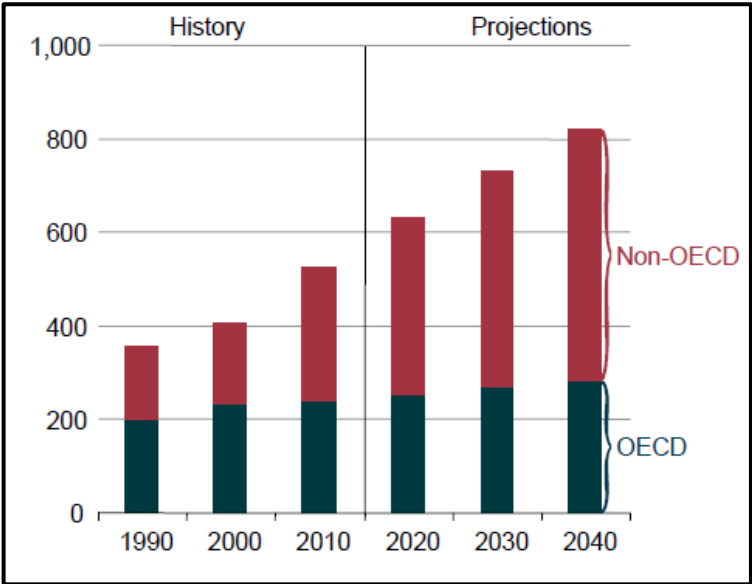


Figure 1. World total energy consumption 1990-2040 (quadrillion BTU) by country grouping [1]

Over the past few decades, there has been emerging evidence and growing concern about global warming. The Arctic warmth has led to the increased melting of ice sheets and glaciers, altering the atmospheric and oceanic circulation that in turn influences weather patterns. For example, the severe weather in the United States last winter was the result of the increased jet stream sinuosity, which tends to bring warm air up from the tropics into the West and carry cold air down from the Arctic to the Great Plains and the East, as the results of rapidly warming Arctic [3]. Among constituents causing warming, anthropogenic CO₂ and CH₄, a result of fossil fuel processing, are believed to have the greatest direct contribution [4]. Therefore, tremendous attention has turned to development and deployment of new technologies across different unconventional resources, including biomass, vegetable oils, animal fat, and algae. For instance, the U.S. Department of Energy has established very specific targets to replace 30% of the liquid fossil fuel with biofuels by 2025 [5].

Currently, the most widely used biofuels for transportation are ethanol and biodiesel. Ethanol is the largest biomass-derived fuel, accounting for 90% of total biofuel usage. The anaerobic fermentation of corn and sugar cane derived sugar produces a dilute aqueous solution of ethanol, which requires an energy-intensive distillation step to completely remove water from the mixture. Low concentration (5%-10%) blends of ethanol with gasoline (i.e. E5-E10) can be employed in current spark ignition engines while ethanol-rich mixtures (E85) require additional engine upgrades [6]. The other drawbacks include low energy content and high corrosion aggressiveness for transportation purpose [7].

Biodiesel, which is a mixture of long-chain alkyl esters typically derived from vegetable oils, is the second most abundant renewable liquid fuel. Similar to ethanol, biodiesel can only be used in low concentration blends with conventional diesel fuel. Another disadvantage of the biodiesel is the unavailability of inexpensive feedstock. Typically, palm, sunflower, canola, rapeseed and soybean oils are used, but they are expensive and can otherwise be used as food sources [8].

Due to the aforementioned limitations of current biofuels, it is desirable to develop technologies to utilize cheap non-edible lignocellulosic biomass feedstock to generate liquid fuels that meet the physical property requirements of liquid fuels and are compatible with modern internal combustion engines.

In addition, the detrimental effect of fossil fuel processing on environment has consequences that reach beyond the transportation fuel sector. Currently more than 90% of the chemical industry relies on fossil fuels as a feedstock. Therefore, the development of technologies to convert renewable lignocellulosic biomass resources for production of chemicals is required as well [9].

The transition from petroleum to biomass feedstock seems feasible for the production of fuels and chemicals based on the current production volume of biomass. However, biomass feedstock, being highly functionalized molecules, is significantly different from petroleum feedstock that is generally non-functionalized, presenting significant technological and economic challenges [10].

References

- [1] International Energy Outlook 2013, DOE Report DOE/EIA-0484 (2013) 1
- [2] Annual Energy Outlook 2013, DOE Report DOE/EIA-0383 (2013) 1
- [3] Z. Liu, K. Yoshimura, G.J. Bowen, N.H. Buenning, C. Risi, J.M. Welker., F. Yuan. Nature Comm. 5:3701 | DOI: 10.1038/ncomms4701
- [4] A. Zecca, L. Chiari. Energy Policy 38 (2010) 1
- [5] H.L. Chum, R. P. Overend. Adv. Solar Energy 15, (2003) 83
- [6] J.C. Serrano-Ruiz, J.A. Dumesic. Energy Environ. Sci. 4, (2010) 83
- [7] M. Balat, H. Balat, C. Oz. Progress Energy Combustion Sci. 34 (2008) 551
- [8] D.Y.C. Leung, X. Wu, M.K.H. Leung. Appl. Energy 87 (2010) 1083
- [9] C.H. Christensen, J.R. Hansen, C.C.Marsden, E. Taarning, K. Egeblad. ChemSusChem 1 (2008) 283
- [10] G.W. Huber, S. Iborra, A. Corma. Chem. Rev. 106 (2006) 4044

A.2. Research Direction

As mentioned above, lignocellulosic biomass material has the great potential for establishing a sustainable platform for the production of energy as well as chemicals. Similar to development of petroleum-based technologies, the catalysis field will inevitably play a crucial role in the growth of biomass-based technologies. However, recent studies have indicated many challenges for catalytic conversion of lignocellulosic biomass. For example, biomass, being a highly functionalized starting material, requires selective oxygen removal while retaining and enlarging carbon number to selectively obtain platform molecules that are stable and fungible to conventional fuel. Furthermore, the presence of an aqueous environment and competing gum formation and polymerization side reactions in most biomass conversion reactions presents challenges for utilizing conventional catalysts. These challenges, among others, create great opportunities for scientific and technological advancements to develop efficient upgrading strategies.

This thesis addresses some of the aforementioned challenges by developing catalytic strategies for the conversion of lignocellulosic biomass-derived C₂ molecules to building block units and platform chemicals utilizing heterogeneous catalysis. Specifically, we focus on two research subjects:

- (i) Catalytic upgrading of acetic acid via ketonization
- (ii) Catalytic conversion of ethanol to 1,3-butadiene

The thesis contains two major parts with a number of different chapters addressing different subtopics of the two research subjects. In each part, literature review and background are followed by a concise description of the goals for the

research, detailed information of experimental and analytical techniques and discussion along with results of completed research topics. Also, conclusion and proposed future research direction are proposed for each project. Each chapter can be viewed as standalone manuscripts and is therefore formatted in that manner.

B. Catalytic Upgrading of Acetic Acid - Derived Biomass by Ketonization

B.1. Biomass Conversion Processes to Liquid Fuel

There have been a number of different processes developed during exploration of biomass to liquid fuel conversions. These techniques can be classified as biochemical and thermo-chemical methods. Typical biochemical process is fermentation while common thermochemical processes include liquefaction, gasification, hydrolysis and pyrolysis [1-3].

Fermentation is primarily used for the production of ethanol, which is not likely a great option as a transportable and inexpensive fuel due to its different chemical properties in comparison to conventional fuel [2,4]. Gasification creates a syngas mixture that could be subsequently upgraded via Fisher-Tropsch synthesis to make transportation-range hydrocarbons [5]. Hydrolysis could effectively break down cellulose and hemicellulose into its constituent C5-C6 sugar molecules, which can be upgrading to form liquid fuels. However, this method involves acid consumption, which might cause serious equipment corrosion and require high cost for acid recovery [6]. Liquefaction, which is usually carried out at high pressures (50-200 atm) and low temperatures (250-450°C) in the presence of reducing gas and/or catalyst can also create liquid fuels, but is largely dismissed as an option due to its high costs [3].

Pyrolysis process is thought to have great promise as a means for converting biomass into liquid fuels. This is due to reasons such as low costs, simple processes, and feedstock flexibility [7,8]. Fast pyrolysis, i.e., rapid heating of biomass in an inert atmosphere at temperatures around 500-800°C in less than 2s, can produce liquids at

high yields. However, this method produces a complex mixture of numerous compounds, which require multi-step separation.

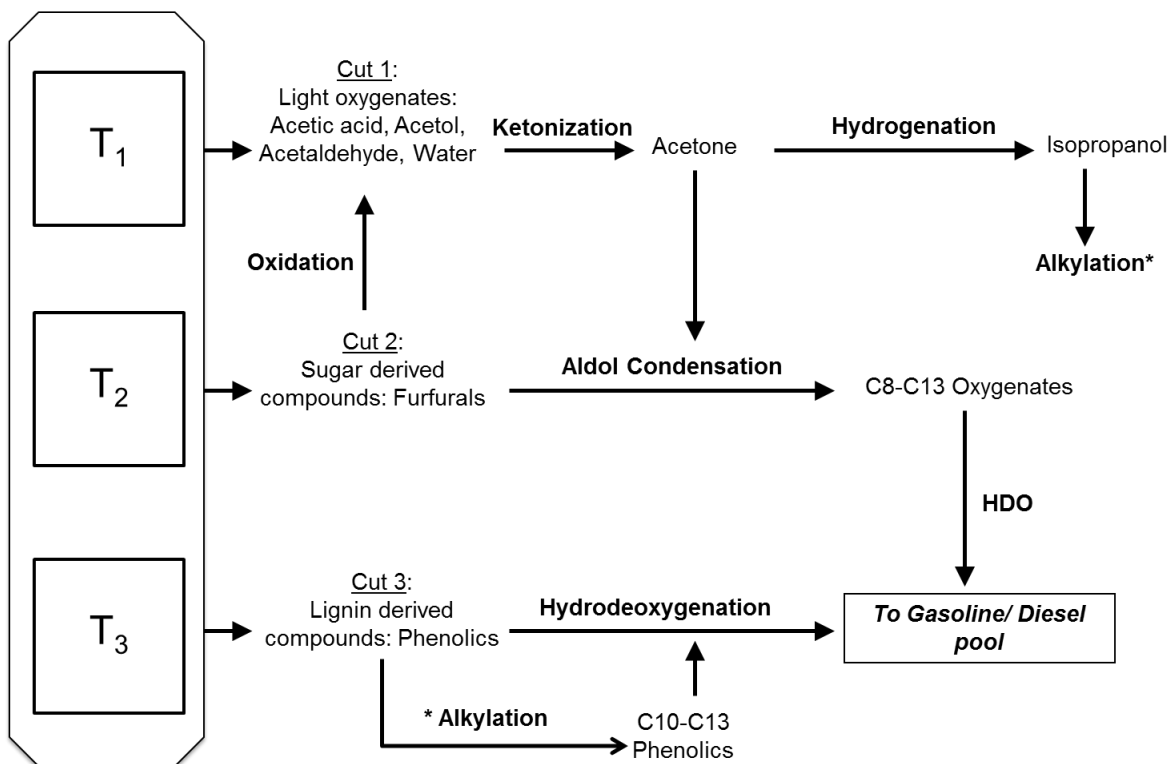


Figure 2. Process Concept: Liquid phase catalytic cascade connected to a multi-stage pyrolysis for biofuel production and upgrading

Staged pyrolysis, taking advantage of the different thermal stabilities of different components in biomass, i.e. hemicellulose, cellulose, and lignin, can selectively thermally breakdown and fractionate different compounds [9]. The concept of a step-wise pyrolysis of lignocellulosic biomass is graphically illustrated in Figure 2. Initial heating at temperatures below 300°C (first torrefaction) results in evolution of small oxygenates (primarily acetic acid and acetol) and water decomposed from hemicellulose. Subsequent heating to 400°C leads to breaking down of cellulose producing mainly levoglucosan and hydroxymethyl furfural (HMF). In the final, fast-

pyrolysis step ($\sim 550^{\circ}\text{C}$), the more stable lignin fraction is decomposed, forming mostly phenolic compounds.

As may be expected from the over-functionalized starting lignocellulosic biomass materials, the inherent characteristics of the resulting bio-oil product, including high viscosity, chemical instability, high corrosiveness and incompatibility with conventional fuels, render it useless as a fuel unless stabilized. Stabilization can be accomplished by oxygen removal from the abundant oxygenated compounds in the product, which include acids, aldehydes, esters, phenolics, furanics and oxygenated oligomers [10,11]. The production of stabilized bio-oils has received increasing attention in the pursuit of economically viable large-scale biomass conversion processes [12].

The various possibilities for stabilization of bio-oil proposed in the literature alleviate some of the aforementioned issues in the use of bio-oil can be divided into three general strategies. The first is to directly contact the vapor exiting the pyrolysis reactor with a catalyst before its condensation. This strategy, which has been under extensive study in recent years [13,14], has the advantage of preventing some of the polymerization and gum formation reactions that occur in liquid phase and greatly reduce viscosity and instability of bio-oil. To this end, a catalytic process to either deoxygenate the oxygenated compounds or utilize the oxygen functionalities to facilitate the formation of C-C bonds, for example, via ketonization of carboxylic acids or aldol condensation of aldehydes and ketones is extensively pursued [15-20].

The second strategy, which has been widely proposed since early 1980s, is hydrotreating, which includes two options (i) hydrotreating after condensation of bio-oil

[21-25]; (ii) high-pressure post pyrolysis hydrotreating integrated with a hydrolysis reactor [26]. In the former case, the pyrolysis vapors are first condensed and the liquid bio-oil is then transferred and treated in conventional hydrotreating units using commercial catalysts such as sulfided Co-Mo and Ni-Mo, similar to those employed in oil refineries. However, it was found that the low chemical and thermal stability of bio-oil make it unprocessable at high temperatures typically used in conventional hydrotreating units. In addition, the hydrogen consumption is exceedingly high. For example, when bio-oil from a poplar wood was hydrotreated over a sulfided Co-Mo catalyst at 355°C and 13.8 MPa, the liquid product contained about 5% oxygen, but the yield was only 23% [23]. More importantly, coke formation and rapid catalyst deactivation is a common problem in hydrotreating of bio-oils. Therefore, an additional pre-hydrogenation deoxygenation (HDO) step at low to medium temperature is required to stabilize the bio-oil, in which the most reactive groups are converted to less active ones to avoid severe coking in a subsequent step. The same catalysts such as sulfided Co-Mo or Ni-Mo have been used for both steps. It has been reported that this two-step process could produce yields up to 0.53 L refined-oil/ L oil feed. However, almost half of this yield is composed of light alkanes, which probably arise from the small oxygenates (C1-C5) in the original bio-oil [22, 23]. Over the last 25 years, much research has been carried out to develop more active and stable catalysts as well as to optimize reactor set-up for hydrotreating process and many progresses have been made. However, the large amount of hydrogen required and a substantial amount of carbon loss in light alkane products have impeded its commercialization. The second option of this strategy is to conduct biomass pyrolysis under medium hydrogen pressure (20-35

bar) in a catalytic fluidized bed (so called hydro-pyrolysis reactor) directly connected to a hydrotreating unit, which can further perform hydrodeoxygenation of liquid products and produce hydrogen by reforming some of the light gases obtained from hydro-pyrolysis [26]. This process has been shown to produce liquid oil with less than 2.2 wt% from a variety of biofeeds including bagasse, corn stover, algae and wood. However, the added complexity and risk of operating the pyrolysis unit under hydrogen does not result in improved liquid yield (>C5). Therefore, the loss of liquid yield remains as a major challenge for the hydrotreating approach.

A third strategy for biofuel production is co-processing pre-hydrogenated pyrolysis oil together with petroleum feedstock in conventional petroleum refinery units such as fluidized catalytic cracking (FCC) and hydrotreating unit [27-31]. The obvious advantage of this approach is the reduced cost of biofuel production by utilizing existing refinery infrastructure and avoiding high capital cost investment into new units exclusively dedicated to biomass processing. To elucidate the possibilities of co-processing approach, many studies have focused on co-feeding hydrocarbon and model oxygenated compounds into a FCC unit. Lappas et al. [27] conducted a study combining hydro-deoxygenation and co-processing in a FCC unit of pyrolysis oil with vacuum gas oil (VGO). Pyrolysis oil was first subject to a thermal hydrogen processing step and then co-fed to the FCC units with VGO. In comparison with VGO, the co-processing with pyrolysis oil resulted in higher coke production (0.5 wt%), lower liquid petroleum gas, and an increased selectivity towards aromatics compounds. Corma et al. [31] studied the catalytic cracking of model bio-oil oxygenates including glycerol and sorbitol, and its mixture with VGO using different FCC catalysts to elucidate the main

reaction pathways and the effect of co-feed. The catalytic cracking of oxygenated compounds involves a complex reaction network. Gas phase products consisting of olefins, CO, CO₂, H₂, and paraffins are produced by dehydration, steam reforming, water gas shift, decarbonylation, and dehydrogenation/hydrogenation reactions. Aromatics are formed by condensation and Diels-Alder reactions of olefins and dehydrated species. Among those tested catalysts, ZSM-5 produced lower level of cokes and high amount of aromatics and olefins, whereas the other catalysts including a commercial FCC catalyst containing Y-zeolite and silica-alumina matrix, a commercial FCC catalyst with V and Ni impurities (ECAT), Al₂O₃ and HY produced high amounts of cokes and low amounts of aromatics and olefins. Addition of oxygenated compounds to VGO did not significantly change the product distribution of the final products as compared with VGO alone. However, bio-oil compounds decreased the gasoline yield and overall conversion, increased the coke amount and the olefin to paraffin ratio of C₂-C₄ hydrocarbons. More studies are needed to understand the synergistic effect of oxygenated compounds and hydrocarbon. Bui et al. [29] studied the co-processing of bio-oil and petroleum model compounds under hydrogen desulfurization conditions. Similar to the catalytic cracking study, decreased catalyst performance at low temperatures and high contact times was observed. This might be due to intermediate phenols competing with sulfur containing molecules on dehydrogenation sites. Although co-processing constitutes a promising route, it presents several challenges including efficiency of the process and catalyst development, which requires more study and investigation.

A fourth alternative for bio-oil upgrading that would avoid some of the problems associated with the above three strategies is to conduct catalytic conversion in liquid phase over pre-fractionated segments of bio-oil. Figure 2 depicts the simplified approach for bio-oil upgrading in liquid phase. As mentioned previously, after a multi-stage pyrolysis of lignocellulosic biomass at different temperatures and reaction times, the obtained bio-oil can be segregated into light, medium and heavy oxygenate components. Therefore, the product mixtures from different stages can be selectively upgraded in liquid phase by different catalysts via different reaction approaches. Specifically, as illustrated in Figure 2, from different bio-oil fractions one could: (i) partially remove unstable oxygen functional groups; (ii) couple C-C bonds to elongate the carbon chain and (iii) completely remove the remaining oxygen functionality.

The upgrading approach for light oxygenates, consisting of water-soluble compounds such as acetic acid, acetol, acetaldehyde, etc. is to undergo ketonization reaction. Ketonization can remove the highly reactive carboxylic functional groups while increasing the size of the carbon chain. The result is a more stable product, ketone, with higher energy content. In addition, the ketones produced are building blocks that can undergo further coupling reactions to expand the fraction of molecules that fall in the gasoline/diesel range. Therefore, in the next hydro-deoxygenation step, the smaller molecules are not eliminated in the form of light gases, but retained as liquid products. For instance, ketone can couple with sugar derived compounds, such as furfurals [32] or hydrogenated to alcohols, which in turn can be used as alkylating agents of phenolic compounds, via acid-catalyzed alkylation [33]. These products,

with enlarged C-chain length, can undergo hydro-deoxygenation to produce long chain hydrocarbons, with minimum loss in liquid yield.

The sugar derived compounds can either couple with acetone as mentioned above, or undergo oxidation to produce acids, which can also be ketonized and further upgraded. The phenolics from lignin fraction of biomass (heavy products) can be alkylated with light alcohols or can undergo direct hydro-deoxygenation. Discussion and research in the following chapters will focus on understanding of ketonization and its potential application in the bio-oil upgrading process.

References

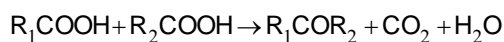
- [1] G.W. Huber, S. Iborra, A. Corma. *Chem. Rev.* 106 (2006) 4044
- [2] P. McKendry, *Bioresource Tech.* 83 (2002) 47
- [3] A. Demirbas. *Energ. Convers. Manage.* 42 (2001) 1357
- [4] M. Balat, H. Balat, C. Oz. *Prog. Energ. Combust. Sci.* 34 (2008) 551
- [5] M.J.A. Tijmensen, A.P.C. Faaij, C.N. Hamelinck, M.R.M. van Hardeveld, *Biomass Bioenerg.* 23 (2002) 129
- [6] Y.Yu, X.Lou, H. Wu. *Energ. Fuels* 22 (2008) 46
- [7] D. Mohan, C.U. Pittman, P.H. Steele, *Energ.Fuels* 20 (2006) 848
- [8] S. Czernik, A.V. Bridgwater, *Energ. Fuels* 18 (2004) 590
- [9] W.H. Chen, P.C. Kuo, *Energy* 36 (2011) 803
- [10] C. A. Mullen, A. A. Boateng, *Energ. Fuels.* 22 (2008) 2104
- [11] C.A. Mullen, A. A. Boateng, K. B. Hicks, N. M. Goldberg, R. A. Moreau. *Energ. Fuels.* 24 (2010) 699
- [12] R. H. Venderbosch, A.R. Ardiyanti, J. Wildschut, A. Oasmaa, H.J. Heeresb, J. *Chem. Tech. Biotechnol.* 85 , (2010) 674
- [13] H.-Y. Li, Y.-J. Yan, Z.-W. Ren, *J. Fuel Chem. & Tech.* 36, (2008) 666
- [14] M. A. Gonzalez-Borja and D. E. Resasco, *Energ. Fuels* 25 (2011) 4155
- [15] C.A. Gaertner, J.C.Serrano-Ruiz, D.J. Braden, J.A. Dumesic, *J. Catal.* 266 (2009), 71.
- [16] T.Q. Hoang, X. Zhu, T. Sooknoi, D.E. Resasco, R.G. Mallinson, *J. Catal.* 271 (2010) 201
- [17] T.Q. Hoang, X. Zhu, T. Danuthai, D.E. Resasco, L.L Lobban, R.G. Mallinson, *Catal. Comm.* 11 (2010) 977.

-
- [18] A. Gangadharan, M. Shen, T. Sooknoi, D.E. Resasco, R.G. Mallinson. *Appl. Catal. A-General* 385 (2010), 385
- [19] S. Sitthisa, D.E. Resasco. *Catal. Lett.* 141 (2011) 784
- [20] X. Zhu, L.L. Lobban, R.G. Mallinson, D.E. Resasco. *J. Catal.* 281 (2011) 21
- [21] D.C. Elliott. *International Sustainable Energy Review* 4 (2010) 56.
- [22] D.C. Elliott, G.G. Neuenschwander. *Developments in Thermochemical Biomass Conversion*. Bridgwater. Blackie Academic and Professional 1996, 611
- [23] D.C. Elliott. *Energ. Fuels*. 21 (2007) 1792
- [24] E. Laurent, B. Delmon. *J. Catal.* 146 (1994) 281
- [25] D.C. Elliott, A. Oasmaa. *Energ. Fuels* 5 (1991) 102
- [26] T.L. Marker, L.G. Felix, M.B. Linck, M.J. Roberts. *Environ. Prog. Sustainable Energy*. 31 (2012) 191
- [27] A.A. Lappas, S. Bezergianni, I.A. Vasalos. *Catal. Today* 145 (2009) 55
- [28] M.E. Domine, A.C. van Veen, Y. Schuurman, C. Mirodatos. *Chemosuschem* 1 (2008) 179
- [29] V.N. Bui, G. Toussaint, D. Laurenti, C. Mirodatos, C. Geantet. *Catal. Today*, 143 (2009), 172
- [30] E. Butler, G. Devlin, D. Meier, K. McDonnell. *Renew. Sustain. Energy Rev.* 15 (2011), 4171
- [31] A. Corma, G.W. Huber, L. Sauvanaud, P. O'Connor. *J. Catal.* 247 (2007) 307
- [32] P.A. Zapata, J. Faria, M. P. Ruiz, D.E. Resasco. *Top Catal.* 55 (2012) 38
- [33] L. Nie, D. E. Resasco. *App. Catal. A: General*. 447 (2012) 14

B.2. Literature Review on Ketonization

B.2.1. Ketonization Mechanism

Ketonization (or ketonic decarboxylation) is a reaction that converts two carboxylic acid molecules into a ketone, carbon dioxide and water, as follows:



The first example of ketonization was reported in 1858 by Friedel [1], who produced acetone by decomposition of calcium acetate. Following the same approach, other low-lattice-energy alkali and alkaline earth oxides were later found to be effective for producing acetone from acetic acid via the decomposition of the corresponding acetate. Later developments have shown that high lattice-energy metal oxides such as TiO_2 , CeO_2 , ZrO_2 and MnO_2 [2-14], as well as zeolites [15] and heteropoly acid catalysts [16] do not follow the decomposition path, but can act as surface catalysts for the ketonization reaction.

Industrial applications of ketonization appeared before WWI, when acetone was commercially produced by dry distillation of calcium acetate, obtained from lime neutralization of wood distillates [17]. More recent cost-effective petrochemical routes of acetone production, such as the cumene process [18] made ketonization less commercially appealing. However, ketonization has regained attention in recent years due to its potential applications in biomass conversion as mentioned previously.

Extensive research efforts on ketonization during the last thirty years have resulted in a variety of mechanistic explanations, with some of them not exempt of controversy. First, it is important to differentiate between bulk ketonization, which occurs via decomposition of the corresponding carboxylate salts, and surface

ketonization, which is catalyzed by solid surfaces. For the bulk ketonization it is necessary to determine what oxides are able to form bulk carboxylates, which decompose releasing ketones. For the surface ketonization, it is crucial to understand the involvement of α -hydrogen and a number of various surface intermediates including ketene, β -ketoacids, adsorbed carboxylates, acyl carbonium ions, and acid anhydrides.

Yakerson *et al.* [19,20] were the first to point out the two entirely different phenomena that can lead to the formation of acetone from acetic acid. They noticed that oxides with low lattice energies (or very high basicity) such as alkali and alkali earth oxides, including MgO, CaO, BaO, SrO and CdO, interact very strongly with acetic acid. This interaction results in the formation of bulk carboxylate salts, which decompose upon thermal treatment, generating acetone, water and CO₂. This reaction has also been observed over highly basic rare earth oxides such as La₂O₃, Pr₆O₁₁ and Nd₂O₃ [21]. In contrast, on oxides with high lattice energies such as TiO₂, CeO₂, ZrO₂, SnO₂, etc., the reaction proceeds via a completely different pathway, which is confined to the catalyst surface. This distinction was later emphasized by Ponec *et al.* [4-6,22] in a series of papers covering several oxides, such as TiO₂, Al₂O₃, ZrO₂ and Cr₂O₃ that are catalytically active to convert acetic acid to acetone. In the presence of H₂ and high enough temperatures, some of them are also active for the hydrodeoxygenation of acetic acid to acetaldehyde. They noticed that, in contrast, low-lattice-energy oxides transformed to acetate salts and only decomposed to acetone, even in the presence of H₂. They tested a number of oxides for ketonization of acetic acid in the vapor phase using H₂ as carrier gas [4]. Periodic sampling was performed during a temperature

ramp and the reactant/product concentrations were plotted against temperature to identify the mechanistic pathway. It was shown that for oxides with high lattice energy, the appearance of acetone, water, and CO₂ occurred simultaneously with the disappearance of acetic acid. In contrast, in the case of MgO, PbO, Bi₂O₃, the decrease in acid concentration occurred significantly before the formation of products. This observation led the authors to support the conclusion of the existence of two separate phenomena, as identified by Yakerson *et al* [19, 20]. It is possible that in some cases, both mechanisms may be simultaneously operative on a given solid, and, depending on the reaction conditions, one of them can prevail. For instance, Kuriacose and Jewur [23] studied the ketonization of acetic acid over iron oxides in the presence of H₂ and found that the activation energy changed at 400 °C signaling a potential change in mechanistic pathway. They proposed that, below 400°C, ketonization proceeds on the catalyst surface by interaction of two adsorbed molecules of acetic acid. By contrast, at higher temperatures, the reaction takes place through the bulk acetate decomposition. More recently, Snell and Shanks [10] have reported similar observations for the case of CeO₂, which has been typically considered a surface ketonization catalyst. They conclude that CeO₂ can promote the ketonization reaction through either the bulk or the surface mode, depending on reaction temperatures. However, opposite to the early study on Fe₂O₃ [23], CeO₂ seems to undergo bulk transformation in the low-temperature range (150-300°C), whereas above 300°C, the reaction only occurs on the catalyst surface. Clearly, different oxides may exhibit different behavior regarding formation/decomposition of bulk carboxylates, and the low/high lattice energy description may need refinement, which will require further

research. In spite of many different mechanistic pathways proposed to explain the bulk carboxylate decomposition pathway there is an agreement in the necessity of two intermediate species, which serve as the source of alkyl and acyl (or carbonyl) fragments to form the ketone product [5,36]. Much of the research conducted on the thermal decomposition of aliphatic and aromatic carboxylate salts suggests that the formation of alkyl and acyl fragments are due to radical-like decomposition at elevated temperatures [24,25]. Such a mechanism does not require the presence of α -hydrogen atoms in the acids, which will be discussed in more detail below. On the other hand, many studies on various carboxylic acids reveal an important effect of α -hydrogen for the surface-catalyzed ketonization. Furthermore, as discussed below, the mechanism and intermediate species formed during the surface catalyzed reaction are subject to debate. For this reason, in the subsequent part of this section, we focus on the role of α -hydrogen, mechanistic pathways, and intermediate structures together with catalyst requirements for the surface-catalyzed ketonization.

One characteristic element that consistently appears in all surface-catalyzed ketonization studies is the need for an α -hydrogen in at least one of the carboxylic acids participating in the reaction. α -Hydrogen is defined as the hydrogen bonded to a carbon atom in the α position relative to a carbonyl group. This atom displays relatively higher acidity in comparison to other alkyl hydrogens. For instance, while the pK_a values for alkyl C-H bond dissociation is typically on the order of 40-50, those for the α -hydrogen atoms are usually in the range of 19-20 [26]. The critical role of the α -hydrogen in the ketonization of carboxylic acids has been well documented,

mostly by H/D exchange studies and the strong dependence of ketonization activity on the number of α -hydrogens present on carboxylic acids.

Neunhoeffer and Paschke [27] were the first to point out that only those carboxylic acids that possess an α -hydrogen can undergo ketonization, i.e. intramolecular ketonization of the dicarboxylic adipic acid to produce cyclopentanone.

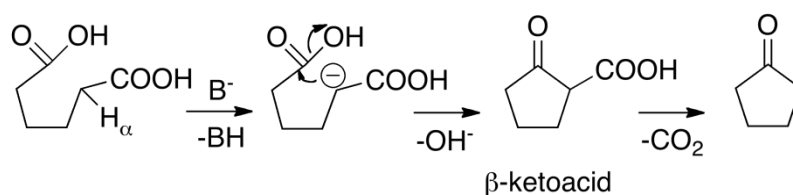


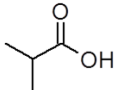
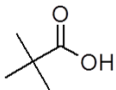
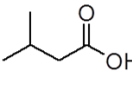
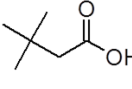
Figure 3. *Ketonization mechanism of adipic acid proposed by Neunhoeffer and Paschke [27]*

As illustrated in Figure 3, their proposed mechanism starts with the abstraction of an α -hydrogen by a basic site of the catalyst surface, which leads to the formation of a nucleophile that can readily attack another carboxylic acid to form a ketone. In a more detailed study, Ponec *et al.* [4] showed a clear trend of increasing ketone formation rate with the greater number of α -hydrogen atoms on the carboxylic acid. This trend indicates that the presence of α -hydrogen atoms is essential for ketonization. The role of α -hydrogen was also emphasized in a study by Nagashima *et al.* [28], whose results are summarized in Table 1.

Here, again, it is seen that the formation of ketones in the reaction of propanoic acid with other α -substituted carboxylic acids depends on the presence of α -hydrogen atoms in the reactants. That is, the self-ketonization of propanoic acid, which has two α -hydrogen atoms, proceeds ten times faster than that of 2-methylpropanoic acid,

which only has one α -hydrogen atom. Finally, with the 2,2-dimethylpropanoic acid, which has no α -hydrogen, the self ketonization activity cannot proceed.

Table 1. Molar composition of effluent flow in the reaction of 1:1 molar ratio of propanoic acid with carboxylic acid at 375°C using CeO_2 - Mn_2O_3 (Mn: 60 mol%)[28]

Propionic acid (P)+ Carboxylic acid (CA)		3- pentanone (2P)	Asymmetric ketone (CA:P)	Symmetric ketone (2CA)	Unreacted propanoic acid	Unreacted counter acid	Others
2-Methylpropanoic acid		1.00	0.97 ^a	0.10 ^b	0.09	1.30	0.12
2,2-Dimethylpropanoic acid		1.00	0.03 ^c	0.00 ^d	0.34	2.16	0.09
3-Methylbutanoic acid		1.00	1.58 ^e	0.25 ^f	0.11	1.58	0.34
3,3-Dimethylbutanoic acid		1.00	0.26 ^g	0.00 ^h	0.30	2.10	0.14

^a:2-methyl-3-pentanone

^b:2,4-dimethyl-3-pentanone

^c:2,2-dimethyl-3-pentanone

^d:2,2,4,4-tetramethyl-3-pentanone

^e:5-methyl-3-hexanone

^f:2,6-dimethyl-4-heptanone

^g:5,5-dimethyl-3-hexanone

^h:2,2,6,6-tetramethyl-4-heptanone

A similar conclusion is reached when the relative rates of cross-ketonization between propanoic acid and other carboxylic acids are considered. For example, the rate of cross-ketonization of propanoic acid and 2-methylpropanoic acid is much higher than the rate of 2,2-dimethyl-3-pentanone formation from propanoic acid and 2,2-dimethylpropanoic acid is. Thus, while the reactivity trend seems to follow the number of α -hydrogen atoms in the molecule (i.e., 2,2-dimethylpropanoic acid < 2-methylpropanoic acid < propanoic acid) one must note that to vary the number of α -

hydrogen atoms in this study, methyl groups have been incorporated. This substitution opens the discussion on steric hindrance, the second important aspect in determining ketonization activity. In fact, Table 1 shows that not only the number of α -hydrogen atoms, but also the number of substituents at the β position influences the reactivity. This is clearly demonstrated in the comparison between 3-methylbutanoic and 3,3-dimethylbutanoic acids. Both, cross- and self-ketonization are greatly lowered with the increase in the number of methyl groups at the β position. Therefore, both the number of α -hydrogens and their steric accessibility are crucial elements to determine ketonization activity.

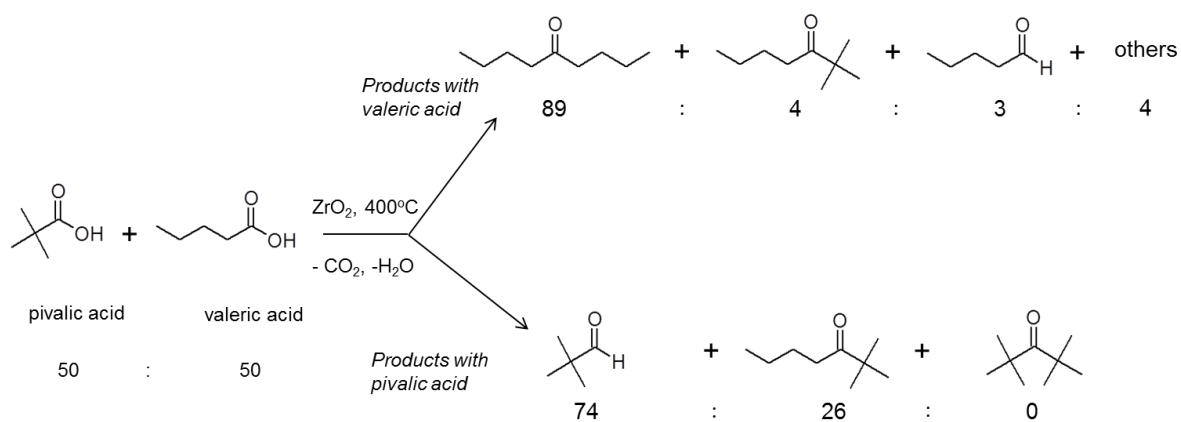


Figure 4. Conversion and product selectivity for ketonization of a mix of valeric and pivalic acid (1:1 molar ratio) [29]

Among the several studies that illustrate the important role of the α -hydrogen in ketonization, Pulido *et al* [29] investigated a mixture of two C5 carboxylic acids, namely valeric and pivalic acids, over a ZrO_2 catalyst. As displayed in Figure 4, valeric acid, with two α -hydrogens and pivalic acid, with no α -hydrogen show clear differences in activity. Valeric acid can be completely converted with 89% selectivity to self-ketonization and 4% selectivity to the cross-ketonization with pivalic acid,

whereas the symmetric ketone of pivalic acid was not obtained. The results lend further support for the requirement of the α -hydrogen in at least one of the carboxylic acids.

Experiments with isotopically labeled compounds have also corroborated the crucial role of α -hydrogen in ketonization reactions. Ponec *et al.* [4-6] found that α -D was present in the acetone product formed by acetic acid ketonization on a pre-deuterated TiO₂ surface, whereas when feeding acetone, no H/D exchange occurred with the deuterated surface. This result clearly suggests that the intermediate for the formation of acetone interacts with the catalyst surface through its methyl group, resulting in α -hydrogen abstraction and exchange. Similar observations were previously reported by Jayamani and Pillai [30] and Munuera *et al.*[31], who found that D in the α -position of ketones formed when unlabeled acid vapors were reacted over deuterated oxide surfaces.

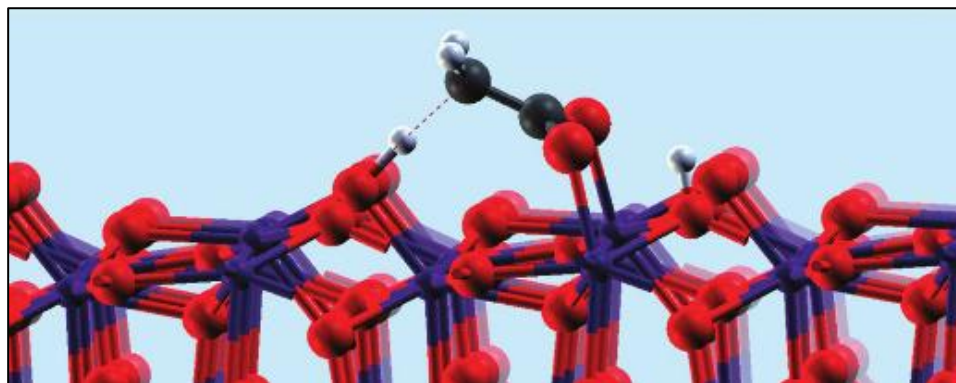


Figure 5. Dianion acetate species on the surface of ZrO₂ [32]

Theoretical modeling was employed to study the activation energy of α -hydrogen abstraction of carboxylic acids, which may help to ascertain the feasibility of this step during ketonization. Ignatchenko [32] calculated the heat of adsorption and α -hydrogen abstraction energy barrier of various acids on a zirconia surface, using

periodic DFT calculations. It was found that the lattice oxygen on the (111) ZrO₂ plane could readily abstract the H atom from the α position relative to the carboxylic group, as shown in Figure 5 [32].

Three carboxylic acids, including acetic, propionic, and isobutyric acids with a varying number of α -hydrogens were investigated in this study. These calculations indicated that the energy barrier for the abstraction of the α -hydrogen that produces a dianion species appears to be 120-159 kJ/mol on the (111) ZrO₂ plane, depending on acid branching. In another theoretical DFT study that also used a periodic slab model of ZrO₂ [29], the reaction pathway involving an α -hydrogen abstraction step was compared to a concerted mechanism that does not involve α -hydrogen abstraction. The calculations indicated that the mechanism involving the α -hydrogen abstraction is kinetically favorable with much lower activation energy, mainly due to the formation of a reactive nucleophilic center formed upon the α -hydrogen abstraction that can easily couple with another adsorbed molecule to produce a β -ketoacid intermediate, which then undergoes decarboxylation to produce the ketone. Details of this pathway will be further discussed below. It is also significant that the reverse reaction, i.e. protonation of the dianion, was reported to have a much lower energy barrier than the abstraction of α -hydrogen to form the dianion. Therefore, a competition between dianion protonation and β -ketoacid intermediate formation, which has comparable activation energy can exist.

In summary, a large part of the published ketonization studies seem to agree on the required participation of α -hydrogen. However, the exact details on how the α -hydrogen is involved in the reaction pathway are still debatable. Nevertheless, the

recognition of the central role of the α -hydrogen has served as the basis for the development of several mechanisms, including the formation and participation of different intermediates, such as ketene and β -ketoacid.

B.2.1.1. Ketene Mechanism

A ketene ($R_2C=C=O$) is formed by dehydration of a carboxylic acid containing at least one α -hydrogen atom [33]. Therefore, due to the connection with the requirement of an α -hydrogen, ketene has been frequently considered as a ketonization intermediate. A mechanism involving the coupling of an adsorbed ketene with a carboxylate was suggested in 1978 by Munuera *et al.* [31] and later further supported by Dooley *et al.* [8,9,34]. In this mechanism, a carboxylate intermediate is first formed on a coordinatively unsaturated metal site and then dehydrated to a surface ketene intermediate. This adsorbed intermediate then couples with the alkyl group of an adsorbed carboxylate species to form the ketone. In this mechanism, the acyl group in the ketone originates from the ketene and not from the carboxylate. The suggested mechanism is illustrated in Figure 6.

While the ketene mechanism is attractive due to its correlation with a central role of an α -hydrogen, the details on how a ketene and carboxylate couple to form a ketone on the surface are missing since this process should involve more than one elementary step. While some evidence that supports the ketene based mechanism is given in the literature, as highlighted below, the common requirement of an α -hydrogen participation for both ketonization and ketene formation is perhaps the only solid argument in favor of the ketene mechanism.

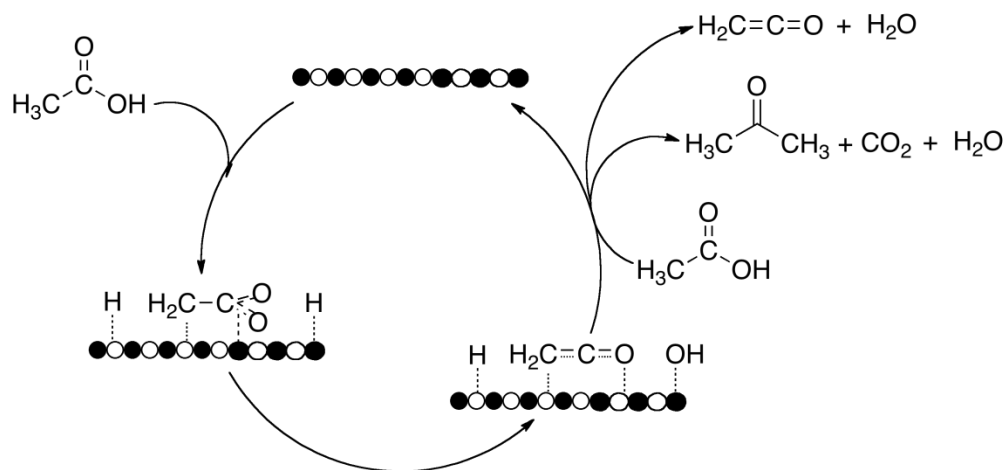


Figure 6. Ketene-based mechanism of acetic acid ketonization

Using a TiO_2 (anatase) catalyst, Munuera *et al.* [31] studied the ketonization of acetic acid combined with FT-IR analysis and isotopic labeling. Specifically, FT-IR was employed to examine the nature of various adsorbed species formed on the surface under different conditions. The similarity between the observed absorption bands with those corresponding to vapor phase ketene (3005 and 1730 cm^{-1}) was taken as an evidence for the existence of ketene on the surface after exposure to acetic acid. Furthermore, acetone was observed to evolve at around $200\text{-}350^\circ\text{C}$ during temperature programmed desorption following exposure to acetic acid. This is about the same temperature range over which disappearance of the bands associated with the ketene occurred. This correspondence was used to conclude that ketene is the most likely ketonization intermediate. In addition, products from the reaction between unlabeled acetic acid with a catalyst surface pretreated with deuterated acetic acid were analyzed by mass spectrometry. Formation of all possible deuterated acetone products was observed. This outcome demonstrates that the reaction involves deuterated species from the surface. However, it is unclear whether they necessarily were deuterated

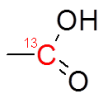
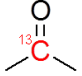
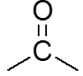
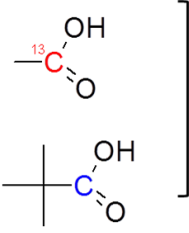

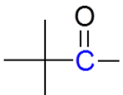
ketene intermediates. It has also been proposed that the rate-determining step is the rate of ketene formation from the adsorbed acetate. The driving force for this step would be the electronic saturation of Ti^{4+} sites with the two surface species formed, -OH and CH_2CO [31].

Likewise, Dooley *et al.* [8,9,34] supported the ketene mechanism by a series of studies that included isotopic labeling experiments on various supported CeO_2 catalysts. For example, they conducted the ketonization of acetic acid and cyclopropane carboxylic acid (CCA) on a 10 wt.% CeO_2/TiO_2 catalyst to produce acetone and methylcyclopropylketone. Using a 3:1:1 mixture of $CD_3COOH:H_2O:CCA$ as a feed, the authors compared the experimentally observed distribution of labeled products with the binomial distribution that one might expect from either the ketene or the direct concerted mechanism. The former should show D-exchange since the acetic acid only contains D atoms at the α -position. By contrast, the latter would result in no D-exchange, producing only CD_3COCD_3 and $CD_3COC_3H_5$. The experimental results showed that the most abundant products were of the type CHD_2COCD_3 and $CHD_2COC_3H_5$, demonstrating both the participation of only one α -hydrogen and the lack of any other exchange with the surface. While these results strongly support the participation of α -hydrogen in the reaction and provide indisputable evidence against the direct concerted mechanism, they are not conclusive about the participation of ketene as a kinetically significant reaction intermediate.

In fact, other authors have expressed opposing views to the participation of ketene as a crucial reaction intermediate. They have offered convincing evidence that seems to demonstrate that ketene may be a side product formed in parallel to the

ketonization pathway rather than being a kinetically significant intermediate. Perhaps the strongest evidence against the ketene mechanism comes from the work of Ponec *et al.* [5] on a TiO_2 catalyst. They carried out reactions with mixtures of ^{13}C ($^{13}\text{C}=\text{O}$) labeled acetic acid and unlabeled pivalic acid, containing no α -hydrogen. As shown in Table 2, their results indicate that the cross ketonization product 2,2-dimethyl-3-butanone (pinacolone) does not contain any ^{13}C , which could only come from the ^{13}C -labeled acetic acid. At the same time, all of the side-product CO_2 was ^{13}C -labeled.

Table 2. Distribution of labeled and unlabeled ketones products in the reaction of $\text{CH}_3^{13}\text{COOH}$ and $(\text{CH}_3)_3\text{COOH}$ over TiO_2 catalyst at 350°C [5]

Reactants	Products	
	Labeled	Unlabeled
	 100%	 0%
	 + C^{13}O_2 0%	 + $^{13}\text{C}\text{O}_2$ 100%

This unambiguous outcome indicates that the carbonyl group remaining on the ketone product has originated from pivalic acid, while CO_2 was produced from acetic acid. However, without an α -hydrogen, pivalic acid cannot form a ketene, while only acetic acid can. This is a strong argument against the involvement of a ketene as an intermediate for ketonization. If acetic acid forms the ketene ($\text{CH}_2=\text{C}=\text{O}$), which serves as the carbonyl group in the cross ketonization product between acetic and

pivalic acid, it then could not generate CO₂. That is, the ketene might be a side product that is in equilibrium with the intermediate adsorbed species on the surface but not an intermediate directly linked to the ketonization reaction.

Similar conclusions can be drawn from a study reported by Martinez and Barteau [3]. They conducted the ketonization of various carboxylic acids at short contact times over titania-functionalized monoliths in the temperature range 533-680 K. Both, ketene and ketones were detected as products. However, the acetone selectivity of the bimolecular ketonization reaction on the titania-functionalized monolith was not affected when varying the conversion from 3-100%. The observed value of acetone carbon selectivity of approximately 75 % agrees with the values given by the stoichiometry of the ketonization reaction (3C: 1C in (CH₃)₂=CO: CO₂). If the reaction were sequential, one would expect to observe significantly lower selectivity at low conversions. These results provide another piece of evidence against the ketene-intermediate pathway and are consistent with previous surface science studies by Barteau's group [2], in which the formation of both ketene and acetone from surface acetates on TiO₂ were indicated as parallel, rather than sequential pathways. In those studies, temperature-programmed desorption (TPD) was employed to investigate carboxylic acid decomposition on single crystal TiO₂ (rutile). Acetate species were shown to be stable intermediates formed by carboxylic acid adsorption on the various TiO₂ surfaces investigated. It was shown that the surface carboxylates can decompose at high temperatures via two parallel pathways, depending on the surface structure and composition. The (011) faceted surface, containing fivefold O-coordinated Ti cations, was shown to decompose surface acetates exclusively via monomolecular dehydration

to ketenes. By contrast, the (114) faceted surface catalyzed the bimolecular ketonization to acetone. These contrasting results indicate that, at high acetate coverage and when adjacent sites are present, the α -hydrogen activation results in ketonization, while isolated acetate species dehydrate to ketene. Clearly, these are parallel, rather than sequential reactions.

B.2.1.2. β -ketoacid Intermediate

In addition to the crucial role of the α -hydrogen in the initial activation, another important component is the coupling of the two species on the surface, with the formation of an intermediate able to decompose with evolution of CO_2 and water. A species that fulfill these requirements is a β -ketoacid, which can be formed by coupling an enolate (enolized carboxylate) (alkyl fragment) and a carboxylate or an acylium (carbonyl or acyl fragment). These β -keto acids (or 3-oxocarboxylic acids) are organic compounds that contain a ketone group at the second carbon (or β position) from the carboxylic acid group.

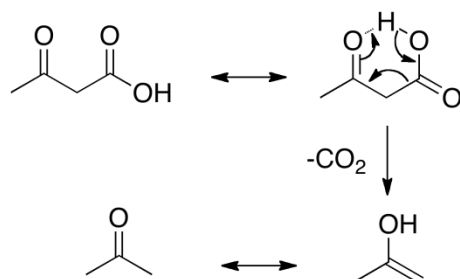


Figure 7. Decarboxylation mechanism of β -ketoacid

This type of compound can undergo decarboxylation to produce a ketone and CO_2 quite readily upon mild thermal treatment. It is generally accepted that the mechanism for decarboxylation of β -ketoacids involves redistribution of six electrons

in a six-membered cyclic transition state to give an enol that can be rapidly tautomerized to form the corresponding ketone, as shown in Figure 7. It is important to note that the easiness of decarboxylation is a unique characteristic of β -ketoacids [35].

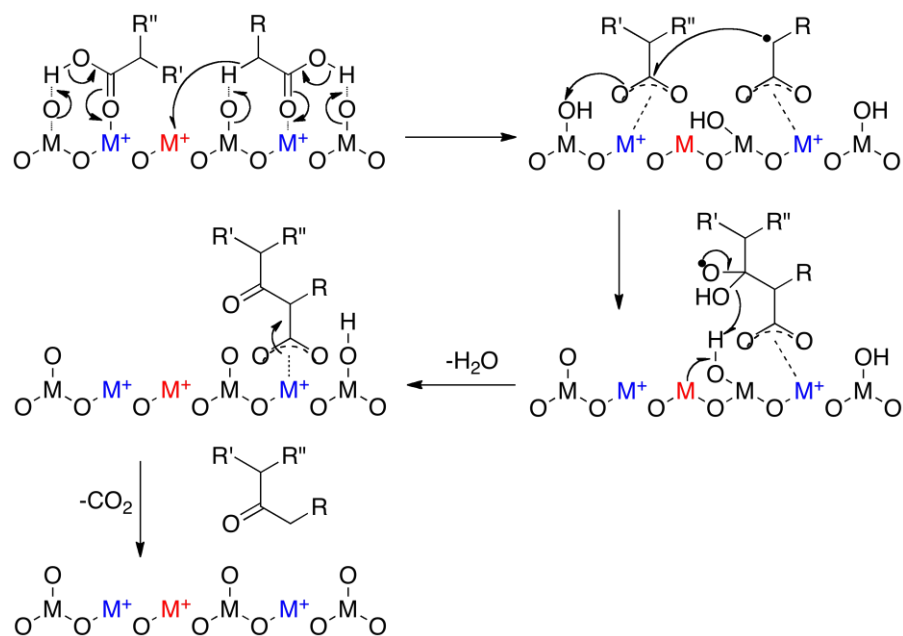


Figure 8. Proposed β - ketoacid based mechanism for vapor phase ketonization of carboxylic acid over $\text{CeO}_2\text{-Mn}_2\text{O}_3$ catalyst [28]

The participation of this intermediate in the mechanism is, in fact, in line with the original proposal of Neunhoeffer and Paschke [27] who recognized the role of a β -keto acid in the formation of cyclopentanone from adipic acid, as already shown in Figure 3 above. Of course, in that case, it was a monomolecular step, while in the case of acetic acid ketonization, it necessarily implies the participation of two adsorbed molecules. There have been a number of studies that support the path involving a β -ketoacid as an intermediate in the ketonization reaction, even though a β -ketoacid has never been detected during ketonization. The rapid decomposition mentioned above makes the detection practically impossible. Among the various studies proposing β -

ketoacid-mediated mechanisms, the one by Nagashima *et al.* [28] is illustrated in Figure 8.

As mentioned above, the formation of surface carboxylates is the first step. Subsequent abstraction of an α -hydrogen atom from the carboxylate results in an anionic radical that attacks another carboxylate and forms the β -ketoacid intermediate, which, as mentioned above, can readily decarboxylate to form the ketone product. This mechanism involves consecutive reduction-oxidation cycles of the catalyst, a process for which redox oxides such as CeO_2 are particularly effective.

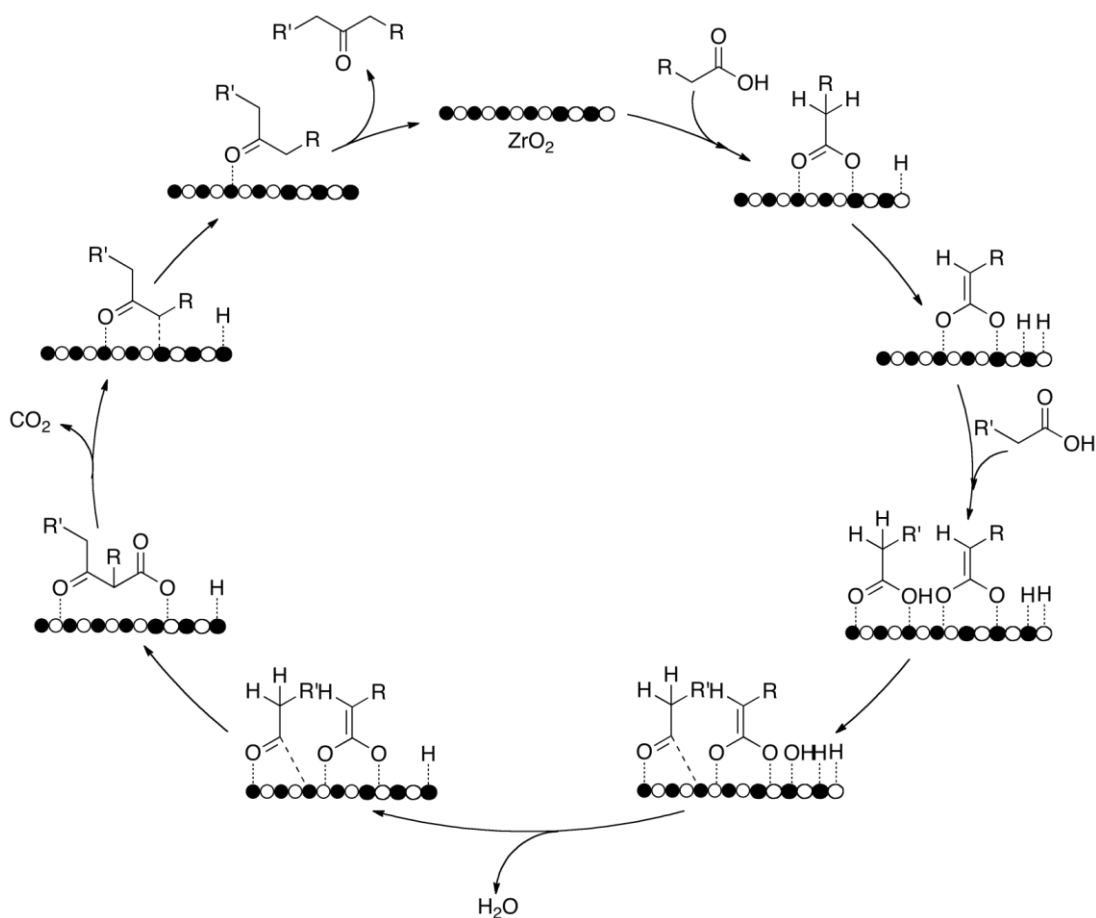


Figure 9. Proposed mechanism for carboxylic acid ketonization over ZrO_2 catalyst via β -ketoacid formed by an acyl and an enolized carboxylate on the surface [29]

In the mechanism described above, the β -ketoacid is proposed to be formed from two adjacent surface carboxylates. An alternative path has been suggested by Renz. *et al.* [29] and Ignatchenko *et al.* [36] who propose that the β -ketoacid results from the coupling of a surface enolate with an acylium ion. The former species is formed by typical deprotonation and α -hydrogen abstraction of a carboxylic acid while the latter is formed by dissociation of OH on the surface, as proposed by Kuriacose *et al.* [66,23]. The mechanistic pathway put forward by Renz *et al.* is summarized in Figure 9. However, on reducible oxides it is hard to differentiate between an acyl and a carboxylate since an acyl can be converted to a carboxylate by nucleophilic addition of lattice oxygen. In fact, surface science studies of carboxylic acids on reducible oxides have only given evidence for the presence of carboxylate species [45,55].

The energy barriers calculated in the DFT study of Pulido *et al.* [29] show that the ketonization via the β -ketoacid route would require a much lower activation energy (108 kJ/mol) than the direct concerted pathway (154 kJ/mol), which is in agreement with the experimental results described above. Unfortunately, the calculations become less convincing when they indicate that the β -ketoacid decarboxylation step that forms the ketone and CO₂ is rate limiting. It is well-known that this step is relatively easy and may occur by simple thermal heating, which makes it unlikely as a rate limiting step.

B.2.1.3. Other Mechanisms

Other mechanisms have also been suggested for the ketonization of carboxylic acids. From their detailed isotopic labeling investigations, Ponc *et al.* [6] concluded that an α -hydrogen is necessary for the ketonization reaction to proceed and that the

rate determinant intermediate is in equilibrium with the ketene. They arrived at this conclusion after inferring that the ketene is not kinetically significant, but its concentration followed very closely the inverse of acetone concentration. The proposed mechanism is displayed in Figure 10.

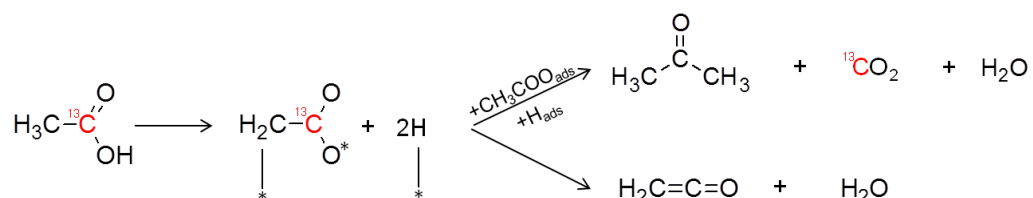


Figure 10. Proposed mechanism for ketonization of carboxylic acid over TiO_2 catalyst by Ponec *et al.* [6]

In this mechanism, after the initial adsorption of a ^{13}C -labeled acid molecule that forms a surface carboxylate, a second hydrogen abstraction occurs, leading to a multiply bonded surface intermediate that ends up parallel to the surface. This configuration allows for the dissociation of the $C-^{13}C$ bond to form a methylene species. This adsorbed species is suggested to be in equilibrium with the gaseous ketene. In this proposal, the methylene species is the crucial intermediate that reacts with a carboxylate in the immediate vicinity to form the ketone product. This mechanism, however, has been questioned by Nagashima *et al.* [28]. They argue that if such methylene species were present during the reaction, methanol should have been produced in measurable amounts by interaction with water, which is present under the ketonization reaction conditions. This is a valid argument against this mechanism.

Bamberger [37] suggested the formation of intermediate acid anhydrides, which decarboxylate to give a ketone. This was based on the observation that over MnO_2 , carboxylic acids yielded both acid anhydrides and ketones. In line with the

ketene mechanism, acid anhydride may be formed by the reaction of a ketene and another carboxylic acid. However, it is still unclear that the decomposition of acid anhydride yields a ketone and CO₂. As ketonization is often observed along with decarbonylation/decarboxylation, one may expect that a similar mechanism may well lead to the formation of ketone. For example, over a Pd catalyst [38], it was proposed that an acid anhydride complex decomposed to acyl and a carboxylic acid as shown in Figure 11.

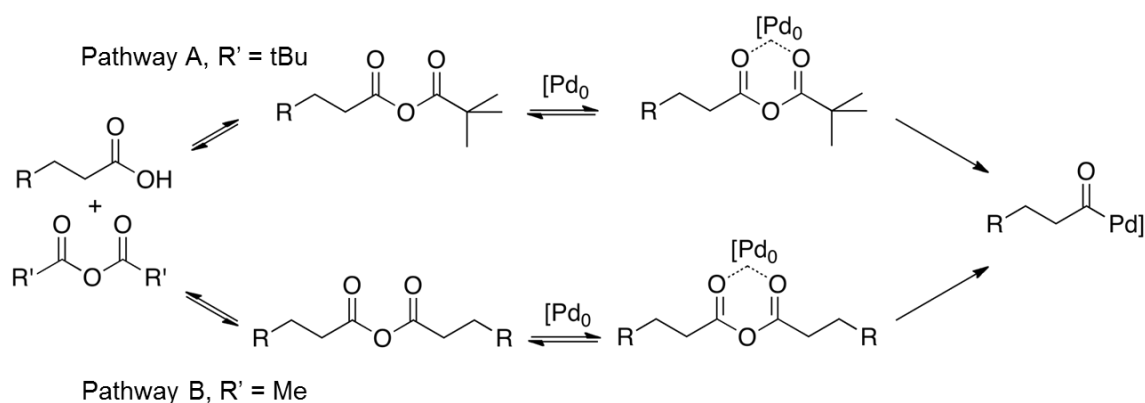


Figure 11. Proposed decomposition pathways of acid anhydride [38]

The decarbonylation of the acyl complex results in a surface alkyl with a redox cycle of Pd²⁺ and Pd⁰. In this case, the alkyl on the surface dehydrogenates to an alkene while water is formed as side product. However, such surface alkyl species may also react with adjacent acyl species to form a ketone. Alternatively, the decomposition of such acid anhydride complex in a redox cycle may lead to coupling of the acyl-M-R complex as shown in Figure 12.

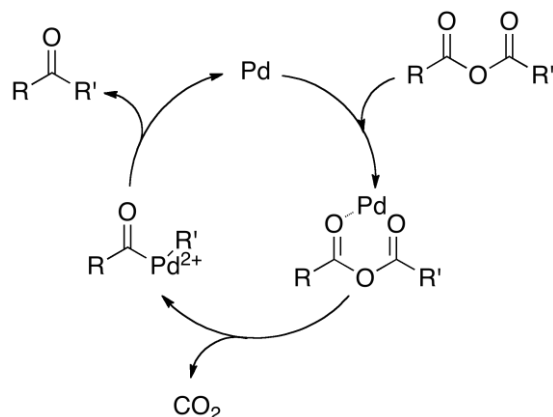


Figure 12. Possible ketone formation mechanism from acid anhydride

B.2.2. Ketonization Catalysts

Over the last thirty years, a large number of metal oxide catalysts have been found to be active for the ketonization of carboxylic acids. Many studies on different types of catalysts have been devoted to find answers to fundamental questions related to the nature of the active sites and structure of the kinetically significant intermediates on the different catalysts. Various techniques and approaches have been employed towards this goal.

A variety of basic, acidic, and amphoteric oxide catalysts have been investigated in the literature for ketonization of different carboxylic acids under various reaction conditions. Glinski *et al.* [39] demonstrated that ketonization can be catalyzed by many different oxides. To show this, they carried out ketonization on twenty different metal oxides supported on silica. The results are listed in Table 3. One can see that amphoteric oxides (CeO_2 , MnO_2 , La_2O_3) appear to be better catalysts than pure acidic or basic oxides. Subsequent investigations [2-13,40,41] have led to the same conclusion. That is, amphoteric reducible oxides possess good ketonization activity and selectivity.

Table 3. Activity of 10 wt% MO_x/SiO_2 catalysts in ketonization of acetic acid [39]

Catalyst	Yield of acetone	
	648K	673K
B_2O_3	2	3
MoO_3	4	5
WO_3	6	5
P_2O_5	10	12
V_2O_5	9	21
Bi_2O_3	11	18
NiO	31	-
Al_2O_3	15	37
CuO	29	39
ZnO	19	33
PbO	36	76
Cr_2O_3	48	39
Fe_2O_3	66	59
CoO	50	63
MgO	53	59
Nd_2O_3	22	61
La_2O_3	50	87
MnO_2	72	96
CdO	76	94
CeO_2	96	97

A generalized description of the adsorption behavior of carboxylic acids on typical amphoteric metal oxides can be derived from surface science studies. As reviewed in the following section, these studies reveal the nature of the key properties that determine ketonization activity, in good agreement with the proposed reaction mechanisms described above. Therefore, an effective oxide catalyst for surface ketonization should be able to dissociatively adsorb the carboxylic acid forming surface carboxylates and have adjacent coordinately unsaturated cation sites to allow the adsorbate-adsorbate interaction that leads to the formation of the crucial

intermediate. Some authors have described this behavior in terms of acid-base or redox properties, as summarized below. However, these are different manifestations of the same fundamental phenomena.

B.2.2.1. Interaction of Carboxylic Acids with Oxide Surfaces

The adsorption geometry and chemistry of carboxylic acids, including formic acid, acetic acid, propanoic acid and higher carboxylic acids on various metal oxides have been thoroughly investigated both, theoretically and experimentally. Investigations on the amphoteric oxides TiO_2 and CeO_2 will be specifically discussed as case studies. The adsorption of carboxylic acids on anatase and rutile TiO_2 has been thoroughly investigated for years, particularly on the most stable planes, i.e., (110) rutile and (101) anatase. Several excellent reviews on the surface science of TiO_2 single crystals have been written by Diebold [42,43] and Barteau *et al.* [44,45]. Carboxylic acids adsorb dissociatively on both surfaces, producing surface carboxylates (RCOO^-) and hydroxyl groups (OH^-) associated to surface cations [46-50]. One can visualize this as a simple proton abstraction of a carboxylic acid by a basic oxygen on the metal oxide surface. Several studies calculated energies for dissociative and non-dissociative adsorption modes of various carboxylic acids. The results of these investigations clearly indicated that dissociative adsorption is more energetically favorable. The carboxylates (RCOO^-) can bind by one or two oxygen atoms binding to the metal cations with three possible coordination structures, namely monodentate, bridging, and chelating bidentate, as shown in Figure 13.

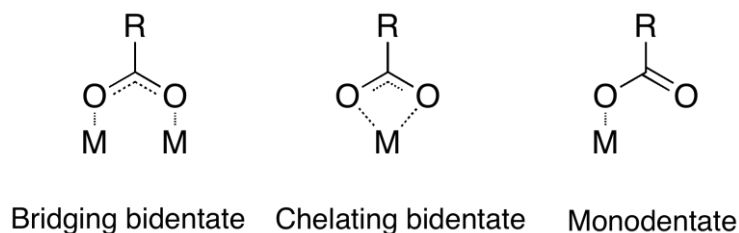


Figure 13. Different adsorption configuration of carboxylates on catalyst surfaces

It is widely established that the most stable carboxylates bind to two surface cations in a bridging bidentate configuration [51], as evidenced by scanning tunneling microscopy [52], FTIR, X-ray photoelectron diffraction [53] as well as by *ab initio* slab and cluster calculations [54]. However, if there exists an oxygen vacancy on the surface, an alternative geometry involving the filling of an oxygen vacancy site by one of the carboxyl oxygen atoms with the other bound to a Ti atom has also been observed. A near edge absorption fine structure spectroscopy (NEXAFS) study of formate, acetate and propionate supported the existence of minority adsorption sites involving oxygen vacancies [48].

Numerous efforts have been aimed at understanding the participation of the adsorbed carboxylates in the catalytic reaction. For example, Pei and Ponec [55] examined the adsorption and surface reaction of acetic acid on TiO₂ using FT-IR. When acetic acid was dosed at room temperature, new strong bands appeared associated with carboxylates in monodentate and bidentate configurations. However, upon heating to 100-300°C, the monodentate band gradually disappeared, leaving only the bands associated to strongly bound bidentate carboxylates. Since only bidentate carboxylates can be observed at 300°C, which is a typical temperature for ketonization activity in a vapor phase flow reactor, these studies suggest that bidentates are species of crucial importance in the catalytic process.

In a surface science study, Kim and Barteau [2] used TPD to explore the decomposition pathway of surface acetates on single crystals at high temperatures. On the TiO_2 (114) plane, where two acetates are bound to the same Ti, acetone evolved at 580 K as a product of ketonization. An equivalent result was observed for propanoic acid, which produced pentanone. However, on the TiO_2 (011) plane, which can only bind one acetate group per Ti center, monomolecular dehydration to ketene was the major pathway. It is noteworthy that in contrast to the well-known bidentate adsorption configuration observed in FT-IR investigation by Pei and Ponec [55], the two acetate species involved in ketonization should be monodentate coordinated to the same Ti on the (114) rutile surface. This suggests the possibility that carboxylate species can bind with metal cations in a number of different conformations during the course of ketonization. The change in binding type might play an important role in determining the ease at which the transition state is formed. For instance, the bidentate, as the most stable adsorbed species, could form initially on the surface. However, during the catalytic cycle this species could undergo a transformation to the less restricted adsorption configuration such as monodentate that can readily undergo the attack from another species to form the ketone with a lower energy barrier.

These results provide strong support for the participation of carboxylates rather than ketene species in the ketonization reaction. In addition, it also sheds some light on the site requirements of metal oxides for ketonization activity. The authors concluded that for ketonization to occur, a surface containing doubly-unsaturated cations must be present [2]. These single crystal studies have helped to identify as an important requirement the creation of coordinatively unsaturated vacancies on the catalyst

surface. While this study indicates that the cations need to retain their 4+ oxidation state, one might anticipate that reduction could be a way to create such coordinatively unsaturated sites on high surface area powder catalysts and thus improve catalytic activity.

Studies of the interaction of carboxylic acids with CeO₂ allow drawing some conclusions about the similarities and differences with those observed with TiO₂. For example, the reaction of acetic acid on the CeO₂ surface has been investigated by employing FT-IR. Zaki *et al.* [56] showed that the adsorption behavior of acetic acid on CeO₂ is essentially similar to the adsorption on TiO₂. Specifically, adsorption bands due to bidentate acetate surface species appeared over the full range of scanned temperature of 200-400°C and a strong shoulder was observed above 300°C, suggesting the occurrence of acetone condensation into mesityl oxide surface species. In another study, Stubenrauch *et al.* [57] studied the adsorption and reaction of acetic acid on CeO₂ (111) and (100) single crystal faces using TPD and HREELS techniques. Dissociation (deprotonation) of the acid and formation of surface carboxylates was observed on both surfaces, similar to the situation observed with TiO₂. However, the specific morphology of the adsorbate on CeO₂ and its relationship with the surface topology are less clearly understood than in the case of TiO₂. During the heating ramp, the acetates were found to decompose and form ketene and acetone on CeO₂ (111), while only ketene was observed on CeO₂ (100) [57].

In summary, adsorption of carboxylic acids gives rise to similar carboxylate species on different oxide surfaces. Upon increasing the temperature, conversion of the adsorbed carboxylate to ketones occurs on certain surfaces, which is entirely consistent

with the picture of a bidentate carboxylate as an initial reaction intermediate. More importantly, the surface science studies are useful in providing concrete insight concerning the nature of the surface properties that dictate the ketonization reaction. Two important requirements for ketonization active sites are: (i) coordinatively unsaturated surface metal cations/oxygen anions for the initial deprotonation of carboxylic acids. (ii) surface cation sites that can bind multiple carboxylates or pairs of adjacent exposed cations for coupling pairs of carboxylates to produce ketones. These surface coordination features, from a catalytic chemistry perspective, are viewed and discussed in terms of acid-base and/or redox properties, as illustrated by the following examples.

B.2.2.2. Acid-base Properties

Amphoteric reducible metal oxides, such as CeO₂, TiO₂ and ZrO₂, have been reported to be the most active catalysts for ketonization. Therefore, acid-base properties, or exposed surface cations/anions with coordination vacancies have been proposed to play a crucial role in their superior ketonization activity. Different characterization techniques including TPD of CO₂ and NH₃ and FTIR of adsorbed acetone/pyridine [58,59] demonstrate the amphoteric character of CeO₂, TiO₂ and ZrO₂. Adsorption of a basic molecule, such as pyridine, shows evidence of Lewis acid sites on three types of oxides. Based on the frequency of pyridine coordinated to Lewis acid sites, the Lewis acid strength of the various metal oxides follows the order TiO₂ > ZrO₂ > CeO₂ [58,60]. On the basis of CO₂ adsorption studies, Martin and Duprez [61] compared the density of basic sites on several oxides and concluded that CeO₂ possesses the highest basic site density (3.23 μmol CO₂ m⁻²), followed by MgO (1.77

$\mu\text{mol CO}_2 \text{ m}^{-2}$), and ZrO_2 ($1.45 \mu\text{mol CO}_2 \text{ m}^{-2}$). However, in terms of strength, CeO_2 and ZrO_2 both have weaker basic sites than MgO . By contrast, while CO_2 adsorbs on TiO_2 , it desorbs upon evacuation at room temperature, indicating a much weaker basicity than that of ZrO_2 and CeO_2 [62]. It is important to note here that CO_2 in the presence of reducible oxides may adsorb in defects on the catalyst surface, and may not be an accurate representation of the number or strength of basic sites.

Exposed metal cations generally act as Lewis acid sites while oxygen anions are Lewis base sites. However, the coordination of oxo oxygen (e.g., ketones, carboxylic groups) to oxophilic coordinatively unsaturated cations or oxygen vacancies is not necessarily due to the acidity of the site. At the same time, for the formation of surface carboxylates discussed above, the oxygen anions must act as Brønsted basic sites rather than Lewis basic sites. Therefore, the ketonization activity of amphoteric oxide catalysts may not necessarily relate to their acid/base character.

As mentioned above, there is ample experimental evidence that links the observed ketonization activity with the presence of surface acid and base sites or, in light of our ongoing discussion, of exposed coordinatively unsaturated metal cations and oxygen anions. At the same time, since CO_2 and acetone have affinity for surface Lewis base and acid sites, they are expected to act as inhibitors of the ketonization reaction as they compete with acid molecules for the coordination sites, i.e. exposed cations and anions [63]. In fact, this inhibition has been verified experimentally [64]. It is worth noting here that the extent of CO_2 adsorption is not only a measurement of Lewis basicity, but also the density uncoordinated cations, which are more relevant for formation of surface carboxylates.

Gaertner *et al.* [65] studied the conversion of hexanoic acid over ceria-zirconia and reported that the catalytic activity decreased to approximately 30 % of its initial value when co-feeding CO₂. More importantly, activity was not regained after the CO₂ flow was stopped. This result not only demonstrates the competitive adsorption of CO₂ with the carboxylic acids, but also an irreversible loss of active sites by permanent coordination of CO₂ to the exposed cations (or oxygen vacancies). At the same time, inhibition by acetone has been observed on Zr-Cr-Fe mixed oxides [66]. Acetone significantly suppressed the reaction rate of acetic acid, suggesting the blocking of required exposed cations for the reaction. In another study, the inhibition of dehydration and dehydrogenation rates of isopropyl alcohol and cyclohexanol by the presence of acetic and propanoic acids has been quantified [67]. It was reported that acetic and propanoic acids suppressed both dehydration and dehydrogenation rates, which take place on acid and base sites of metal oxides, respectively [68,69]. A correlation between ketonization rates and the extent to which they suppress the dehydration and dehydrogenation was established. These results suggest that carboxylic acids utilize both dehydration and dehydrogenation sites, implying the involvement of both acid and base sites for ketonization.

B.2.2.3. Redox Properties

Together with acid-base properties, the redox capacity of the solid (i.e. how easily coordination vacancies can be formed) has been linked to its ketonization activity, especially in the case of CeO₂ [4,9].

The exceptional redox properties of CeO₂ are well known for its application in automotive catalytic converters, since this oxide is able to undergo fast and deep

reduction/oxidation cycles (i.e., $\text{CeO}_2 \leftrightarrow \text{CeO}_{2-x} + \text{O}_x$). Therefore, it effectively stores and releases oxygen during the fuel-lean (excess O_2) and fuel-rich phases (no O_2), respectively [70]. In reference to ketonization, Nagashima *et al.* [28] proposed that the surface oxide may be reduced by α -hydrogen abstracted from the feed and reoxidized through the combination of its proton and hydroxyl group from the acid to form water as seen in Figure 7. In this sense, the redox cycle was considered key in maintaining the ketonization activity. While the bulk redox ability of ZrO_2 and TiO_2 is much lower than that of CeO_2 [71,72], they are still able to form oxygen vacancies and exposed surface cations with a high degree of unsaturation. Therefore, their ketonization activity may be more closely related to the capacity to form these sites than the bulk reducibility.

B.2.2.4. Effect of Dopants and Catalyst Pretreatments

The enhancement of ketonization activity by the addition of dopants such as transition metals and metal oxides and by pre-reduction treatments has been a matter of interest in various investigations. Doping or pre-reduction of the catalyst can presumably affect the density of several of the potential characteristics that can be linked to ketonization activity:

- a) oxygen vacancies,
- b) coordinatively unsaturated cations,
- c) acid sites
- d) basic sites
- e) redox properties.

These studies have shed some more light on our understanding of surface active sites for ketonization. Glinski *et al.* [39] examined the effects of oxide supports, including SiO₂, TiO₂, and Al₂O₃ on the ketonization activity of MnO₂ and CeO₂. The authors observed a significant enhancement in catalytic activity without a change in selectivity over MnO₂ and CeO₂ deposited on Al₂O₃ and TiO₂ supports in comparison with those on SiO₂ supports, despite their lower surface areas. It is reasonable to associate the observed changes in catalytic activity to the incorporation of the acidic function of the support to basic sites of the supported oxides at the interface. Teterycz *et al.* [73] in their study of conversion of *n*-butanol have observed significant changes in selectivity of the products upon the addition of MgO to ZrO₂. The selectivity toward *n*-butene and butyraldehyde was found to decrease whereas that of dipropylketone increased. The authors proposed that butyraldehyde was oxidized to butyric acid by picking up a lattice oxygen. The acid in turn would undergo ketonization to yield the observed ketone. The ease of oxygen vacancies formation on the mixed oxide surface was suggested to promote formation of the acid and its conversion to ketone.

The addition of ZrO₂ to CeO₂ to produce mixed oxides has also been found to enhance the ketonization activity. Several explanations have been proposed in the literature. The addition of ZrO₂ leads to the formation of a highly defective surface, higher Lewis acid content and oxygen vacancies, indicated by X-ray photoelectron spectroscopy characterization. As a result, ketonization activity of CeZrO₂ has been found to be higher than that of pure CeO₂. On the other hand, the addition of ZrO₂ leads to a reduction of the bulk oxide at lower temperatures. The reduction temperature of the mixed oxide was found to be at 250°C, as compared to 500°C for CeO₂. This

phenomenon results in a great enhancement of the redox properties of the mixed oxides, or as discussed above, a higher density of uncoordinated cations. As a result, the CeZrO_2 obtained improved oxidation-reduction cycling through high temperature reduction and a subsequent oxidation while pure CeO_2 's redox abilities were significantly hindered [74].

In addition to ZrO_2 , other dopants have been investigated and found to promote ketonization activity. For example, a mixed $\text{CeO}_2\text{-Al}_2\text{O}_3$ catalyst was found to have similar redox properties to the mixed CeZrO_2 catalysts in the sense that the bulk CeO_2 was more easily reduced when supported on alumina [75]. In addition, the catalytic activity of $\text{CeO}_2\text{-Al}_2\text{O}_3$ and $\text{CeO}_2\text{-TiO}_2$ for ketonization was studied as a function of time on stream and number of regeneration cycles. It was reported that the catalyst performance of $\text{CeO}_2\text{-Al}_2\text{O}_3$ and $\text{CeO}_2\text{-TiO}_2$ improved with time on stream during the first 2-5 regeneration cycles. This activity enhancement was attributed to a higher dispersion of CeO_2 facilitated by consecutive reduction/oxidation cycles inherent to the reaction, causing gradual dispersion on the support [8].

Likewise, addition of transition metals to CeO_2 also causes significant improvement in ketonization activity. For example, Dooley *et al.* [9] studied the effects of adding Co and Pd to alumina-supported CeO_2 particles in the vapor phase ketonization of isobutyric, acetic, and decanoic acids. Both the Pd- and Co- $\text{CeO}_2/\text{Al}_2\text{O}_3$ catalysts were shown to be more active for ketonization, as compared to the $\text{CeO}_2/\text{Al}_2\text{O}_3$ catalyst under the same conditions. XANES and EXAFS characterization showed a significant enhancement in the number of oxygen vacancies

around each Ce atom upon the incorporation of small amounts of Pd and Co (both at 0.8%) when compared to the base CeO₂/Al₂O₃ catalyst.

The addition of alkali and alkali earth metals as promoters of metal oxide catalysts has been explored as well. In a study conducted by Parida [76], all the alkali metals (Na, K, Cs) except Li were found to increase the ketonization activity of ZrO₂ at 623-698K. A decrease in activity in the case of the Li-doped sample may have been due to the drastic decrease in surface area observed on this catalyst. Among all tested alkali metals, Na was the most effective for ketonization, followed by K and Cs. A 5 mol% Na doped ZrO₂ catalyst reached 99% conversion with 94% selectivity toward acetone at 623K and a gas hourly space velocity (GHSV) of 160 ml g⁻¹min⁻¹. The authors claimed that Na favors the formation of surface carbonates and stabilizes the tetragonal phase of ZrO₂, resulting in the observed increase in ketonization activity. With respect to the requirement for acid-base properties mentioned earlier, the addition of alkali would incorporate a basic center to accompany the acidic ZrO₂. In contrast, it has been found that doping of alkali on CeO₂ catalysts only promotes the formation of heavy products by aldol/Michael condensations of the ketones produced. The excessive number of basic sites on the alkali-doped surface appears to be the main reason.

Direct H₂ reduction is another method that has been employed to improve ketonization activity. Zaytseva *et al.* [77] showed that ketonization of valeric acid gave higher conversion and comparable selectivity over CeO₂, ZrO₂ and CeO₂/ZrO₂ at 628K in a H₂ environment, as compared to runs in inert gas. The increased amount of coordinatively unsaturated Lewis acid sites under H₂ flow, as observed in X-ray

photoelectron spectroscopy analysis, was suggested to be responsible for the change in catalytic activity. The importance of surface reduction is not only limited to ketonization reactions. For example, Calaza *et al.* [78] examined adsorption and enolization of acetaldehyde for the aldol condensation reaction on a fully oxidized and a highly reduced thin film CeO₂ (111) by employing a combination of reflection absorption infrared spectroscopy and periodic density functional theory calculations. The mechanism of aldol condensation shares several mechanistic steps with ketonization. For instance, they both need an α -hydrogen to form an enolate that acts as a nucleophile to attack the electrophilic acyl C of another aldehyde. Acetaldehyde predominantly adsorbs weakly through its carbonyl oxygen on top of a Ce⁴⁺ cation on the fully oxidized CeO₂ (111) surface without any coupling reaction. The adsorption energy of this state was calculated to be weak, -0.21 and -0.09 eV at 1/4 and 1/2 monolayer coverage, respectively. The lack of reaction on the fully oxidized CeO₂ surface suggests that lattice Ce⁴⁺ cations evidently cannot stabilize the carbonyl O and form a stable electrophilic carbonyl C to be attacked by an enolate species. On the reduced surface containing about 60% Ce³⁺, the carbonyl group is indicated to be strongly stabilized on coordinatively unsaturated Ce³⁺ sites (oxygen vacancies), resulting in stronger adsorption of acetaldehyde. This stable adsorption enables the formation of a strong electrophilic center on acyl C, thus enabling the coupling reaction.

Based on all these studies, it is reasonable to suggest that the presence of adjacent Lewis acid and Brønsted basic sites is the key for ketonization on most oxides. The coordination of primary intermediate species, adsorbed carboxylates,

produced by dissociative adsorption of carboxylic requires the availability of Brønsted basic sites on the surface. More importantly, basic sites are required to perform α -hydrogen abstraction or keto/enol tautomerization to generate the enolate species with a nucleophile center at an α -carbon. An adjacent Lewis acid (or coordinatively unsaturated cation site) is needed to stabilize and activate another carboxylic acid for the coupling reaction. At the same time, the bulk redox ability of the oxide may also correlate well with the ketonization activity since the redox properties are strongly linked to the acid-base properties of the solid and the ability to expose surface cations.

References

- [1] C. Ann. Friedel, 108 (1858) 125
- [2] K.S. Kim, M. A. Barteau, J. Catal. 125 (1990) 353
- [3] R. Martinez, M.C. Huff, M.A. Barteau, J. Catal. 222 (2004) 404
- [4] R. Pestman, R.M. Koster, A. van Duijne, J.A.Z. Pieterse, V. Ponec, J. Catal. 168 (1997) 265
- [5] R. Pestman, R.M. Koster, J. A. Z Pieterse, V. Ponec, J. Catal 168 (1997) 255
- [6] R. Pestman, R.M. Koster, J. A. Z Pieterse, V. Ponec, J. Mol. Catal. A 103 (1995) 175.
- [7] C. Doornkamp, V. Ponec, J. Mol. Catal. A. 162 (2000) 19
- [8] S.D. Randery, J.S Warren, K.M. Dooley, Appl. Catal. A 226 (2002)265
- [9] K.M. Dooley, A. K. Bhat, C. P. Plaisance, A. D. Roy, Appl. Catal. A 320 (2007) 122
- [10] R.W. Snell, B.H. Shanks, ACS Catal. 2013, 3, 783
- [11] R.W. Snell, B.H. Shanks, Appl. Catal. A : General 2013, 451, 86
- [12] T.N. Pham, D. Shi, T. Sooknoi, D.E. Resasco, J. Catal. 2012, 295, 169
- [13] C. A. Gaertner, J. C. Serrano-Ruiz, D. J. Braden, J. A. Dumesic, Ind. Eng. Chem. Res. 49 (2010) 6027
- [14] E. Karimi, A. Gomez, S. W. Kycia, M. Schlaf, Energy Fuels. 24 (2010) 2747
- [15] J.A. Martens, M. Wydoodt, P. Espeel, P.A. Jacobs, Stud. Surf. Sci. Catal. 78 (1993) 527
- [16] M.A. Alotaibi, E.F. Kozhevnikova, I.V. Kozhevnikov, Appl. Catal. A 447 (2012) 32

-
- [17] S. Sifniades, A. B. Levy, "Acetone" in Ullmann's Encyclopedia of Industrial Chemistry, (2005), Wiley-VCH, Weinheim,.
- [18] M. Weber, M. Kleine-Boymann, "Phenol" in Ullmann's Encyclopedia of Industrial Chemistry (2004) Wiley-VCH.
- [19] V.I. Yakerson, L.I. Lafer, A.L. Klyachko-Gurvich, A.M. Rubinshtein, Bull. Acad. Sci. of the USSR. 15 (1966) 65
- [20] V.I. Yakerson, English version is translated from Izvestiya Akademi Nauk SSSR 6 (1963) 1003
- [21] Y. Yamada, M. Segawa, F. Sato, T. Kojoma, S. Sato, J.Mol. Catal. A: Chem 346 (2011) 79
- [22] R. Pestman. Ph.D Dissertation, (1995) Leiden University.
- [23] J.C. Kuriacose, S.S. Jewur, J. Catal. 50 (1977) 330
- [24] R.A. Hites, K. Biemann, J. Am.Chem.Soc. 94 (1972) 5772
- [25] Y. Sakata, C.A. van Tol-Koutstaal, V. Ponec, J. Catal. 169 (1997) 13
- [26] J.E. McMurry, Fundamentals of Organic Chemistry. (2010) 7th edition, Cengage Learning Publisher.
- [27] O. Neunhoeffer, P. Paschke, Chem. Ber. 72B (1939) 919
- [28] O. Nagashima, S. Sato, R. Takahashi, T. Sodesawa, J. Mol. Catal A: Chemical. 227 (2005) 231
- [29] A. Pulido B. Oliver-Tomas, M. Renz, M. Boronat, A. Corma, ChemsusChem. 6 (2013) 141
- [30] M. Jayamani, C.N. Pillai, J. Catal. 87 (1984) 93

-
- [31] F. González, G. Munuera, J. Prieto, *J. Chem. Soc., Faraday Trans.* 74 (1978) 1517
- [32] A.V. Ignatchenko, *J. Phys. Chem C* 115 (2012) 16012
- [33] H. Staudinger, *Ber. Chem. Gesell.* 38 (1905) 1735
- [34] T.S. Hendren, K.M. Dooley, *Catal. Today*, 85 (2003) 333
- [35] F.A. Bettelheim, Brown, W.H.; Campbell, M.K.; Farrell, S.O. Book "Introduction to General, Organic and Biochemistry", 9th edition, (2010)
- [36] A. Ignatchenko, E. Kozliak, *ACS Catal.* 2 (2012) 1555
- [37] Bamberger, *Chem. Ber.*, 43 (1910) 3917
- [38] J. L. Notre, E. L. Scott, M. C. R. Franssen, J. P. M. Sanders, *Tetrahedron Lett.* 51 (2010) 3712
- [39] J. Kijenski, M. Glinski, A. Jakubowski, *Appl. Catal. A: General.* 128 (1995) 209
- [40] K. Parida, A. Samal, N.N. Das, *Appl. Catal. A*, 166 (1998) 201
- [41] A.D. Murkute, J.E. Jackson, D.J. Miller, *J. Catal.* 278 (2011) 189
- [42] U. Diebold, *Surf. Sci. Rep.* 48 (2003) 53
- [43] U. Diebold, *Appl. Phys. A* 76 (2003) 681
- [44] H. Idriss, M.A. Barteau, *Adv. Catal.* 45 (2000) 261
- [45] H. Idriss, K. S. Kim, M. A. Barteau, *Stud. Surf. Sci. Catal* 64 (1991) 327
- [46] A.G. Thomas, K.L. Syres, *Chem. Soc. Rev.* 41 (2012) 4207
- [47] C.L. Pang, R. Lindsay, G. Thornton, *Chem. Soc. Rev.* 37 (2008) 2338
- [48] A. Gutierrez-Sosa, P. Martinez-Escolano, H. Raza, R. Lindsay, P.L. Wincott, G. Thornton, *Surf. Sci.* 471 (2001) 163

-
- [49] I.D. Cocks, Q. Guo, R. Patel, E.M. Williams, E. Roman, J.L. de Segovia, *Surf. Sci.* 377 (1997) 135
- [50] H. Onishi, T. Arugawa, Y. Iwasawa, *Surf. Sci.* 193 (1988) 33
- [51] C. Martin, V. Rives, *J. Mol. Catal.* 73 (1992) 51
- [52] K. Fukui, H. Onishi, Y. Iwasawa, *Chem. Phys. Lett.* (1997) 280
- [53] S. A. Chambers, S. Tevuthasan, Y. J. Kim, G. S. Herman, Z. Wang, E. Tober, R. Ynzunza, J. Morais, C. H. F. Peden, K. Ferris, C. S. Fadley, *Chem. Phys. Lett.* 267 (1997) 51
- [54] S. P. Bates, G. Kresse, M. J. Gillan, *Surf. Sci.* 409 (1998) 336
- [55] Z-F. Pei, V. Ponc, *Appl. Surf. Sci.* 103 (1996) 171
- [56] M.A. Hasan, M.I. Zaki, L. Pasupulety, *Appl. Cat. A* 243 (2003) 81
- [57] J. Stubenrauch, E. Broscha, J.M. Vohs, *Catal. Today.* 28 (1996) 431
- [58] M.I. Zaki, M.A. Hasan, L. Pasupulety, *Langmuir* 17 (2001) 768
- [59] M.I. Zaki, M.A. Hasan, F.A. Al-Sagheer, L. Pasupulety, *Colloid. Surf. A* 190 (2001) 261
- [60] C. Binet, M. Daturi, J.-C. Lavalley, *Catal. Today* 50 (1999) 207
- [61] D. Martin, D. Duprez, *J. Mol. Catal. A: Chemical.* 118 (1997) 113
- [62] K. I. Hadjiivanov, D.G. Klissurski, *Chem. Soc. Rev.* 25 (1996) 61
- [63] J.A. Lercher, C. Grundling, G. Eder-Mirth, *Catal. Today* 27 (1996) 353
- [64] T.N. Pham, D. Shi, D.E. Resasco, *Top. Catal.* 57 (2014) 706
- [65] C. A. Gaertner, J. C. Serrano-Ruiz, D. J. Braden, J. A. Dumesic, *J. Catal.* 266 (2009) 71
- [66] S. Rajadurai, J.C. Kuriacose, *Mater. Chem. Phys.* 16 (1986) 17.

-
- [67] J.C. Kuriacose, R. Swaminathan, *J. Catal.* 14 (1969) 348
- [68] E. Iglesia, D.G. Barton, J.A. Biscardi, M.J.L. Gines, S. L. Soled, *Catal. Today* 38 (1997) 339
- [69] H. Noller, J.A. Lercher, H. Vinek, *Mater. Chem. Phys.* 18 (1988) 577
- [70] L. Vivier, D. Duprez, *ChemSusChem.* 3 (2010) 654
- [71] T. Yamaguchi, *Catal. Today* 20 (1994) 199
- [72] D. Martin, D. Duprez, *J. Phys. Chem.* 100 (1996) 9429
- [73] H. Teterycz, R. Klimkiewicz, M. Łaniecki, M. Appl. *Catal A: General* 249 (2003) 313
- [74] F. Fally, V. Perrichon, H. Vidal, J. Kaspar, G. Blanco, J.M. Pintado, S. Bernal, G. Colon, M. Daturi, J.C. Lavalley, *Catal. Today*, 59 (2000) 373
- [75] L. Ilieva, G. Pantaleo, I. Ivanov, A.M. Venezia, D. Andreeva, *Appl. Catal. B: Environ.* 65 (2006) 101.
- [76] K. Parida, H.K. Mishra, *J. Mol. Catal. A*, 139 (1999) 73
- [77] Yu A. Zaytseva, V. N. Panchenko, M. N. Simonov, A. A. Shutilov, G. A. Zenkovets, M. Renz, I. L. Simakova, V. N. Parmon, *Top. Catal.* 56 (2013) 1
- [78] F.C. Calaza, Y. Xu, D.R. Mullins, S.H. Overbury, *J. Am. Chem. Soc.* 134 (2012) 18034

B.3. Research Objectives

In this study, we would like to address the aforementioned challenges associated with acetic acids in bio-oil by developing a highly active and selective catalyst for aqueous phase ketonization to convert this acid molecule into ketone.

A natural continuation following the catalyst development from liquid phase ketonization is to explore the mechanistic aspects of this reaction. In addition, examination of the literature revealed the scarceness of research on ketonization process at a more fundamental level, which further justified the necessity of research endeavor in this direction. Toward that goal, we dedicated our efforts onto two aspects: 1) catalyst characterization, which was largely dismissed in most other research efforts; 2) kinetics study, which was carried out in vapor phase because it has proven to be a powerful means in comparison to liquid phase in acquiring kinetically meaningful data. However, probing into the catalyst surface and its evolution in the course of a reaction and connecting it to the kinetics data is conceivably the only way to achieve concrete understanding on the fundamental level, which is the goal and hope of this work.

B.4. Ketonization of Acetic Acid over Ru/TiO₂/Carbon Catalysts in the Aqueous Phase

B.4.1. Introduction

As mentioned in chapter 1, the production of stabilized bio-oils from biomass pyrolysis has received increasing attention in recent years since this method seems to offer technical and economic advantages over other methods for large-scale conversion of biomass [1-3]. The stabilization of pyrolysis oil requires the conversion of oxygenated compounds that include acids, alcohols, aldehydes, esters, phenolics, furans and heavier oxygenates. Without stabilization, bio-oil exhibits low heating value, high viscosity, chemical instability, and corrosiveness, which impede its storage, transportation, and industrial applicability [1-6]. Among many oxygenates present in bio-oil, acetic acid is one of the most abundant single components. For example, the bio-oil produced from sawdust contains about 10% of acetic acid [7]. This compound is particularly undesirable due to its high corrosiveness and the instability that it imparts to the bio-oil. As a result, ketonization is an important upgrading pathway because it converts acetic acid into acetone, which can be further converted with other bio-oil products such as furan compounds via aldol condensation/hydrogenation or phenolic compounds through hydrogenation/alkylation routes to produce longer chain (i.e. C9-C14) hydrocarbons which could be readily utilized as fuels [8-10].

Vapor-phase ketonization of acetic acid on oxides has been extensively studied in the past as summarized in section 3 [11-22]. However, as mentioned earlier, biomass contains highly oxygenated structures that upon depolymerization result in liquid

products of low vapor pressure, high solubility in water, and high reactivity. Therefore, it would be advantageous to carry out this reaction in the liquid phase at temperatures low enough to minimize decomposition and re-polymerization of bio-oil. Furthermore, in order to convert acetic acid in the most economic and effective way, it would be beneficial to use aqueous phase as the reaction medium.

Different transition metal oxides have been investigated as catalysts for ketonization reaction. In general, these oxides can be divided into two categories depending on lattice energies. On oxides with low-lattice-energy or high basicity, such as those from groups 1 and 2 in the periodic table, bulk acetate salts are formed and can decompose at high temperatures to produce acetone. Under steady state conditions, the reactions might process throughout the volume of the catalysts and alter the catalyst surface layers into salts. On the metal oxides with high lattice energy, such as TiO_2 , ZrO_2 , CeO_2 , the conversion to acetone takes place on the surface, leaving the oxide structure unchanged [11-19]. Among the numerous high lattice energy oxides, TiO_2 has been proved to possess high ketonization activity and selectivity to acetone [11-13]. It has been reported [18-23] that the addition of catalytic metals with high hydrogen dissociation activity, such as Pd, Pt, Rh and Co, significantly improves the reducibility of the metal oxides and consequently their ketonization activity.

In this contribution, we have investigated the catalytic conversion of acetic acid in the liquid phase using TiO_2 as the reducible oxide ingredient. Our working hypothesis is that activated carbon with its characteristically high surface area not only can enhance the dispersion of TiO_2 particles, but may also increase the adsorption of acetic acid from water. In recent years, there have been many contributions that

describe different preparations of TiO₂/carbon composite catalysts with enhanced properties for a number of reactions [24,25]. The results reported here indicate that the combination of Ru, TiO₂, and activated carbon (Ru/TiO₂/C) creates a unique catalyst system with potential for reactions in the aggressive liquid media of hot liquid acids. To investigate the interactions of the three components in the Ru/TiO₂/C catalysts, several characterization techniques were employed (XPS, TPR, TEM). They provide fairly detailed information about the structure and functionality of this catalyst.

B.4.2. Experimental Techniques

B.4.2.1. Catalyst Preparation

5 wt% Ru/TiO₂ catalyst used in this study was prepared by incipient wetness impregnation of an aqueous solution of RuCl₃·nH₂O (Sigma Aldrich, 99.5%) onto TiO₂ support (Degussa P25), using a liquid/solid ratio of 0.25 ml/g. After impregnation, the catalyst was dried overnight at 90°C in a vacuum oven. The dry catalyst was then heated for 3 h at 400°C under 100 ml/min flow of high purity air, and stored. Similarly, Ru/C was also prepared by conventional incipient wetness impregnation of activated carbon (C) (Darco, from Aldrich) with RuCl₃·nH₂O (Sigma Aldrich, 99.5%) to yield the Ru loading of 1.5 and 5 wt%.

TiO₂/C catalyst was prepared by conventional incipient wetness impregnation of activated carbon (C) (Darco, from Aldrich) with anhydrous titanium (IV) isopropoxide (from Fluka). After impregnation, the sample was left for two days in ambient air to slowly hydrolyze by normal humidity of the room. Subsequently, it was dried in a vacuum oven at 100°C and then heated under flowing He (50 ml/min) to 400°C for 3 h. This catalyst, identified as TiO₂/C, had a TiO₂ loading of 30 wt%.

To prepare Ru/TiO₂/C, Ru was incorporated by incipient wetness impregnation onto the previously prepared TiO₂/C sample using an aqueous solution of RuCl₃·nH₂O (Sigma Aldrich, 99.5%) to obtain a Ru loading of 1.5 wt% (i.e., 5 wt% with respect to TiO₂). After impregnation, the sample was dried at 100°C overnight and calcined in flowing air (100 ml/min) at 400°C for 4 h. The resulting catalyst is labeled Ru/TiO₂/C.

B.4.2.2 Catalyst Characterization

The BET surface areas were measured by N₂ physisorption at liquid nitrogen temperature on a Micromeritics ASAP 2010 instrument. For these measurements, the sample was degassed for 3 h at 250°C prior to analysis.

X-ray diffraction (XRD) analysis was conducted on a Rigaku automatic diffractometer (Model D-MAX A), equipped with a curved crystal monochromator and system setting of 40kV and 35 mA. The data were collected in the angle ranging 5-40° with a step size of 0.05 and a count time of 1.0 s. The catalysts were evacuated at 350°C for 3 h prior to analysis.

Temperature programmed reduction (TPR) analysis of 30-50 mg catalysts was carried out in a gas mixture of 5% H₂ in Argon at a flow rate of 30 ml/min with a linear heating ramp of 5°C/min up to 600°C. The amount of H₂ consumed was monitored as a function of temperature on a thermal conductivity detector (TCD). Deconvolution of the TPR peaks was carried out with PeakFit software.

X-ray Photoelectron spectroscopy (XPS) analysis was conducted on a Physical Electronics PHI 5800 ESCA system with standard non-monochromatic Al X-rays (1,486.6 eV) operated at 250W and 15 kV in a chamber pumped down to a pressure of approximately 1.0×10⁻⁸ Torr. A sealed transfer cell was used to transport the ex-situ

reduced samples from a glove box to the analysis chamber without exposure to air. A 93.9 eV and 58.7 eV pass energy were typically used for survey and specific element analysis, respectively. The electron takeoff angle was 45° with respect to the sample surface. The binding energies were adjusted to the C signal at 284.8 eV as an internal reference. The curve fitting was done using PeakFit program.

Electron paramagnetic resonance (EPR) measurements were recorded on a Bruker EMX spectrometer equipped with a nitrogen cryostat at a frequency of 9.43 GHz, microwave power of 2.03×10^{-1} mW, receiver gain of 1×10^5 , and modulation frequency of 100 KHz. The pre-reduced sample was prepared by reduction in water at 250°C under 400 psi of H₂ and then dried in the vacuum oven.

Transmission electron microscopy (TEM) analysis was carried out on a JEOL JEM-2010F field emission microscope, operating at an acceleration voltage of 200 kV. Catalyst leaching was tested and measured by UV-Vis spectroscopy. To prepare the sample, 0.5 mL of filtered solution from the reaction was diluted in water and mixed and stirred with 30% H₂O₂ to allow the formation of yellow Titanium-hydrogen peroxide complex, which absorbs at a wavelength of about 300 nm.

B.4.2.3. Reaction Studies

Experiments for ketonization of acetic acid (CH₃COOH 99%, Sigma Aldrich) in liquid phase were carried out in a 100-mL batch stainless steel autoclave reactor (Parr Corporation), equipped with impeller, temperature and pressure controllers, and sampling unit. Reaction temperature was at 180°C and pressure was varied in the range of 400-800 psi, respectively. In a typical experiment, measured amounts of catalyst were mixed with water or organic solvent (n-hexane, or N-methylpyrrolidone) and

placed in the reactor vessel. After the reactor was sealed, it was purged with N₂, then pressurized with H₂ to 400 psi, and heated up to 250°C for 3 h in order to reduce the catalyst. After completing the reduction period, the reactor was cooled down to room temperature, the pressure was released, and H₂ was purged out with N₂ at atmospheric pressure. The reactor was pressurized again in N₂ and heated to the desired reaction temperature. Mechanical stirring at 700 rpm kept the catalyst suspended to avoid external mass transfer limitations. At this point, acetic acid was fed into the reactor, which denotes the start of the reaction time. In all experiments, the initial concentration of acetic acid was kept constant at 1.7 M. The reaction was then stopped by rapid cooling. Liquid product samples were filtered and analyzed using gas chromatography (GC). GC-MS was used for product identification and GC-FID for quantification, using the corresponding chemical standards to obtain response factors.

B.4.3. Results

B.4.3.1 Catalyst Characterization Results

Table 4 summarizes the BET surface areas and pore volumes of the TiO₂/C and Ru/TiO₂/C catalysts, compared to those of the bare activated carbon (C) support. The deposition of TiO₂ and/or Ru causes significant decreased surface area and pore volume compared to those of the original carbon. As proposed in earlier studies [26-27], the micropores of the activated carbon may become partially blocked by fine particles, in this case TiO₂ and Ru, causing the observed drops in pore volume and surface area.

XRD diffractograms of the Ru/TiO₂/C and TiO₂/C catalysts, along with that of a commercial TiO₂ powder (Degussa P25, Sigma Aldrich) as a reference, are shown in Figure 14.

Table 4. BET surface area and pore volumes of the synthesized catalysts

Catalyst	Surface area ± 10 (m ² /g)	Pore Volume ± 0.02 (cm ³ /g)
Activated Carbon (C)	620	0.55
TiO ₂ /C	540	0.52
Ru/ TiO ₂ /C	390	0.40

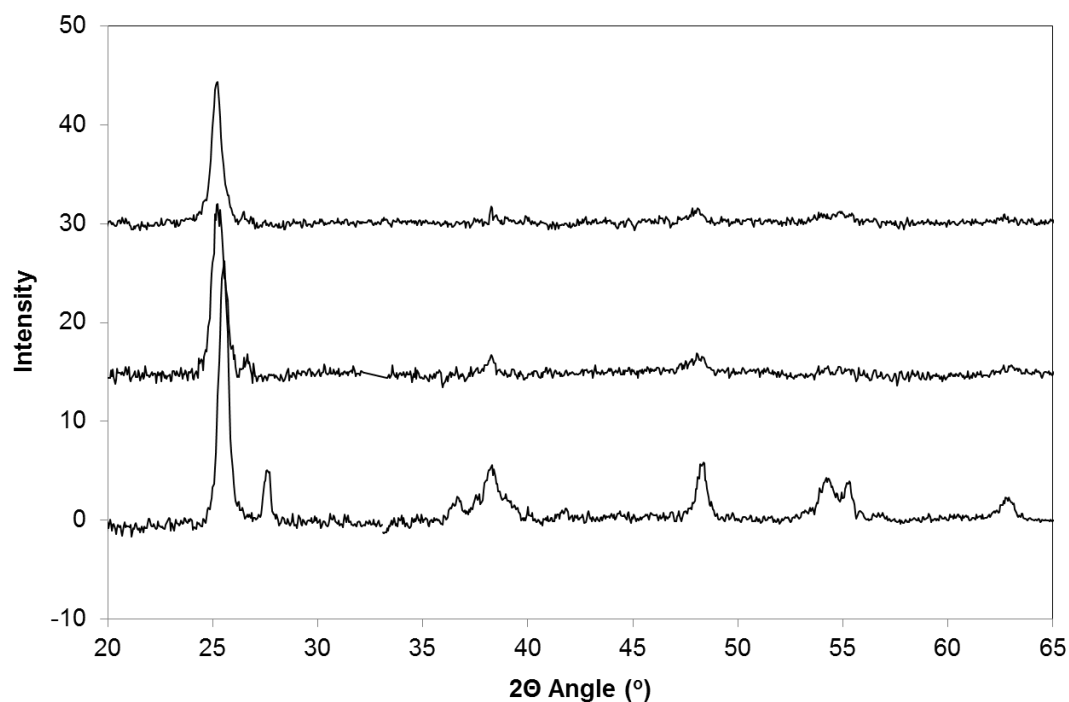


Figure 14. XRD patterns of commercial TiO₂ powder P25, TiO₂/C, and Ru/TiO₂/C

It is clear that anatase is the dominant TiO₂ species in both TiO₂/C and Ru/TiO₂/C catalysts, similar to the commercial P25 TiO₂. However, as clearly shown in the inset, there is a significant shift in the position of the main peak from $2\theta = 25.55$ for the P25 TiO₂ to $2\theta = 25.25$ for TiO₂/C and Ru/TiO₂/C catalysts. Those values correspond to the d -spacing of 3.48 and 3.53 Å, respectively. The former is in good agreement with the reported d -spacing of anatase (101) planes [28]. The slightly larger

d-spacing exhibited by the carbon-supported TiO₂ species might indicate a lattice distortion induced by strong interaction between TiO₂ and the carbon support. As previously reported [28-31], lattice structure of TiO₂ can be distorted by the support via (i) diffusion of support into the microstructure of the oxides or (ii) rearrangement of oxide atoms at the interface with the support during the growth of the oxide. In this particular case, it is believed that the latter case might occur at the interlayer of TiO₂/carbon during the formation TiO₂ [30]. This lattice distortion may facilitate the creation of defect sites on this catalyst, as discussed below in XPS analysis.

Figure 15 displays the TEM images of the TiO₂/C and Ru/TiO₂/C catalysts compared to the bare activated carbon support. Small TiO₂ clusters dispersed over the surface of activated carbon are clearly evident in the TiO₂/C sample. A histogram of 75 particles indicates that the average size of the TiO₂ clusters was about 6 ± 2 nm.

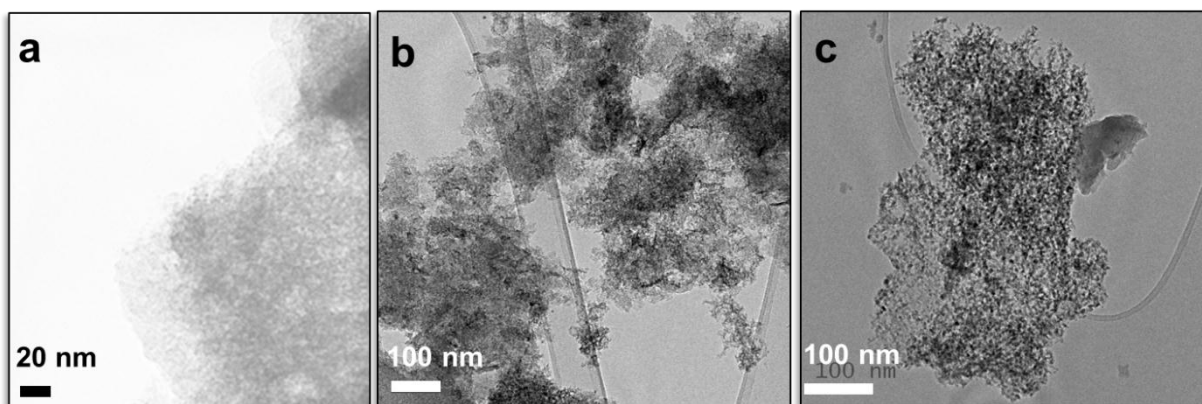


Figure 15. TEM images of a) activated carbon support; b) TiO₂/C; and c) Ru/TiO₂/C

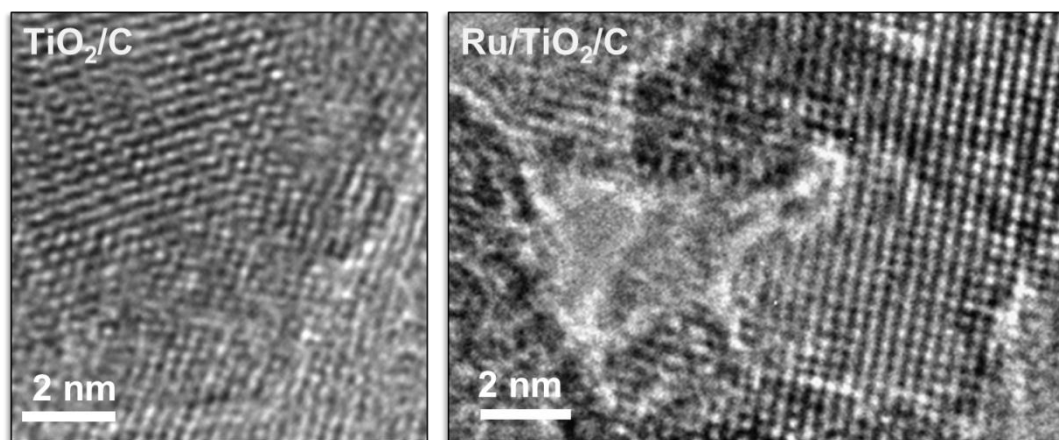


Figure 16. High Resolution TEM images of TiO_2/C ; and $\text{Ru}/\text{TiO}_2/\text{C}$

The high resolution TEM images in Figure 16 clearly show the lattice fringes of TiO_2 in both catalysts. The Ru-containing sample shows the presence of small dark spots over the TiO_2 crystals with sizes of less than 2 nm, which can be ascribed to Ru particles. However, the distinction between Ru and TiO_2 particles in carbon-supported catalysts is not as clear as those typically observed on conventional Ru/TiO_2 [32-33].

Temperature-programmed reduction (TPR) profiles of the two catalysts, TiO_2/C and $\text{Ru}/\text{TiO}_2/\text{C}$, as well as two reference samples with 1.5% and 5% Ru supported on the activated carbon are compared in Figure 17. The TPR profiles of the two Ru/C samples exhibit a single sharp reduction peak, whose position depends on the Ru loading. This peak is ascribed to the reduction of Ru oxide particles to metallic Ru, which is in good agreement with other TPR data reported in literature [26]. Since the one with higher Ru loading (5%) appeared shifted to higher temperatures (195°C) compared to that (180°C) of the lower loading (1.5%), it can be concluded that the smaller particles are easier to reduce on the activated carbon support than the larger particles. As expected, TiO_2/C showed no significant hydrogen consumption below

500°C, but only a broad consumption in the 500-700°C range, which can be attributed to the partial reduction of TiO₂, as previously reported [34].

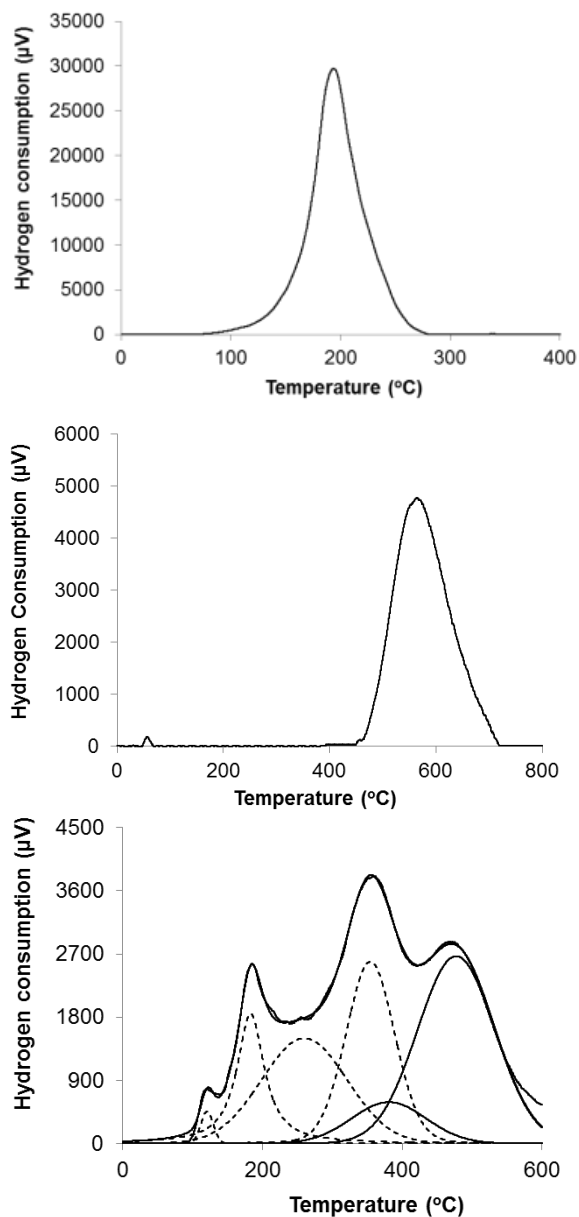


Figure 17. TPR profiles of (top) 5%Ru/C; (middle) TiO₂/C; and (bottom) Ru/TiO₂/C

When both Ru and TiO₂ are incorporated onto the C support, the TPR profile shows significant differences. For example, instead of the single peak observed with Ru/C, the Ru/TiO₂/C catalyst shows multiple reduction peaks ranging from 100°C to 600°C and can be fitted with five Gaussians. Based on the results observed with Ru/C, the sharp peak at 183°C and the small shoulder at 121°C observed in Ru/TiO₂/C can be tentatively ascribed to the complete reduction of Ru oxide particles dispersed on activated carbon, of larger and smaller sizes, respectively. The peaks appearing at higher temperatures can be ascribed to a combination of the reduction of Ru oxide and that of TiO₂, in close interaction with each other. That is, this interaction delays the reduction of Ru, but enhances the reduction of TiO₂ [35].

It is well known that by adding a transition metal, the hydrogen adsorption and reducibility of reducible metal oxides can be greatly increased by spillover, in which the hydrogen atoms formed upon dissociation on the metal surface can migrate to the reducible oxide [14,15,33,36-43]. According to Pestman et al. [14], the addition of Pt greatly improved the activity for selective hydrodeoxygenation of acetic acid to acetaldehyde on TiO₂ catalyst. This is because the H atoms spillover from the metal to the oxide creates O vacancies, which are then replenished by O from acetic acid (i.e., Mars-van Krevelen-like mechanism) [15].

In our case, we can expect that H atoms adsorbed on Ru can migrate onto TiO₂ and reduce some Ti⁴⁺ cations to Ti³⁺. At lower temperatures (e.g. < 400°C), Ti⁴⁺ ions in closer contact with Ru particles can get reduced, whereas at higher temperatures (e.g. > 450°C), more Ti⁴⁺ species, not necessarily in direct contact with Ru, can also get

reduced [36]. As a result, one can expect that the Ru/TiO₂/C catalyst can have a much larger density of Ti³⁺ sites than the TiO₂/C catalyst.

As can be seen, the presence of Ru greatly enhances the amount of reduced TiO₂ at low temperatures. It is worth mentioning that the reduction temperature chosen for the pretreatment before reaction (250°C) is a compromise between the operating temperature range of the reactor and the TPR results. In this case, it is important to take into account that during the reduction step, a hydrogen partial pressure (400 psi) much higher than in the TPR experiments is employed, which certainly enhances the reduction rate of Ru and TiO₂.

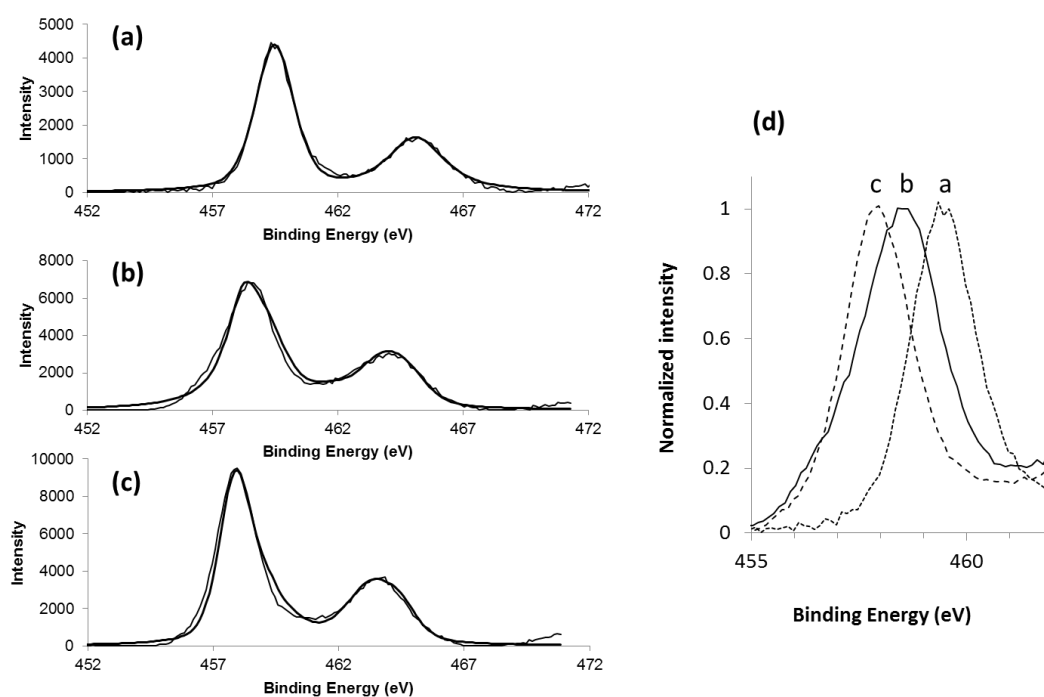


Figure 18. Ti 2p XPS spectra of (a) TiO₂/C (as-synthesized) ; (b) Ru/TiO₂/C (as-synthesized); (c) Ru/TiO₂/C (ex-situ reduced at 500°C in H₂ before XPS experiment); and (d) normalized Ti 2p_{1/2} peak for the three samples.

Figure 18 shows the XPS spectra of the Ti 2p regions for TiO₂/C, Ru/TiO₂/C, reduced at 500°C in H₂ and non-reduced, and commercial P25 (as-received). The binding energies of the Ti 2p core levels of TiO₂/C catalyst, appearing at around 459.5 and 465.1 eV for Ti 2p_{3/2} and Ti 2p_{1/2}, respectively, agree well with values of TiO₂ P25 and those reported in literature for stoichiometric TiO₂ [11]. Interestingly, upon deposition of Ru, a significant amount of TiO₂ was stabilized in a state of lower binding energy. That is, the Ti 2p_{3/2} peak shifts from 459.5 eV for TiO₂/C to 458.2 eV for Ru/TiO₂/C. This indicates "pseudo partial reduction" of TiO₂ possibly due to electronic effect from Ru. Upon the ex-situ reduction treatment in H₂ at 500°C, the binding energies shift to even lower values, i.e. 457.9 eV for Ti 2p_{3/2}. These low binding energies indicate the reduction of Ti by H₂ from Ti⁴⁺ to Ti³⁺ [11, 35].

The relative dispersion of Ti species on Carbon over the two different catalysts can be evaluated in terms of the Ti/C ratio calculated from the atomic surface concentrations as determined by XPS (see Table 5). It is interesting to note that the Ti/C ratio is higher for Ru/TiO₂/C than for TiO₂/C, even though some Ru may cover TiO₂. This enhanced fraction of exposed Ti may be the result of smaller TiO₂ stabilized by Ru.

Table 5. Surface composition of TiO₂/C and Ru/TiO₂/C catalysts as determined by XPS characterization

Catalyst	Atomic Composition (%)				Ti/C ratio
	C	O	Ti	Ru	
TiO ₂ /C (as-synthesized)	50.7	39.4	9.9	0	0.19
Ru/TiO ₂ /C (as-synthesized)	42.9	43.4	10.4	3.3	0.24

To further investigate the presence of Ti^{3+} species in the reduced catalysts, a detailed EPR study was conducted for as-synthesized Ru/TiO₂/C as well as Ru/TiO₂/C pretreated with H₂ at 250°C in the water phase for 4 hours and dried in vacuum. Due to its electronic structure, i.e., full valence band and empty conduction band with no unpaired electrons, stoichiometric TiO₂ is not active for EPR. However, reduced Ti^{3+} species can produce EPR signals. Figure 19 presents the EPR spectra of as synthesized and reduced Ru/TiO₂/C catalysts. Only one signal at $g = 2.02$ was observed for the as-synthesized catalyst whereas two signals at $g = 2.01$ and $g = 1.95$ were observed for the reduced one. The common signals of the two samples at $g > 2$ can be assigned to superoxo or hydroperoxo species associated with Ti^{4+} [44,47]. These species are postulated to be formed during the air calcination of the Ru/TiO₂/C catalyst.

The signal at $g = 1.95$ with peak width of 115 Gauss can be attributed to electrons trapped in Ti^{3+} , which is in good agreement with values previously reported [45-47]. We can rule out the possibility of the presence of Ru ions because Ru signal appears at higher g values with wider peak width [48,49]. In addition, the reduction of Ru can complete at 250°C under the high pressure of hydrogen. The observation of Ti^{3+} signal from EPR further proves that upon pre-reduction, reduced Ti^{3+} species can be formed and retained on Ru/TiO₂/C catalyst in liquid water.

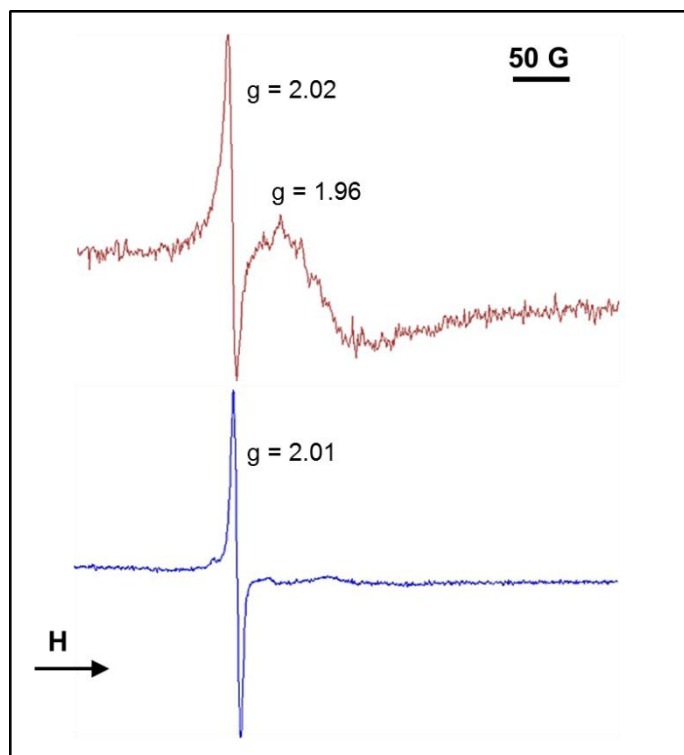


Figure 19. EPR spectra of as synthesized and reduced Ru/TiO₂/C catalysts

B.4.3.2 Catalytic performance of TiO₂/C and Ru/TiO₂/C catalysts

A number of different mechanisms have been proposed in literature for vapor phase ketonization reactions over high lattice energy oxides, such as TiO₂ [11-18]. While the mechanisms differ in the nature of the intermediates and reaction pathways, there is a general agreement that coordinatively unsaturated sites i.e. oxygen vacancies play a crucial role in ketonization reaction [11-18]. The need for generating those active sites by reduction and by addition of transition metals has been emphasized in several studies [14, 19-23]. For example, it is well known that addition of small amounts of yttrium to Ce_{0.6}Zr_{0.4}O₂ support in three-way catalysts enhances the oxygen uptake capacity and increases the concentration of Ce³⁺ - O vacancy sites, as confirmed by XPS [21]. Similarly, DFT studies [23] have shown that doping TiO₂ anatase with Au or Fe

weakens the M-O bonds around the dopants and reduces the energy required to form an O vacancy from 2.7 eV in pure TiO₂ to 1.24 eV in Fe-doped catalyst.

More relevant to the current work, Dooley et al. [19] studied the effects of adding Co and Pd to alumina-supported CeO₂ particles in vapor phase ketonization of isobutyric, acetic, and decanoic acids. By using XANES and EXAFS characterization techniques, they showed a significant enhancement in the number of oxygen vacancies around each Ce atom upon the incorporation of small amounts of Pd and Co (0.8%) to the base CeO₂/Al₂O₃ catalyst.

While a large number of catalysts have shown high activity and selectivity in vapor phase at temperatures above 300°C, it must be emphasized that the study reported here focuses on ketonization reaction at low temperatures, in the liquid phase, and in the presence of solvents, including water. Moreover, under these conditions, the conversion of acetic acid on TiO₂/C and Ru/TiO₂/C catalysts operate at 100% selectivity towards ketonization, i.e. acetone is the only product.

Table 6 compares the catalytic activity of the TiO₂/C, Ru/TiO₂/C, Ru/C, and Ru/TiO₂ catalysts in aqueous phase at 180°C. It is clear that the activity of pure Ru supported on activated carbon is very low (only 1.3 %). That is, Ru does not impart any significant ketonization activity, and cannot be directly responsible for the high activity exhibited by the TiO₂-containing catalysts (conversion ~ 15-54 %). However, the participation of Ru is crucial for enhancing the activity of TiO₂. That is, the conversion of the catalysts containing both Ru and TiO₂ is at least twice that of TiO₂/C. If we normalize the moles of acetic acid converted to the mass of TiO₂ in the catalyst, the highest activity is that of Ru/TiO₂/C. Since the TiO₂ particles present in TiO₂/C and in

Ru/TiO₂/C catalysts are similar in size, we can conclude that the presence of Ru enhances the specific activity of TiO₂. Likewise, when we compared the activity of Ru/TiO₂ P25 to that of the bare TiO₂ P25, the activity is increased by a factor of more than 3. As discussed earlier, the strong interaction between Ru and TiO₂ results in higher reducibility of TiO₂ and creation of more Ti³⁺ sites, as suggested by TPR and XPS.

Table 6. Catalytic activity of 5%Ru/C, TiO₂/C, Ru/TiO₂/C, TiO₂ P25 and 5% Ru/TiO₂ catalysts for the reactions at 180°C in 5 hours in water phase.

Catalyst	Pre-treatment	Acetic acid converted /TiO ₂ mass (mmol/g)	Acetic acid converted /TiO ₂ surface area (mmol/cm ²) (x 10 ⁶)
5%Ru/C	pre-reduced	-	
TiO ₂ /C	pre-reduced	250	141
Ru/TiO ₂ /C	pre-reduced	440	249
Ru/TiO ₂ P25	pre-reduced	170	252
TiO ₂ P25	None	8	12
TiO ₂ P25	Pre-reduced	60	89

It is important to point out that, as has been clearly demonstrated for vapor-phase reactions, we have found here that in the case of liquid-phase reaction, the pre-reduction of the catalyst is vital. One might expect that during reaction, when the catalyst is exposed to hot liquid water, it might get re-oxidized, erasing any effect of a pre-reduction treatment. However, this is not the case. We measured the conversion of

acetic acid over 200 mg of as-received and pre-reduced TiO₂ P25 catalyst at 180°C in water phase. It was observed that while only 1.5% of acetic acid was converted to acetone over non-reduced TiO₂, indicating that non-reduced TiO₂ is inactive for ketonization. Interestingly, however, with pre-reduction in hydrogen at 250°C, the ketonization activity of TiO₂ increased significantly to 10%. This result indicates that the pre-reduction step generates the reduced Ti³⁺ required for ketonization reaction.

However, to retain the high selectivity toward ketonization reaction, the reaction must be carried out in non-hydrogen environment. In a separate test, under hydrogen environment, acetic acid underwent hydrogenation to produce ethanol, acetaldehyde and ethyl acetate. This result is in good agreement with what was reported in [32], in which Corma et al. studied the reaction of various acids including lactic acid, levulinic acid, succinic acid and itaconic acid over 0.6% Ru/TiO₂ under high pressure of hydrogen (32 bar, or 470.4 psi). Under this condition, only hydrogenated products were observed. Also, it is interesting to analyze the higher activity exhibited by Ru/TiO₂/C as compared to Ru/TiO₂. On the carbon support, Ru and TiO₂ may not interact as effectively as in the case of the Ru/TiO₂ since some of the Ru may just be supported on carbon rather than on the TiO₂ particles. However, the carbon support is able to stabilize the TiO₂ in smaller particles giving a larger fraction of exposed TiO₂ species. Moreover, as shown in the XRD data, the presence of activated carbon support can induce distortion of TiO₂ lattice and generate more defect sites, leading to the formation of more Ti³⁺ sites in the catalyst.

As previously shown, oxygen vacancies are crucially needed to catalyze ketonization reaction, which, however, is difficult to form and persist in liquid water,

since the presence of liquid water can attack those sites. Recent theoretical and surface science studies have observed the filling of oxygen vacancies by water. It is important to note that the mechanism of liquid water attack is substantially different from the filling by dioxygen. In the latter case, O₂ is thought to dissociate on the surface O vacancy. One O atom fills the vacancy while the other O remains on a neighboring Ti site [50]. In the former case, while O vacancies are also the active sites to dissociate H₂O, the final result is different from that obtained with O₂. That is, the vacancy is filled by an OH group and a proton is transferred to a nearby O atom. So, two adjacent hydroxyl groups are formed for every original vacancy [51]. Under reaction conditions, it is possible that the O vacancy can be regenerated by dehydration of these adjacent hydroxyls [52].

Proposed mechanism for the ketonization in the presence of liquid water is shown in Figure 20. In our particular case, with highly dispersed Ru, surface Ti³⁺ site can be readily formed upon reduction in H₂ in the liquid water, as evidenced by EPR experiment (Figure 19). A hydroxyl would be consecutively generated at the adjacent Ti⁴⁺ site according to mechanism mentioned above. In aqueous solution, this reduced Ti³⁺, a Lewis acid site, would be readily associated with water [a]. In the presence of acetic acid, the coordinated water at the Ti³⁺ site [a] can be equilibrated with acetic acid [b]. This proposed step is supported by a theoretical investigation about the adsorption of formic acid and sodium formate on the hydrated surface of anatase (101). The DFT calculation clearly indicated that formic acid and formate can displace the water pre-adsorbed on the surface of anatase and energetically favor the direct attach to the surface of anatase. Furthermore, it was suggested that for the formate, the stable

adsorption configuration was bridging bidentate structure with a net adsorption energy of 0.79eV. For the acid, on the other hand, the more favorable structure is a monodentate dissociated geometry which is stabilized by a hydrogen bond to a surface hydroxyl.

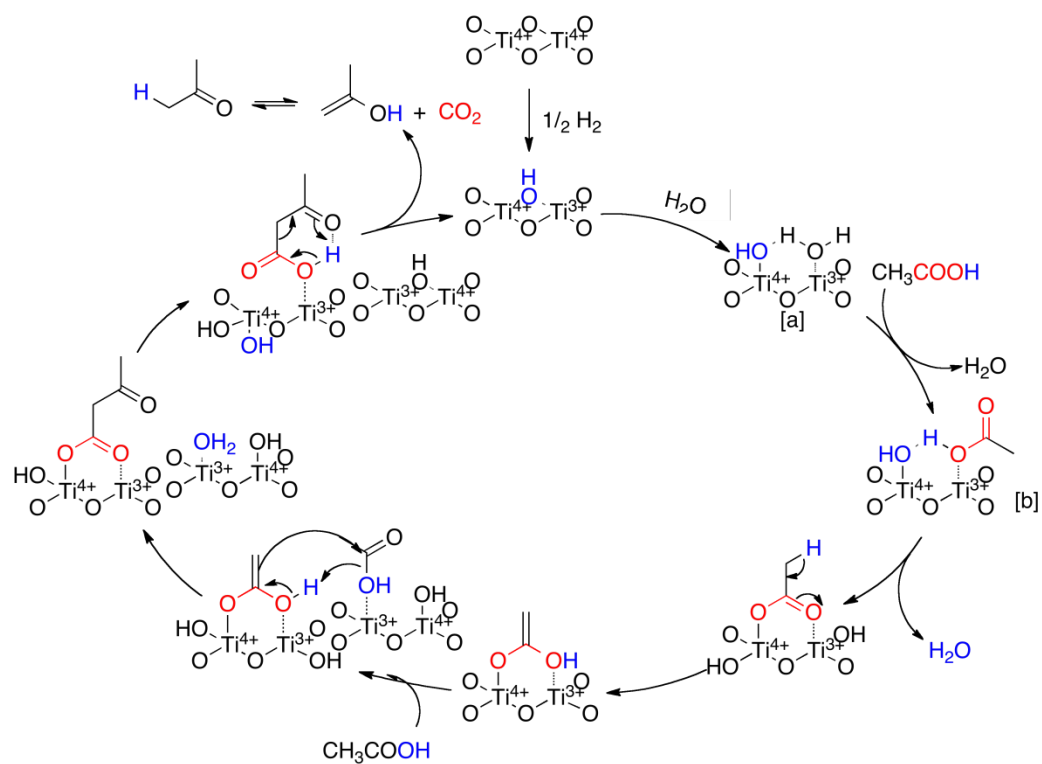


Figure 20. Proposed mechanism for liquid phase ketonization of carboxylic acid over TiO_2 catalyst

It is believed that the hydroxyl at the proximate Ti^{4+} site may also react with the coordinated acetic acid forming “Ti-acetate species” on the surface as shown in Figure 20. The formation of such “Ti-acetate species” appears to be irreversible since water produced by this reaction would be strongly associated with the Lewis-acid Ti^{3+} site. In turn, this water can be equilibrated with another acetic acid molecule, in a manner similar to the preceding step. This would result in a couple Ti^{3+}/Ti^{4+} intermediate, in

which one acetic acid is coordinated with Ti^{3+} site while the other forms “Ti-acetate species” at the adjacent Ti^{4+} site. Decomposition of such intermediate is believed to proceed in a manner similar to those [53] known as the decarboxylation of organic acid over alkali-earth cationic sites, namely Mg^{2+} and Ca^{2+} . However, as “Ti-acetate species” is in proximate with the acetic acid- Ti^{3+} site, the decarboxylation readily yields acetone and carbon dioxide. Both products are less adsorptive, as compared to water, and the couple Ti^{3+}/Ti^{4+} active sites can be readily recovered after the decomposition.

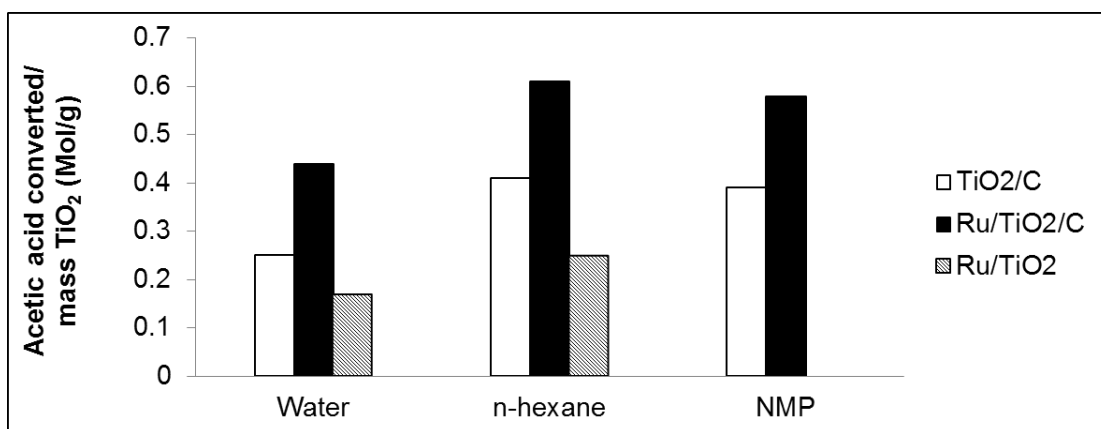


Figure 21. Catalytic activity of TiO_2/C , Ru/TiO_2 P25 and $Ru/TiO_2/C$ catalysts for the reactions at $180^\circ C$ in 5 h in three different solvents: water, *n*-hexane and *N*-methyl pyrrolidone. All the catalysts were pre-reduced before the reaction

According to the proposed reaction pathway, competitive adsorption between water and acetic acid would play a marked role in the formation of the reaction intermediate. In fact, Fig. 21 shows the results obtained after 5 h reaction at $180^\circ C$ in three different solvents: *N*-methyl pyrrolidone (NMP), *n*-hexane, and water. It is clear that the activity of all three tested catalysts increased when organic solvents were used. This is presumably due to the fact that both coordination of acetic acid at the Ti^{3+} site and the formation of “Ti-acetate species” can be readily facilitated in the absence of water.

Similar effects have been observed in vapor phase with basic oxides such as CeO₂ and CeO₂-ZrO₂ [54-55]. Also, as observed, the incorporation of Ru or activated carbon drastically enhanced the activity of TiO₂/C or Ru/TiO₂ by up to more than 50% in all three solvents, which according to this description, would suggest that the presence of Ru helps stabilizing a higher density of Ti³⁺ sites.

As the reaction involves coordination of water and acid, leaching of Ti³⁺ sites could happen and be responsible for the catalyst deactivation in aqueous phase. In the leaching test of the filtered solution after 2 hour reaction, 3.31% of the total titanium contained in the fresh catalyst was detected in the solution. It is likely that Ti³⁺, a Lewis acid site, can be readily leached in solution, which would result in deactivation of the catalyst.

B.4.4. Conclusion

In this study, a new and efficient catalyst composed of TiO₂ and Ru supported on activated carbon (Ru/TiO₂/C) has been developed and tested for the liquid phase ketonization of acetic acid. This Ru/TiO₂/C catalyst has been shown to possess high activity and selectivity toward ketonization at 180°C in organic solvents including n-hexane and NMP. More importantly, the catalyst also retains the high catalytic activity in aqueous phase. Several characterization techniques including XPS and TPR demonstrated that the incorporation of transition metal Ru resulted in the formation of more Ti³⁺ sites and oxygen vacancies. Also, the hydrophobic activated carbon support might help to protect the catalytic sites from water blockage and maintain the activity of catalyst in water phase. This new catalyst has paved the way for the effective

conversion of bio-oil through multistep reactions consisting of ketonization, aldol condensation and hydrogenation deoxygenation.

References

- [1] G.W. Huber, S. Iborra, A. Corma. *Chem. Rev.* 106 (2006) 4044.
- [2] D. M. Alonso, J. Q. Bond, J. A. Dumesic. *Green Chem.* 12 (2010) 1493.
- [3] G.W. Huber, A. Corma. *Angew. Chem. Int. Ed.* 46 (2007) 7184.
- [4] J. Lede, F. Broust, F.T. Ndiaye, M. Ferrer. *Fuel*, 86 (2007) 1800.
- [5] V.R. Wiggers, A. Wisniewski, L.A.S. Madureira, A.A. Chivanga Barros, H.F. Meier. *Fuel Proc. Technol.* 88 (2009) 2135.
- [6] S. Czernik, A. V. Bridgwater. *Energy Fuels.* 18 (2004) 590.
- [7] R. Aguado, M. Olazar, M. J. San Jose, G. Aguirre, J. Bilbao. *Ind. Eng. Chem. Res.* 39 (2000) 192.
- [8] P. A. Zapata, J. Faria, M. P. Ruiz, D. E. Resasco. *Top. in Catal.* 55 (2012) 38.
- [9] S. Crossley, J. Faria, M. Shen, D. E. Resasco. *Science.* 327 (2010) 68.
- [10] W. Shen; G. A. Tompsett; K. D. Hammond; R. Xing; F. Dogan; C. P. Grey; W. C. Conner; S. M. Auerbach; G. W. Huber. *Appl. Catal. A General*, 392 (2011) 57.
- [11] K.S. Kim and M. A. Barteau., *J. Catal.* 125 (1990) 353.
- [12] R. Martinez, M. C. Huff, M. A. Barteau. *J. Catal.* 222 (2004) 404.
- [13] R. Pestman, R. M. Koster, A. van Duijne, J. A. Z. Pieterse, V. Ponec. *J. Catal.* 168 (1997) 265.
- [14] R. Pestman, R. M. Koster, J. A. Z. Pieterse, V. Ponec. *J. Catal.* 168 (1997) 255.
- [15] R. Pestman, A. van Duijne, J. A. Z. Pieterse, V. Ponec. *J. Mol. Catal. A* 103 (1995) 175.
- [16] C. Doornkamp, V. Ponec. *J. Mol. Catal. A.* 162 (2000) 19.
- [17] S.D. Randery, J.S. Warren, K. M. Dooley. *Appl. Catal. A* 226 (2002) 265.

-
- [18] Rajadurai S. *Catal. Rev.: Sci. and Eng.* 36 (1994) 385.
- [19] C. A. Gaertner, J. C. Serrano-Ruiz, D. J. Braden, J. A. Dumesic. *J. Catal.* 266 (2009) 71.
- [20] K. M. Dooley, A. K. Bhat, C. P. Plaisance, A. D. Roy. *Appl. Catal. A* 320 (2007) 122.
- [21] H. He, H.X. Dai, L.H. Ng, K.W. Wong, C.T. Au. *J. Catal.* 206 (2002) 1.
- [22] H. Idriss, C. Diagne, J.P. Hindermann, A. Kiennemann, M.A. Barteau. *J. Catal.* 155 (1995) 219.
- [23] M. Boronat, A. Corma. *Catalysis Today.* 169 (2011), 52.
- [24] R. Leary, A. Westwood. *Carbon*, 49 (2011) 741.
- [25] J.R. Osman, J.A.Crayston, A. Pratt, D.T. Richens. *Mat. Chem. Phys.* 110 (2008) 256
- [26] B. Tryba, A. W. Morawski, M. Inagaki. *Appl. Catal. B* 41 (2003) 427.
- [27] L.B. Okhlopkova, A.S. Lisitsyn, V.A. Likholobov, M. Gurrath, H.P. Boehm, *Appl. Catal. A* 204 (2000) 229.
- [28] L. Wang, Y. Sun, and B. Xu. *J. Mater. Sci. Technol.* 23 (2007) 604.
- [29] D.S. Gill, A. A. Anderson, R.W. Eason, T.J. Warburton, D.P. Shepherd. *Appl. Phys.. Lett.* 69 (1996) 11.
- [30] U. Diebold, *Surf. Sci. Rep.* 48 (2003) 53
- [31] A. Sasahara, T.C. Droubay, S. A. Chambers, H. Uetsuka, H. Onishi. *Nanotechnol.* 16 (2005) 18.
- [32] A. Primo, P. Concepcion, and A. Corma. *Chem. Commun.* 47 (2011) 3613.

-
- [33] X. Shen, L-J. Garces, Y. Ding, K. Laubernds, R.P. Zerger, M. Aindow, E. J. Neth, S. L. Suib. *Appl. Catal. A* 335 (2008) 187.
- [34] L. Miao, P. Jin, K. Kaneko, A. Terai, N. Nabatova-Gabain, S. Tanemura. *Appl. Surf. Sci.* 212 (2003) 255.
- [35] G.L. Haller, D.E. Resasco, *Adv. Catal.* 36 (1989) 173.
- [36] C. Milone, C. Gangemi, R. Ingoglia, G. Neri, S. Galvagno. *Appl. Catal. A* 184 (1999) 89.
- [37] J. Strunk, W. C. Vining, A. T. Bell. *J. Phys. Chem. C* 114 (2010) 16937.
- [38] P. Panagiotopoulou, A. Christodoulakis, D.I. Kondaries, S. Boghosian. *J. Catal.* 240 (2006) 114.
- [39] T. Huizinga, J. van Grondelle, R. Prins, *Appl. Catal.* 10 (1984) 199.
- [40] J.G. Kim, J.Z. Shyu, J.R. Regalbuto, *J. Catal.* 139 (1993) 153.
- [41] E. D. Reddy, L. Davydov, P. G. Smirnotis. *J. Phys. Chem. B.* 106 (2002), 3394.
- [42] R.J. Tauster, S.C. Fung, R.L. Garten. *J. Am. Chem. Soc.* 100 (1978), 170.
- [43] R. Prins, *Chemical Reviews* (2012); DOI:10.1021/cr200346z
- [44] T. Berger, M. Sterrer, O. Diwald, E. Knözinger, D. Panayotov, T.L. Thompson, J.T. Yates Jr., *J. Phys. Chem. B* 109 (2005) 6061.
- [45] T. M. Salama, H. Hattori, H. Kita, K. Ebitani, T. Tanaka, *J. Chem. Soc. Faraday Trans* 89 (1993) 2067
- [46] J. C. Conesa, P. Malet, G. Munuera, J. Sanz, J. Soria, *J. Phys. Chem.* 92 (1988), 189
- [47] R. Bal, K. Chaudhari, D. Srinivas, S. Sivasanker, P. Ratnasamy, *J. Mol. Catal. A.* 162 (2000) 199

-
- [48] P. Castillo-Villalon, J. Ramirez, M.J. Peltre, C. Louis, P. Massiani. *Phys. Chem. Chem. Phys.*, 6 (2004), 3739
- [49] G. I. Pilipenko, A.A. Sabirzyanov, D.V.Oparin, V.G. Stephano, F.F. Gavrilov *J.Phys.: Condens. Matter*, 4 (1992), 4055
- [50] O. Bikondoa, C. L. Pang, R. Ithnin, C. A. Muryn, H. Onishi, G. Thornton, *Nature Materials* 5 (2006) 189.
- [51] R. Schaub, P. Thostrup, N. Lopez, E. Lægsgaard, I. Stensgaard, J. K. Nørskov, and F. Besenbacher, *Phys. Rev. Lett.* 87 (2001) 266104
- [52] M. Aizawa, Y. Morikawa, Y. Namai, H. Morikawa, Y. Iwasawa, *J. Phys. Chem. B* 109 (2005) 18831
- [53] A. Zhang, Q. Ma, K. Wang, X. Liu, P. Shuler, Y. Tang. *Appl. Catal.* 303 (2006), 109
- [54] A. Gangadharan, M. Shen, T. Sooknoi, D.E. Resasco, R.G. Mallinson. *Appl. Catal.* 385 (2010) 80.
- [55] D. Mansur, T. Yoshikawa, K. Norinaga, J-I. Hayashi, T. Tago, T. Masuda. *Fuel*. DOI:10.1016/j.fuel.2011.04.003.

B.5. Reaction Kinetics and Mechanism of Ketonization of Aliphatic Carboxylic Acids with Different Carbon Chain Lengths over Ru/TiO₂ Catalyst

B.5.1. Introduction

As discussed in section 3, ketonization of carboxylic acids is a well-known reaction, discovered in 1858 by Friedel [1], and widely used in the early 20th century for commercial production of acetone [2]. In recent years, ketonization has received renewed attention for its potential application in the production and upgrading of renewable fuels and chemicals from conversion of cellulosic biomass [3-6]. Fast pyrolysis, i.e., rapid heating of biomass in inert environment, produces bio-oil, a complex liquid rich in oxygenated molecules, among which small acids such as acetic acid are particularly abundant [7]. Therefore, an effective method to remove these undesirable acids is ketonization, which not only reduces O content, but also creates C-C bonds.

For more than thirty years, extensive research efforts have been devoted to the study of surface-catalyzed ketonization. It is generally accepted that reducible amphoteric metal oxides, such as TiO₂, CeO₂, ZrO₂, and MnO₂ are the most effective catalysts for this reaction [8,10]. However, while some aspects of the mechanism are well established, others remain unsettled. For example, there is compelling evidence in favor of the crucial role of α -hydrogen on at least one of the two participating carboxylic acid molecules [3,9-11]. However, the exact nature of the reaction intermediates is controversial and several possibilities have been considered. For

example, important roles of acid anhydrides, β -ketoacids, ketene, and ketene-like species have been proposed in different studies [9-14].

Rigorous catalytic kinetics analysis is a powerful tool for determining kinetic and thermodynamic parameters that can help to shed light on the reaction mechanisms and has been used successfully for various reactions [15,16]. In the present contribution, we attempt to gain a deeper understanding of the ketonization reaction mechanism and reaction intermediates through a detailed kinetic investigation, using a Langmuir-Hinshelwood model combined with transition state theory analysis. This combination has allowed us to determine the kinetically relevant step and its true activation energy instead of the apparent activation energies typically calculated when not using a detailed kinetic model. More interestingly, the data analysis based on the transition state theory provides useful information about the nature of the activated complex.

B.5.2. Experimental

B.5.2.1. Catalyst Synthesis

The 5 wt% Ru/TiO₂ catalyst used in this study was prepared by incipient wetness impregnation of an aqueous solution of RuCl₃·nH₂O (Sigma Aldrich, 99.5%) onto TiO₂ support (Degussa P25), using a liquid/solid ratio of 0.25 ml/g. After impregnation, the catalyst was dried overnight at 90°C in a vacuum oven. The dry catalyst was then heated for 3 h at 400°C under 100 ml/min flow of high purity air, and stored.

B.5.2.2. Catalyst Characterization

BET surface area of the catalyst was measured by N₂ physisorption at liquid nitrogen temperature on a Micromeritics ASAP 2010 unit. For these measurements, the sample was degassed for 3 h at 250°C prior to analysis. X-ray diffraction (XRD) analysis was conducted on a Rigaku automatic diffractometer (Model D-MAX A), equipped with a curved crystal monochromator at a system setting of 40 kV and 35 mA. Data were collected over 5–40° angle range with a step size of 0.05° and a count time of 1.0 s. X-ray photoelectron spectroscopy (XPS) data were recorded on a Physical Electronics PHI 5800 ESCA system with standard non-monochromatic Al X-rays (1486.6 eV) operated at 250W and 15 kV in a chamber pumped down to a pressure of approximately 1.0×10^{-8} Torr. A 93.9 eV and 58.7 eV pass energy were typically used for survey and specific element analysis, respectively.

B.5.2.3. Kinetic Measurements

The vapor-phase conversion of three carboxylic acids of varying alkyl chain lengths (acetic, propionic, and butyric acids) was measured over Ru/TiO₂ in an isothermal tubular reactor equipped with high-precision flow and temperature controllers. In each run, a fresh catalyst sample was held at the center of a vertical tubular quartz reactor (6 mm I.D.) between two layers of quartz wool. Before the reaction, the catalyst was reduced in situ for 1 h at 400 °C under a 50 ml/min flow of H₂. After reduction, the reactor was cooled down to the selected reaction temperature (275-335 °C) under He flow. The acid feed was continuously injected from a syringe pump and vaporized into the He carrier gas stream to reach the selected space times (W/F) and partial pressures. The outlet of the reactor was connected to a six-way gas

sampling valve, heated at 180-200 °C to avoid condensation. The reactants and products were analyzed online by gas chromatography using flame ionization detector (FID) and thermal conductivity detector (TCD). The GC-FID analyses were performed using a Hewlett Packard 6890 GC equipped with a Phenomenex ZB-Wax polyethylene glycol column (30 m x 0.25 mm x 0.25 µm). The GC-TCD analyses were conducted on a Carle 400 AGC with a built-in MultiCoat™ column. In each run, the carbon balance was checked and found to be higher than 90% in all cases. In order to compare the runs under identical conditions, a fresh catalyst was used in each separate experiment.

B.5.3. Results

B.5.3.1. Catalyst Characterization

Figure 22 compares the X-ray diffractogram of the Ru/TiO₂ catalyst to that of the bare TiO₂ support, before any treatment. It is seen that the XRD patterns of the two samples were similar, indicating that the crystallinity of TiO₂ was not altered upon the impregnation and heating processes. No peaks due to ruthenium oxide could be observed, which is consistent with a relatively high Ru dispersion previously observed on this type of catalyst [17].

In agreement with the XRD results, BET analysis showed that the Ru/TiO₂ catalyst and the bare TiO₂ P25 support had very similar surface areas, 60-62 m²/g, indicating that the surface area of TiO₂ was not affected upon Ru loading.

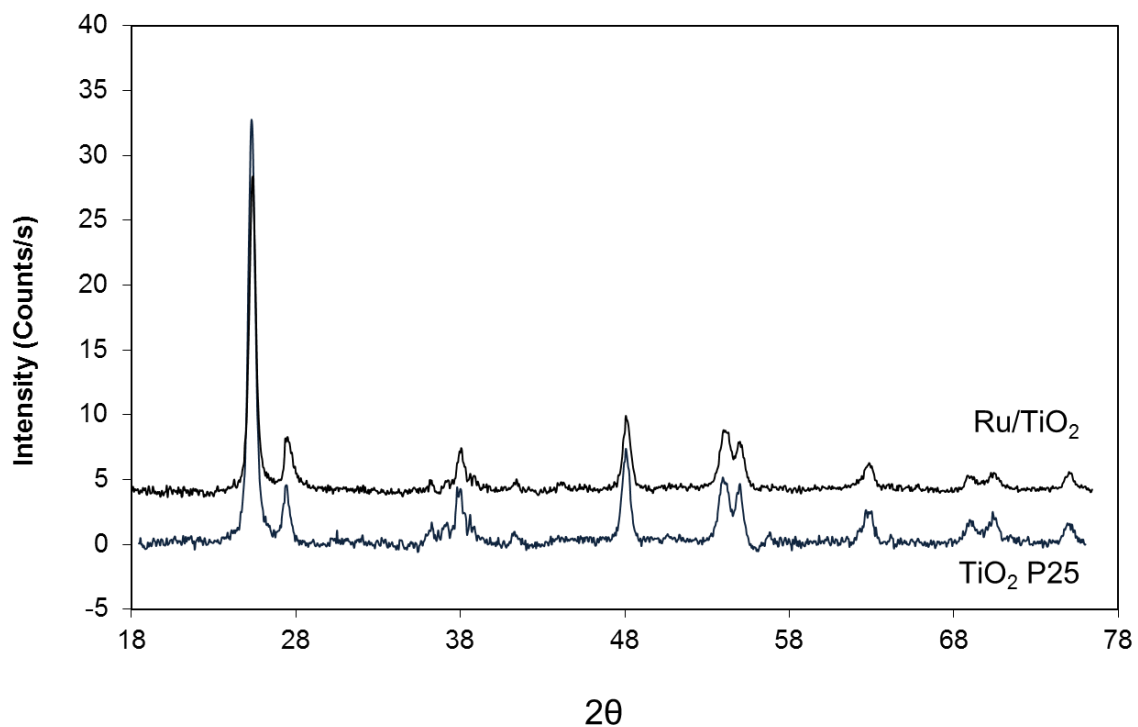


Figure 22. X-ray Diffractogram (XRD) of Ru/TiO₂ and bare TiO₂ P25

On the other hand, XPS revealed an atomic content of Ru of ~16% with respect to Ti on the catalyst surface, larger than that calculated from 5wt% of Ru on TiO₂. In addition, as opposed to previous results which showed broadened and shifted Ti2p peaks of Ru/TiO₂/C in comparison to TiO₂/C, no noticeable difference was observed in this study over Ru/TiO₂ without activated carbon support. The difference could be due to an enhancement effect of activated carbon on the interaction between Ru and TiO₂ but the exact reason is still unclear.

B.5.3.2. Catalytic Activity Measurements

B.5.3.2.1. Removal of transport and thermodynamic limitations in kinetic measurements

To obtain kinetic parameters that can be used to evaluate a given reaction mechanism, it is important to conduct the measurements in the absence of mass transport limitations. It is well established [18] that rates need to be obtained at

sufficiently small particle sizes and sufficiently high gas velocity to avoid internal and external mass transfer limitations, respectively. A useful criterion proposed by Fogler [18] is that transport limitations are absent when the measured rate no longer increases as the value of $(\text{carrier gas velocity}/\text{particle size})^{1/2}$ increases. We measured the reaction rates as a function of He carrier gas flow from 30 to 140 sccm and catalyst particle sizes varying from $< 20 \mu\text{m}$ to $250 \mu\text{m}$. As shown in Figure 23, when the measured rates are controlled by mass transport limitations, the rate increases practically linearly with this value. By contrast, when it reaches about $194 \text{ cm}/\text{min}^{0.5}$, mass transfer effects disappear. Therefore, employing a flow rate greater than $100 \text{ ml}/\text{min}$ and catalyst particles smaller than $20 \mu\text{m}$ are adequate for operating in the kinetic regime, without mass transfer limitations.

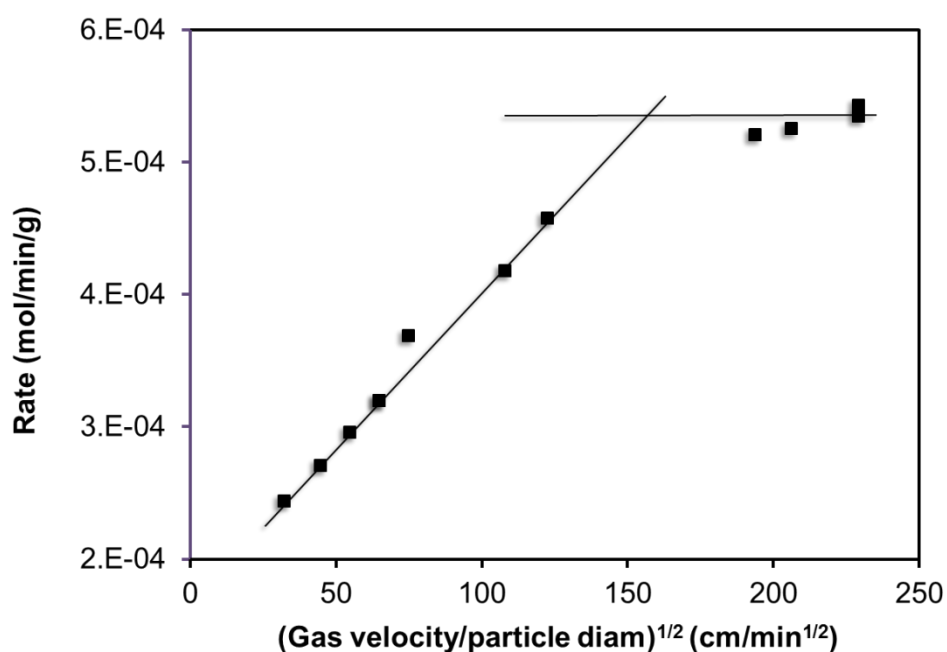


Figure 23. . Effect of carrier gas velocity and catalyst particle sizes on ketonization rate at 275°C on pre-reduced Ru/TiO_2

Furthermore, internal diffusion limitations were also tested by applying Weisz-Prater criterion [19], that is:

$$N_{W-P} = \frac{rR_p^2}{C_s D_{\text{eff}}} \leq 0.3$$

with the following values for our operating conditions: r (reaction rate per volume of catalyst) = 3.77×10^{-5} moles/min/cm³; R_p (catalyst particle radius) = 2×10^{-3} cm; C_s (reactant concentration at particle surface) = 6.87×10^{-7} moles/cm³. D_{eff} (effective diffusivity) = 1.748×10^{-2} cm²/s, which is Knudsen diffusivity in this case. This is because Ru/TiO₂ catalyst has an average pore size diameter of around 11.92 nm (obtained from BET measurement), much less than the calculated value of mean free path of acetic acid in the gas phase (320 nm), making Knudsen diffusion dominant.

$$D_{\text{eff}} = D_{\text{Kn}} = \frac{v d_p}{3} = \frac{(4.4 \times 10^4 \text{ cm s}^{-1}) (11.92 \times 10^{-7} \text{ cm})}{3} = 1.748 \times 10^{-2} \text{ cm}^2 \text{ s}^{-1}$$

in which v is average velocity of acetic acid molecules in gas phase at 548 K and 1 atm and d_p is average pore size diameter of the catalyst. Accordingly, the calculated Weisz-Prater number obtained over Ru/TiO₂ at 275°C is 0.013, which assured the absence of internal mass transfer limitations.

It is worth mentioning that even though we used small catalyst particles for the reactions, the small amounts of catalyst used avoided a significant pressure drop through the bed, which did not exceed 3-5 psig.

Besides the absence of mass transfer limitation, kinetic measurements also require the absence of thermodynamic restriction to ensure the measured concentrations of acetic acid and products are far from equilibrium. Table 7 shows the calculated equilibrium constant K by using Thermosolver software together with calculated

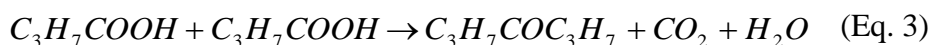
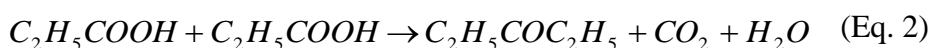
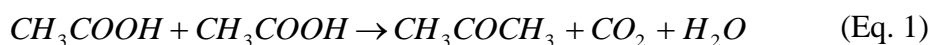
thermodynamic conversion of acetic acid ketonization at three different temperatures in this study. As shown, the thermodynamic conversions are >99.8%, which are much higher than the conversion range used in this study.

Table 7. *Thermodynamic equilibrium constants and conversion values of acetic acid ketonization at different temperatures*

	Temperature (°C)		
	275	280	285
K_{eq}	2.41×10^5	2.50×10^5	2.60×10^5
$X_{thermodynamic}$ (%)	99.7	99.8	99.8

B.5.3.2.2. *Ketonization products from the various acids*

One of the advantages of ketonization reaction is its very high selectivity to the desired products, which greatly simplifies analysis. Water, CO₂, and corresponding ketones are practically the only products obtained, in line with the following expressions:



With acetic and propionic acids, these products were the only ones detected. With butyric acid, they represented > 99% of the products; only trace amounts of larger condensation products were obtained.

B.5.3.2.3. Kinetics results. Differential reactor analysis

To determine the reaction order with respect to acid in ketonization, we chose acetic acid as the probe molecule. The partial pressure of acetic acid was varied by modifying the inlet flow and adjusting the flow of carrier gas accordingly, while the total pressure was kept constant (1 atm). The rates were calculated according to the expression

$$r = X \cdot (F/W) \text{ [(mol/min)/g cat.]} \quad (2)$$

where X = conversion, F = molar flow rate (mol/min), W = catalyst weight.

Assuming that under differential reactor conditions, the partial pressure of the products is negligible, the slope of the $\log r$ vs. $\log P_{\text{Acid}}$ straight line yields a reaction order with respect to acetic acid of 1.6 ± 0.1 .

In order to quantify the effect of product concentration on reaction rate in the differential reactor, we injected varied amounts of acetone, water or CO_2 , while keeping the rest constant at 275°C over the pre-reduced Ru/TiO_2 catalyst. The resulting ketonization rates measured at conversions below 18 % for varied partial pressures of acetone, water or CO_2 , at a constant partial pressure of acetic acid of 12.67 Torr clearly indicated that all three products have an inhibiting effect on ketonization activity.

Acetone seems to have the strongest inhibition effect, suggesting a strong competitive adsorption on the same surface sites. In comparison, the inhibition effect of water and CO_2 is much lower. From the slopes of the fitted straight lines, the reaction orders with respect to acetone, water, and CO_2 are -0.4 ± 0.06 , -0.1 ± 0.02 , and -0.2 ± 0.04 , respectively.

B.5.3.2.4. Reaction rate data and kinetic fitting. Integral reactor analysis

The analysis from differential reactor suggested that the ketonization reaction is about second order with respect to the acid, with all the reaction products competing for adsorption on active sites and inhibiting the reaction rate. From these preliminary results, a series of elementary steps can be proposed and incorporated in a conventional Langmuir-Hinshelwood kinetic model to describe the reaction kinetics.



where * represents a surface active site.

It is noteworthy to mention that for the rate determining step (5), the important kinetic parameter is the rate constant, which provides information about the activation barrier. This barrier is the energy difference between the stable reacting species, i.e. $RCOOH *$ and the transition state, the species at the maximum energy point along the reaction coordinate, which leads to products, i.e. $RCOR*$, CO_2 , and H_2O . While the formation of the stable products may still require several subsequent steps, the formation of the intermolecular C-C bond is the crucial, rate-limiting step. There are two possible transition states that can be considered in this step, as illustrated in Figure 24. In the first case, the transition state would be one in which the C-C bond is still rather long while the C-COO bond that connects the CO_2 to the molecule is still rather short. We can consider this as an *early* transition state. By contrast, in the second case,

the C-C bond to be formed is shorter and the C-COO bond that will break upon reaction is now rather long. We therefore consider this as a *late* transition state.

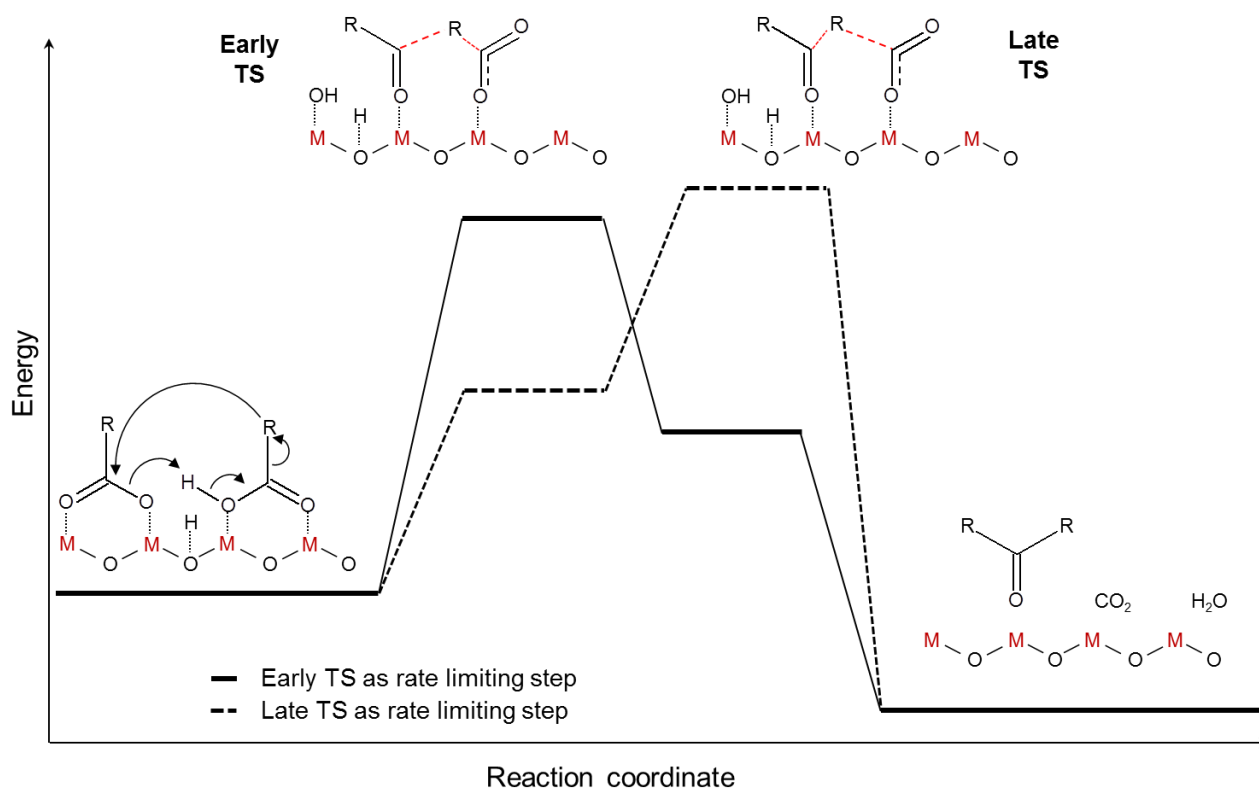
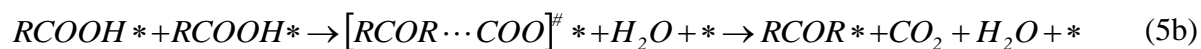
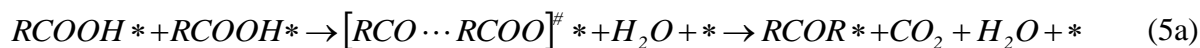


Figure 24. Proposed early and late transition state (TS) structures for ketonization of carboxylic acids

Accordingly, the measured activation energy will be either the energy required to bring the two C atoms together and form the C-C bond between the two adsorbed acid species (*early* transition state) or the energy needed for decarboxylation (i.e., CO₂ detachment) of the β -ketoacid intermediate (*late* transition state). As will be discussed below, the two proposed transition states are subject to steric effects that may vary to different extents with different alkyl chain lengths.

Based on the elementary steps proposed above with step (5) as the rate-limiting step, the overall reaction rate can be expressed as:

$$rate = k (\Theta_{RCOOH})^2 \quad (6)$$

where Θ_{RCOOH} is the fractional coverage of the carboxylic acid and can be derived from the adsorption equilibrium and the pseudo-equilibrated steps by the conventional expressions:

$$\Theta_{RCOOH} = K_{RCOOH} P_{RCOOH} \Theta_V \quad (7)$$

$$\Theta_{RCOR} = K_{RCOR} P_{RCOR} \Theta_V \quad (8)$$

$$\Theta_{CO_2} = K_{CO_2} P_{CO_2} \Theta_V \quad (9)$$

$$\Theta_{H_2O} = K_{H_2O} P_{H_2O} \Theta_V \quad (10)$$

where Θ_V is the fraction of empty sites, while Θ_{RCOR} , Θ_{H_2O} , and Θ_{CO_2} are the fractional surface coverages of ketone, water, and CO₂, respectively.

Applying the conventional Langmuir Hinshelwood kinetics derivation, the rate expression becomes:

$$rate = k \frac{(K_{RCOOH} P_{RCOOH})^2}{(1 + K_{RCOOH} P_{RCOOH} + K_{RCOR} P_{RCOR} + K_{CO_2} P_{CO_2} + K_{H_2O} P_{H_2O})^2} \quad (11)$$

To better validate the kinetic model and fit parameters obtained, two sets of data were used for the analysis of the ketonization of acetic acid at 275 °C. The first set of data obtained with the same (initial) acetic acid feed composition was analyzed by the integral reactor method at different space times (W/F). The second set of data was analyzed by the differential reactor method, in which the composition of the feed is varied with different concentrations of acetic acid and products, working at short W/F's

and consequently low conversions. Both sets of data were successfully fitted with the same values of kinetic fitting parameters, which reflect the robustness of the fitting.

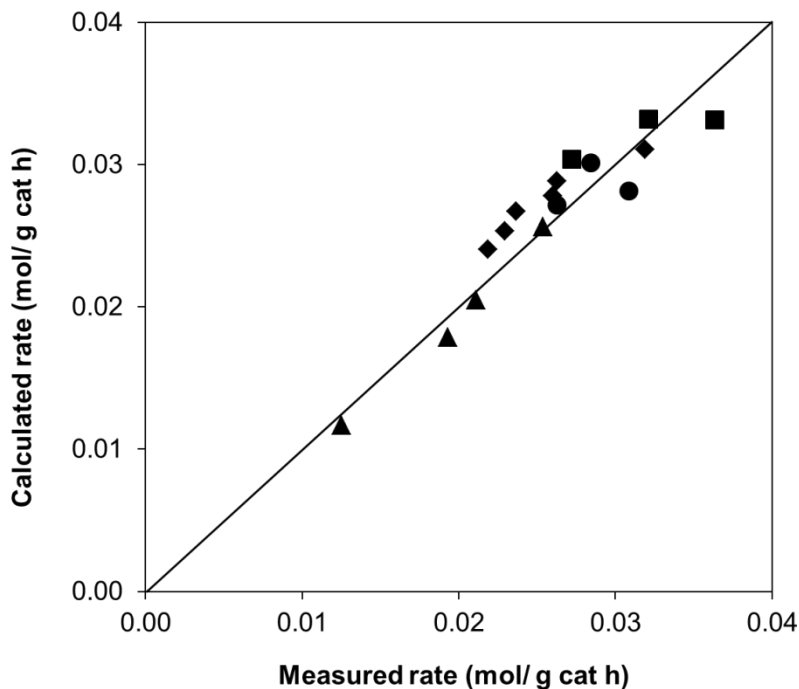
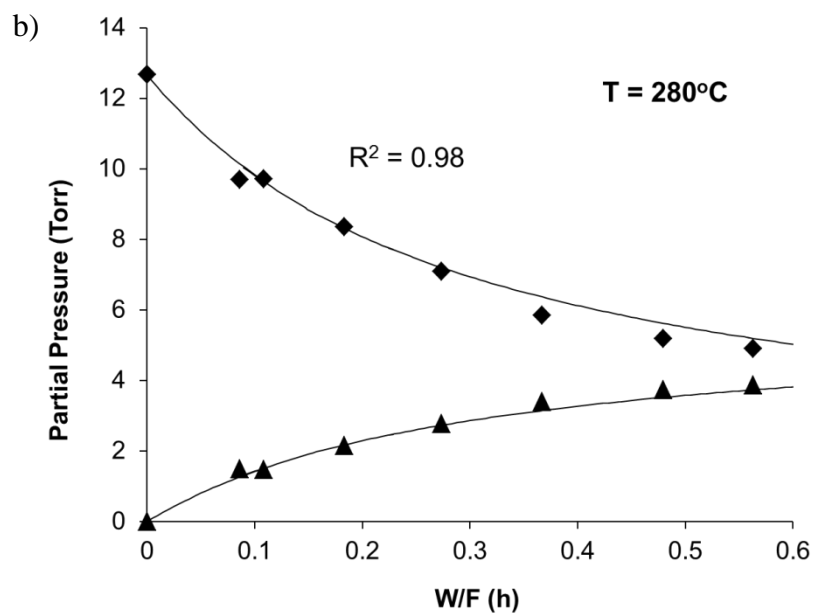
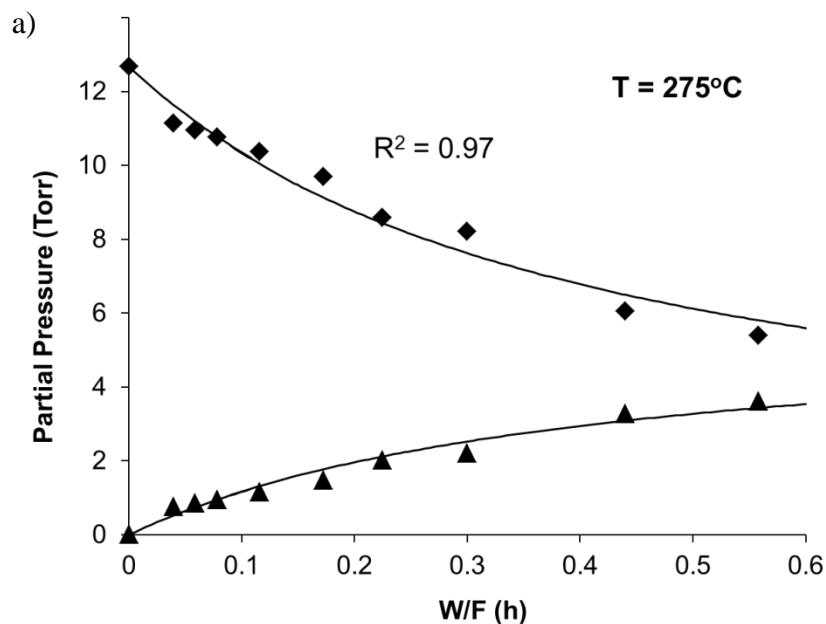


Figure 25. Parity plot comparison of experimental data (points) obtained with differential reactor model with the fitted data from Langmuir Hinshelwood model (line).

Figure 25 shows a parity plot of the experimental rates of acetic acid ketonization obtained with different feed compositions to the calculated rates by using equation (11) in the differential reactor method. The fitting parameters were obtained simultaneously with the data set obtained from the runs using the same initial feed composition at different space times (W/F) in the integral reactor, which is illustrated in Figure 26(a).

Figures 26 a, b, and c show the evolution of partial pressures of reactant and product as a function of W/F for three different temperatures (275, 280, and 285 °C) in an isothermal integral reactor. The corresponding results obtained for propionic acid

(290, 300 and 310 °C), and butyric acid (315, 325 and 335 °C) are shown in Figures 27 and 28, respectively. The solid lines in each case represent the fitted partial pressures using the same Langmuir-Hinshelwood model described above.



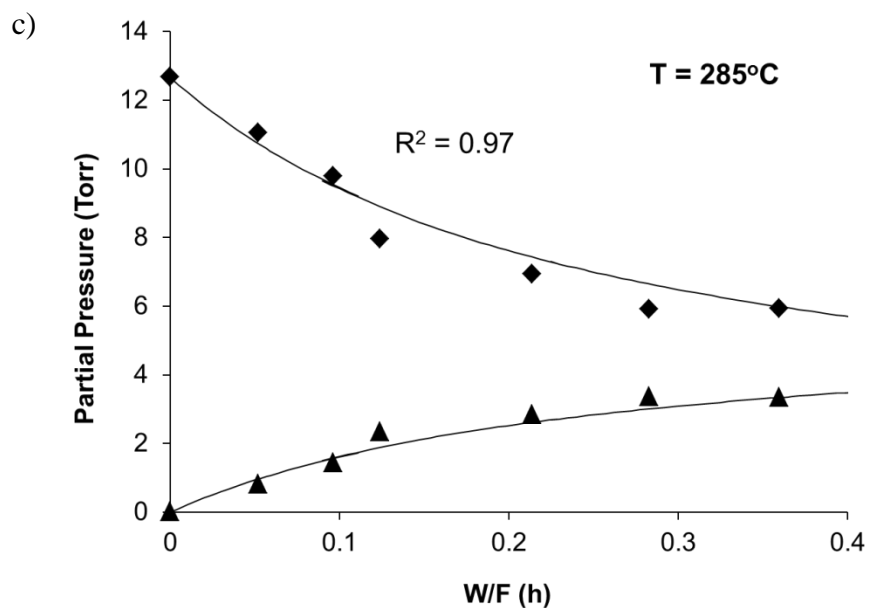
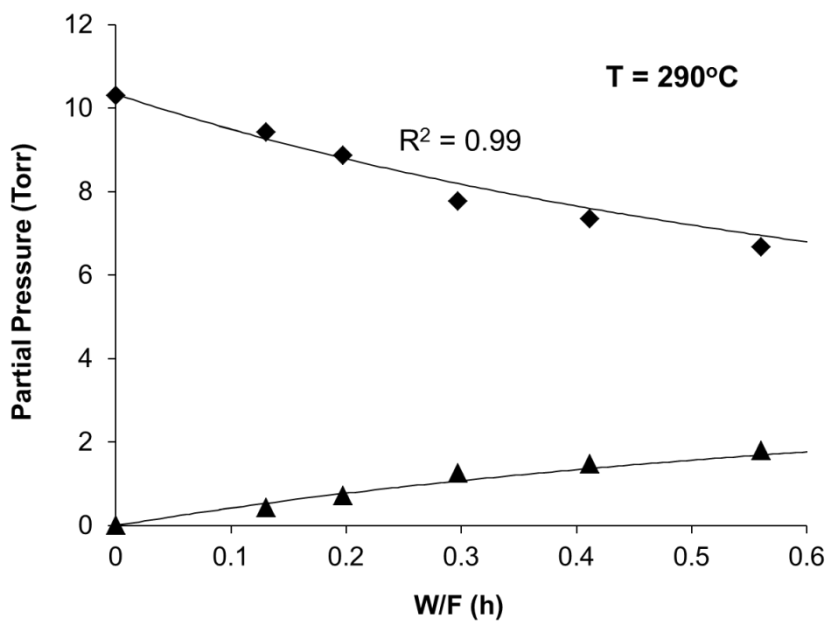


Figure 26. Partial pressures of acetic acid and acetone as a function of W/F at 30 minutes time on stream on Ru/TiO₂ at 275 (a), 280 (b) and 285°C (c). Catalysts were pre-reduced in H₂ stream at 400°C in 1 hour. The points are experimental data and the lines are fitted data from the Langmuir-Hinshelwood fitting model



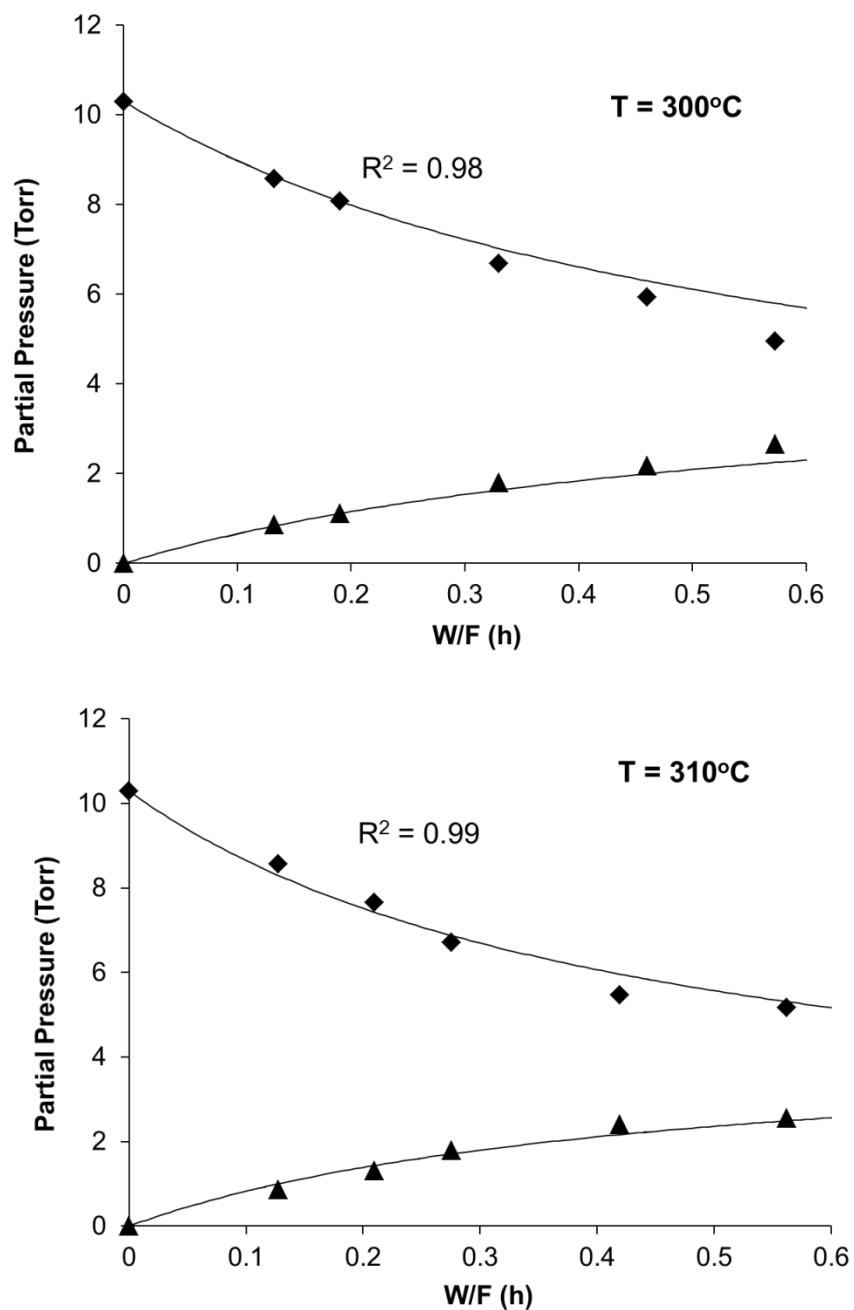
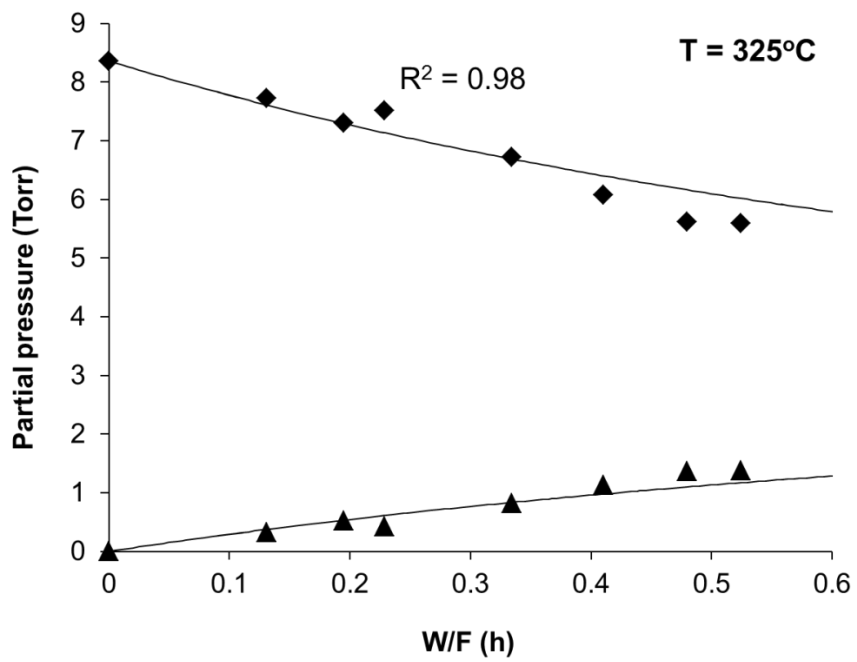
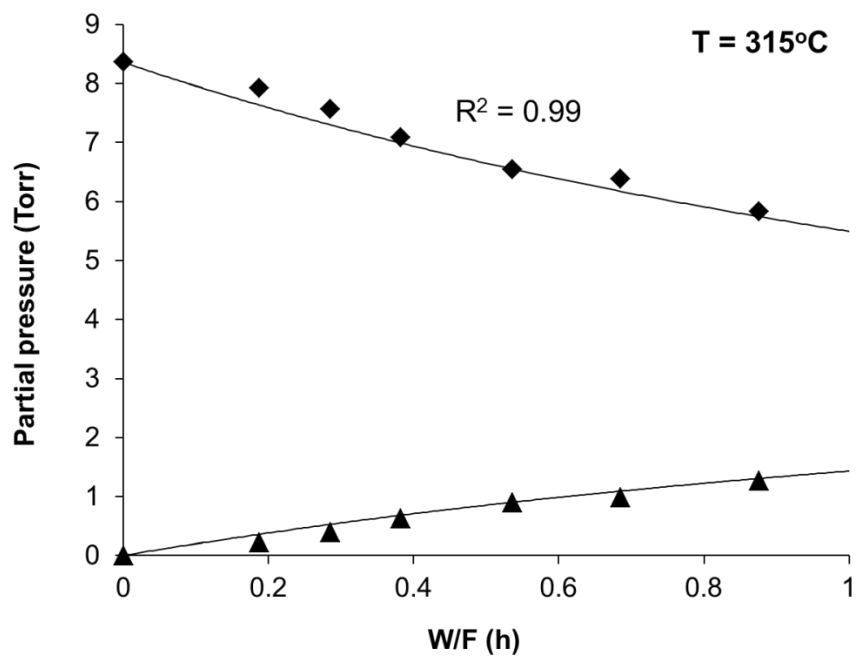


Figure 27. Partial pressures of propionic acid and 3-pentanone as a function of W/F at 30 minutes time on stream on Ru/TiO₂ at 290, 300, and 310°C. Catalysts were pre-reduced in H₂ stream at 400°C in 1 hour. The points are experimental data and the lines are fitted data from the Langmuir-Hinshelwood fitting model



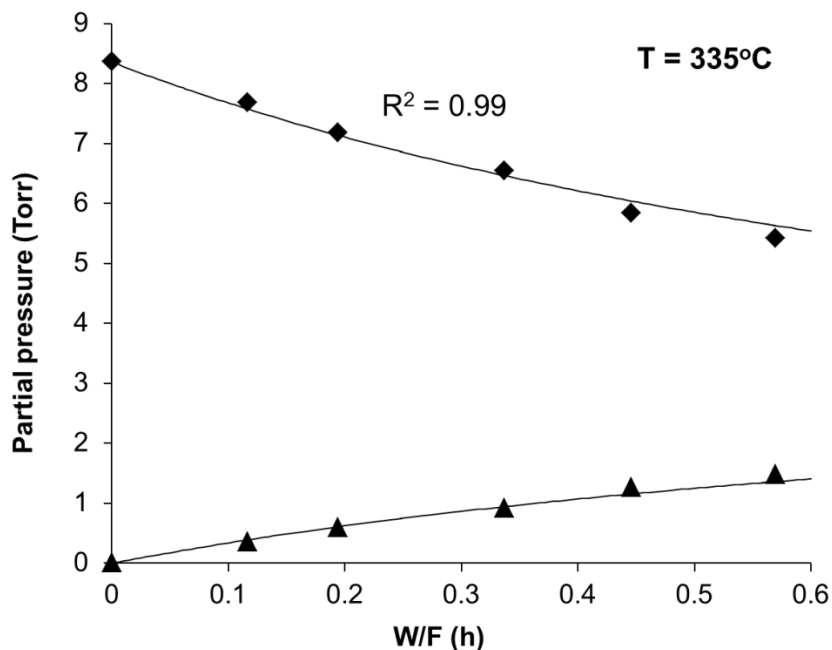


Figure 28. Partial pressures of butyric acid and 4-heptanone as a function of W/F at 30 minutes time on stream on Ru/TiO₂ at 315, 325, and 335°C. Catalysts were pre-reduced in H₂ stream at 400°C in 1 hour. The points are experimental data and the lines are fitted data from the Langmuir-Hinshelwood fitting model

The thermodynamic and kinetic constants are expressed as a function of temperature according to the conventional Arrhenius and Van't Hoff equations in terms of the true activation energy (E) and enthalpies (ΔH) and entropies (ΔS) of adsorption, respectively. That is, $k_i = A e^{\frac{-E_i}{RT}}$ and $K_i = e^{\frac{\Delta S_i}{R}} e^{\frac{-\Delta H_i}{RT}}$. It must be noted that the adsorption enthalpy and entropy values for water and CO₂ were kept the same in the fitting of the three acids at all temperatures.

The equilibrium adsorption constants for the three acids, three ketones, water, and CO₂ resulting from the fitting at different temperatures are summarized in Tables 8-10. The resulting enthalpies of adsorption for the three acids are shown to be

significantly higher than those of the reaction products, which decrease in the order of ketones > CO₂ > water.

Table 8. Optimized kinetic and thermodynamic parameters for the ketonization of acetic acid obtained from fitting the experimental data with the Langmuir-Hinshelwood model

Temp (°C)	Rate constant k (mol/g cat h)	Adsorption constant (Torr ⁻¹)			
		K _{Acetic acid}	K _{Acetone}	K _{Water}	K _{CO₂}
275	0.057	0.362	0.231	0.033	0.019
280	0.080	0.274	0.194	0.029	0.016
285	0.108	0.214	0.150	0.024	0.014
		Acetic	Acetone	Water	CO ₂
	$\Delta H_{\text{adsorption}}$ (kJ/mol)	-134.0	-109.7	-81.8	-87.5
	$\Delta S_{\text{adsorption}}$ (J/mol K)	-197.7	-157.1	-122.4	-137.4
	S_{gas} (J/mol K) (upper bound)	282.8	293.1	188.8	213.8

Table 9. Optimized kinetic and thermodynamic parameter values for the ketonization of propionic acid obtained from fitting the experimental data with the Langmuir-Hinshelwood kinetic model

Temp (°C)	Rate constant k (mol/g cat h)	Adsorption constant (Torr ⁻¹)			
		K _{Propionic acid}	K _{Pentanone}	K _{Water}	K _{CO₂}
290	0.023	0.396	0.273	0.021	0.011
300	0.050	0.230	0.174	0.015	0.008
310	0.088	0.148	0.115	0.011	0.006

	Propionic	Pentanone	Water	CO ₂
$\Delta H_{\text{adsorption}}$ (kJ/mol)	-134.2	-117.8	-81.8	-87.5
$\Delta S_{\text{adsorption}}$ (J/mol K)	-190.2	-169.7	-122.4	-137.4
S_{gas} (J/mol K) (upper bound)	-	-	188.8	213.8

Table 10. Optimized kinetic and thermodynamic parameter values for the ketonization butyric acid obtained from fitting the experimental data with the Langmuir-Hinshelwood kinetic model

Temp (°C)	Rate constant k (mol/g cat h)	Adsorption constant (Torr ⁻¹)			
		K _{Butyric acid}	K _{Heptanone}	K _{Water}	K _{CO₂}
315	0.012	0.584	0.275	0.010	0.005
325	0.024	0.304	0.179	0.007	0.004
335	0.055	0.102	0.051	0.003	0.002
		Butyric	Heptanone	Water	CO ₂
	$\Delta H_{\text{adsorption}}$ (kJ/mol)	-134.6	-129.5	-81.8	-87.5
	$\Delta S_{\text{adsorption}}$ (J/mol K)	-178.4	-175.7	-122.4	-137.4
	S_{gas} (J/mol K) (upper bound)	353.3	-	188.8	213.8

As illustrated in Fig. 29, it is interesting to note that all three acids have very similar heats of adsorption (i.e., about 134 kJ/mol), but the entropies of adsorption exhibit a significant change with increasing alkyl chain length from acetic acid to butyric acid (i.e., from -198 to -178 J/mol K).

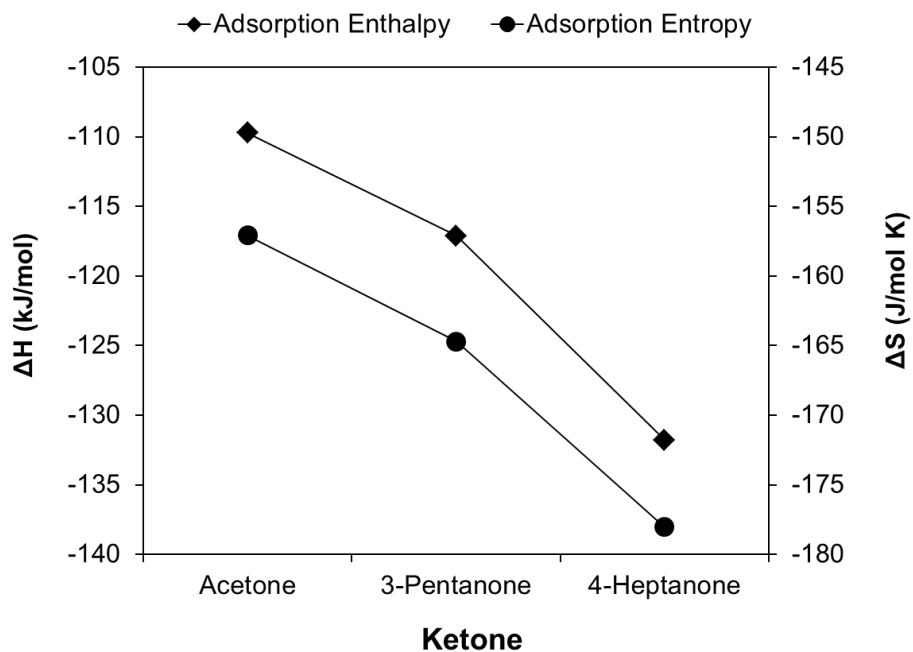
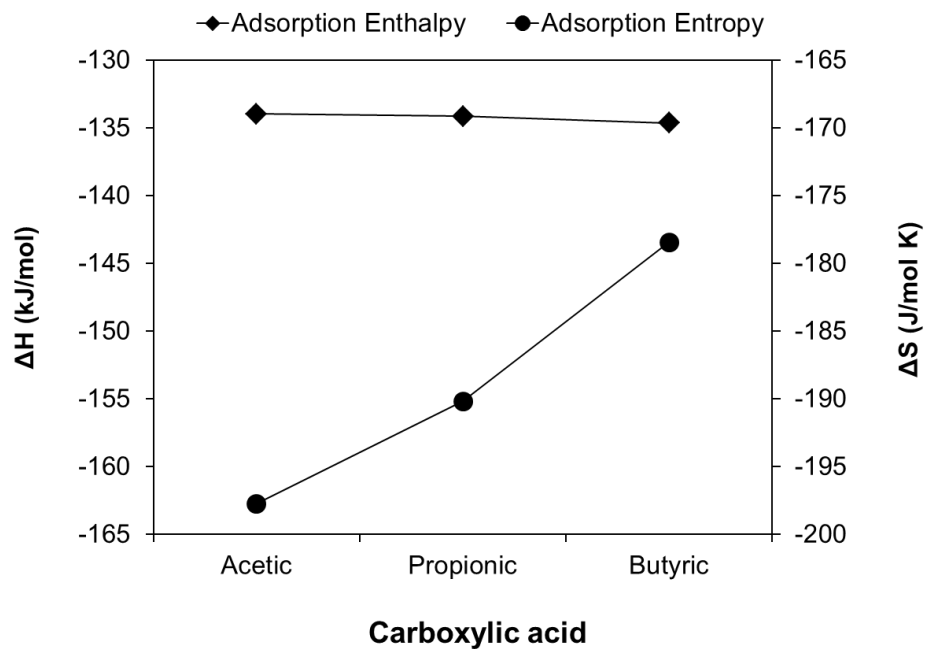
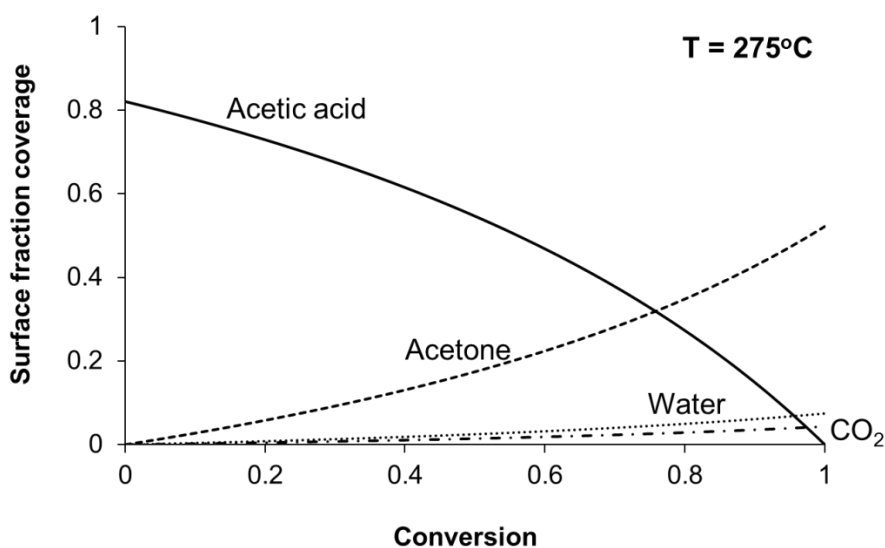


Figure 29. Adsorption enthalpies and entropies as function of carbon chain length of acid and ketones over Ru/TiO₂ catalyst

It is important to note that Vannice [20] has recommended a set of criteria to validate the thermodynamic parameters extracted from kinetic fittings. The ΔS_{ads} must

be negative and its absolute value must be smaller than the standard entropy in the vapor phase. Indeed, both criteria have been met for the calculated ΔS_{ads} values of all species involved in the kinetics analysis.

In contrast to the acids, the absolute values of the changes in both adsorption enthalpy and entropy of the ketones increase with the alkyl chain length with respect to the gas phase (see Figure 29 (b)). In comparison to the adsorption constants of the acids (K_{Acid}), the constants of the ketones (K_{Ketone}) are smaller, but still significantly higher than those of water and CO_2 , which indicates that these two products would only compete weakly for adsorption sites during the reaction. In fact, as shown in Figure 30, when the fractional surface coverages of acid, ketone, water, and CO_2 are calculated as a function of conversion, we can see that, at low conversion, the surface is practically covered by the carboxylic acid, and only at the highest conversion levels is the ketone a strong adsorption competitor. The coverages of water and CO_2 were kept very low in all cases for the entire conversion range. Therefore, during the course of the reaction, ketones are the strongest inhibitors of ketonization activity.



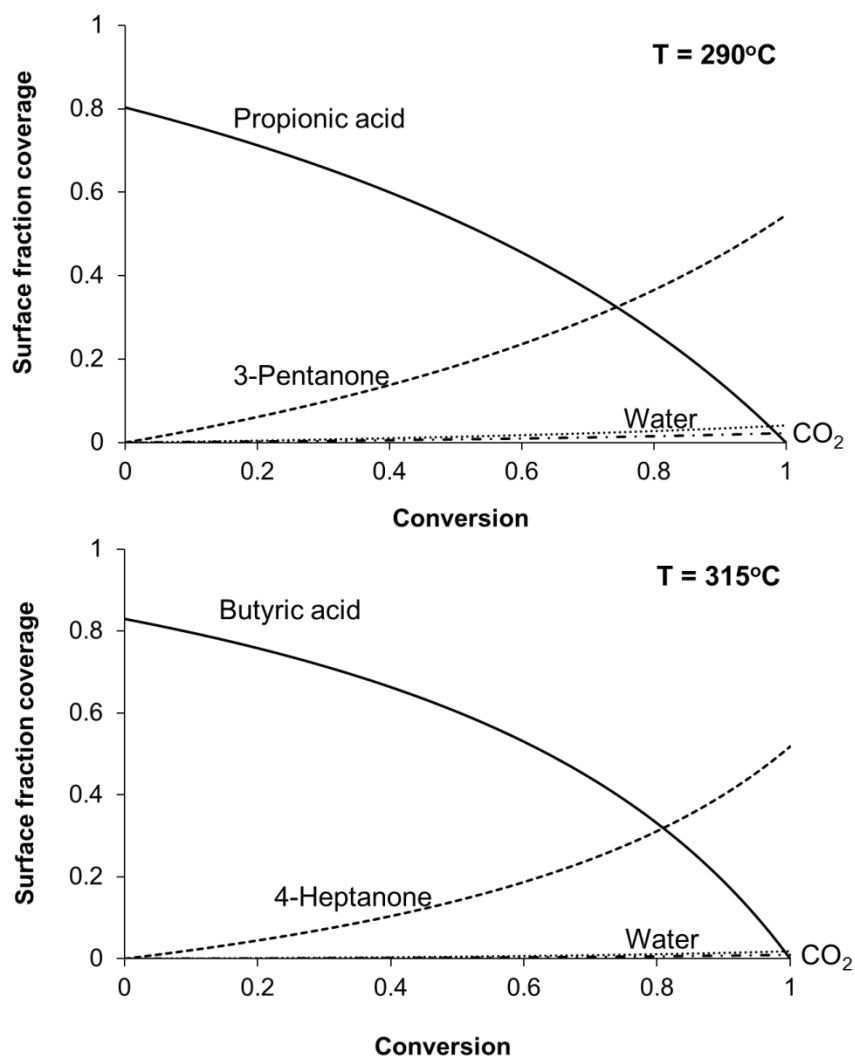


Figure 30. Surface fraction coverage of acid, ketone, water and CO₂ as a function of conversion over Ru/TiO₂ catalyst

Tables 8-10 also include the kinetic rate constants (k_i) obtained from the fittings for three acids. Since this rate constant corresponds to the individual rate constant of the rate-limiting step in the mechanism, the E/R values calculated for each acid from the slopes of the Arrhenius plots (Fig. 31) correspond to true activation energies. Accordingly, the resulting values are 161, 186, and 225 kJ/mol for the ketonization of acetic, propionic, and butyric acids, respectively.

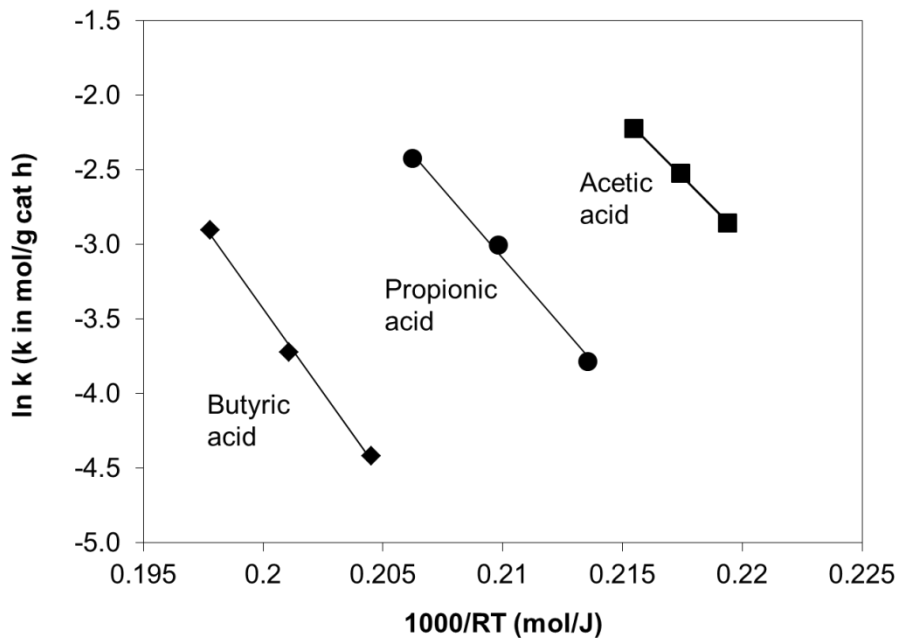


Figure 31. Natural log of kinetic rate constant (k) as a function of inverse reaction temperature

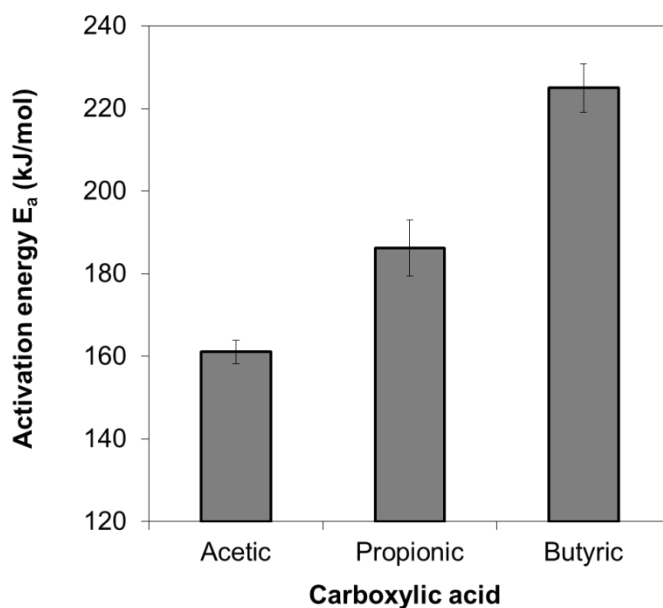


Figure 32. Ketonization activation energies as a function of carbon chain length. Error bars indicate 95% confidence interval

The value of 161 kJ/mol found for acetic acid is in close agreement with activation energy values previously reported. For example, Kuriacose and Rajadurai [21] working below 400°C obtained a value of 159 kJ/mol for the true activation energy over Zn:Cr:Fe mixed oxides and 141 kJ/mol over iron oxide [22]. By contrast, the value reported for the reaction over ZrO₂ was noticeably higher, 193 kJ/mol [11,23].

As shown in Figure 32, a clear trend is observed in the true activation energy as a function of alkyl chain length. As discussed in more detail below, this trend can shed light on the nature of the transition state for the ketonization reaction since the true activation energy is the difference in enthalpy between the adsorbed species and the transition state.

Table 11. Measured rate obtained at 275°C and after 30 minute time on stream using different pre-treated Ru/TiO₂

Catalyst pretreatment	W/F (hr)	Conversion (%)	Measured rate (mol./h/g)
Pre-reduction	0.116	18.23	2.66E-02
As-synthesized	0.116	12.78	1.86E-02
Reduction+ Oxidation	0.116	10.85	1.58E-02
Pre-reduction	0.384	36.9	1.61E-02
As-synthesized	0.384	25.8	1.13E-02
Reduction+ 30-min Oxidation	0.384	22.3	9.75E-03
Reduction+ 60-min Oxidation	0.384	22.7	9.92E-03

To investigate the nature of catalytically active sites for ketonization more closely, a comparison in acetic acid ketonization rate obtained at 275°C was conducted over as-synthesized Ru/TiO₂ catalysts pre-treated in different ways: (i) pre-reduced in H₂, (ii) pre-reduced in H₂ and then reoxidized in 5% O₂/He for 30 to 60 mins and (iii) no pretreatment.

The results are summarized in Table 11. As displayed, the reduced catalyst has the highest activity among the three, suggesting the generation of more active sites upon reduction. However, after the re-oxidation step, a significant decrease in activity was observed, indicating a decrease in the number of active sites by the oxidation process.

B.5.4. Discussion

B.5.4.1. Nature of Catalyst Active Sites

The liquid phase ketonization as discussed in Chapter 5 has demonstrated that Ru alone is inactive for ketonization but the addition of Ru enhances the ketonization activity of a reducible oxide, such as TiO₂. A detailed characterization of the catalysts indicated that the catalytically active sites for ketonization are coordinatively unsaturated Ti cations, whose presence can be enhanced by Ru which greatly facilitates the reducibility of TiO₂, i.e., formation of surface Ti³⁺ species. The comparison in activity between pre-reduced/reoxidized surfaces presented above serves as another important evidence. As can be seen, the activity drops after the re-oxidation step, suggesting the elimination of the active sites by oxygen titration of the unsaturated cations. All of these evidences support the hypothesis that the active sites should be the coordinatively unsaturated cations. Similar mechanisms have been proposed in earlier

literature [24,25]. The detailed kinetic investigation in this study provides more evidence to support this conclusion.

For all the temperatures and acid types tested in this study, the adsorption of acids was found to be significantly stronger than that of ketones, water, or CO₂, which favors the ketonization reaction. Among the three products, ketones are the more strongly adsorbed and, as shown in Figure 30, they compete more effectively with the acids for active sites than the other products. Ketones have been shown to preferentially bind to coordinatively unsaturated Ti cation sites through the oxygen atom of the carbonyl group in an η^1 coordination [26], which correlates well with the proposed nature of the ketonization active sites.

Similarly, the observed negative effect of water on catalyst activity is likely due to its competitive adsorption with acid to the surface cations as coordination sites [27]. Likewise, CO₂ could potentially impede the reaction through either the formation of carbonate or adsorbed CO₂ via Ti–O–C–O bonding on the catalyst surface [28]. However, in comparison with ketones, water and CO₂ have a much lower inhibiting effect on ketonization activity. The weak adsorption of water on TiO₂ is consistent with previous reports by Deng et al [29]. By contrast, the influence of CO₂ on ketonization activity seems to be highly dependent on the support properties. For example, Gaertner et al. [30] have shown that the ketonization activity of a ZrO₂-CeO₂ catalyst was drastically reduced upon the addition of CO₂ and water. This apparent contradiction with the results reported here is most likely due to the higher basicity of CeO₂ than TiO₂, forming strongly adsorbed carbonate on CeO₂ surface.

B.5.4.2. Nature of the Adsorbed Species under Reaction Conditions

The strong heats of adsorption derived from the kinetics for the three acids do not depend on the length of the alkyl chain. As shown in Figure 29, the Langmuir Hinshelwood kinetic fitting results yield almost identical heats of adsorption for acetic, propionic, and butyric acids on Ru/TiO₂ catalyst. Moreover, experimental studies, such as scanning tunneling microscopy [31] and vibrational spectroscopy [34], as well as computational studies involving ab-initio slab calculations [32] have shown that the most stable adsorption mode of monocarboxylic acids, such as formic and acetic acids, on either anatase or rutile TiO₂ is the bridging (bidentate) configuration, in which two oxygen atoms of carboxylates bound to two surface Ti cations. Therefore, one can conclude that, under the reaction conditions, the acids adsorb on the oxide via formation of a bidentate species with the surface via the two O on the carboxylic group, with little or no interaction of the alkyl chain with the surface.

Reported direct measurements of heats of adsorption of these acids on TiO₂ include a distribution of values, which are in the same range as those derived from our kinetics study. For example, Bowker et al. [33] have measured heats of dissociative adsorption of formic acid on TiO₂ (110) single crystals on the order of 125 kJ/mol. For Wang et al. [34] the heat of adsorption of acetic acid on anatase was around 100 kJ/mol. Idriss et al. [35, 36] obtained essentially the same heats of adsorption, about 160 kJ/mol, for formic and acetic acids on TiO₂ (110). While the absolute value is somewhat higher than those found in our work, the constant heat of adsorption for different acids is in good agreement with our observations.

While the adsorption enthalpies were essentially constant for the three acids, the adsorption entropies changed considerably and systematically. It was found that, relative to their gas phase values, acetic acid showed the highest loss of entropy upon adsorption, while butyric acid showed the lowest. That is, the loss in entropy upon adsorption appears to decrease with increasing length of the alkyl group. This trend can be rationalized in terms of the proposed adsorption species. That is, the number of degrees of freedom that can be retained in the molecule upon anchoring the end carboxylic group to the surface while leaving the alkyl chain free directly increases with the alkyl chain length. Therefore, together with the observed constant adsorption enthalpy values, the observed trend in entropy gives further support to the picture of a bidentate carboxylate adsorbed species, with the alkyl group not interacting with the surface or interacting only weakly.

B.5.4.3. Nature of the Transition State

The transition state theory can provide a physical justification to the kinetic parameters derived from the fitting as well as some insight into the structure and configuration of the transition state involved in the chemical reaction. The transition state theory assumes the occurrence of an activated complex that is in equilibrium with reactants and readily converts into products in a single vibration.

As proposed above, the rate limiting step (5) can be described by the following equations:



Where $[2RCOOH^\ddagger]$ can be either $[RCO \cdots RCOO^\ddagger]$ or $[RCOR \cdots COO^\ddagger]$ for early and late transition states, respectively.

From this equation, the ketonization rate as derived from transition state theory will be equal to the concentration of the activated complex multiplied by the frequency at which the new C-C bond is formed.

$$rate = \nu^\# K^\# [2RCOOH^*]^2 \quad (14)$$

where $\nu^\#$, the vibration along the reaction coordinate, corresponds to the vibration of the C-C bond being formed. Equilibrium constant $K^\#$, based on statistical mechanics, can be written as:

$$K^\# = q_{vib}^{asym} K'^\# \quad (15)$$

in which q_{vib}^{asym} is the partition function for the loose anti-symmetric vibrational mode along the reaction coordinates, leading to the formation of the new C-C bond and $K'^\#$ represents the equilibrium constant with the loose vibration removed. The loose vibration is fully excited (high temperature limit) and can be described by:

$$q_{vib}^{asym} = \frac{1}{1 - e^{-h\nu^\# / k_B T}} \approx \frac{k_B T}{h\nu^\#} \quad (16)$$

Canceling $\nu^\#$ in (14) with the derived partition function for the C-C bond vibration stretch at the transition state (16) gives:

$$rate = \nu^\# \frac{k_B T}{h\nu^\#} K'^\# [2RCOOH^*]^2 = \frac{k_B T}{h} K'^\# [2RCOOH^*]^2 \quad (17)$$

where k_B and h are the Boltzmann and Planck constants, respectively, and $K'^\#$ is the transition-state equilibrium constant (calculated from partition functions for the activated complex which exclude the C-C bond stretch along the reaction coordinate). According to Polanyi-Eyring, this $K'^\#$ value reflects the enthalpy and entropy of activation, which can be calculated using the following equation:

$$rate = \frac{k_B T}{h} e^{-\Delta H / RT} e^{\Delta S / R} [2RCOOH^*]^2 \quad (18)$$

It is noteworthy that the rate in transition state analysis is on a per catalytic active site basis, which is calculated as follow:

$$\text{Number of catalyst sites} = \text{Catalyst mass (g)} \times \text{Catalyst surface area (m}^2\text{/g)} \times \text{Ti cation density (Ti sites/nm}^2\text{)} \times 10^{18} \text{ nm}^2\text{/m}^2$$

The catalyst surface area was obtained from BET measurements. The Ti cation density value was obtained from relevant literature in surface science [37].

In some kinetics studies, the barriers derived from fitting pseudo first-order rate expressions are “apparent” values, relative to the gas phase [16,38]. It is important to note that since we use a full LH equation to fit the reaction rate measurements, the rate constant thus derived includes the true enthalpy and entropy of activation for the C-C bond formation (or breaking) with respect to the surface adsorbed species (single elementary step (5)). Therefore, the values of ΔH^\ddagger and ΔS^\ddagger in Eq. 18 refer to the differences between the H and S values of the transition state and those of the adsorbed reactants (i.e. two adsorbed acid molecules).

The goodness of the kinetic fitting for a second order LH model with respect to adsorbed acid coverage supports the suggested mechanism involving two adsorbed carboxylate species on the surface that form a β -ketoacid intermediate, as previously proposed [10,23].

Table 12 summarizes the resulting activation enthalpies and entropies of acetic, propionic and butyric acid, respectively. It is clear that the activation enthalpy (ΔH^\ddagger) increases monotonically with increasing alkyl chain length, which can be described as an increased energy barrier for the rate-limiting step as the size of the alkyl chain increases. Similarly, the changes in activation entropies ΔS^\ddagger are positive and also

increase as a function of carbon chain length. That is, the entropy of the transition state is higher than that of the two adsorbed acids and, more interestingly, the entropy gain increases with the length of the alkyl chain. That is, there seems to be a correlation between entropy and enthalpy.

Table 12. Activation enthalpies and entropies for ketonization of acetic, propionic and butyric acid over Ru/TiO₂ catalyst

	Activation enthalpy ΔH (kJ/mol)	Activation entropy ΔS (J/mol K)
Acetic acid	156.4	3.4
Propionic acid	181.5	32.4
Butyric acid	220.0	78.2

In fact, as shown in Figure 33 a, the well-known compensation effect [39-41] is clearly apparent in these data. Bond et al. [42,43] have suggested that the compensation effect may be a result of using apparent activation enthalpy and entropy. However, we must emphasize that, in this work, the compensation effect is observed with true enthalpy and entropy (see Figure 33 b).

Many years ago, Everett [44] made the observation of the commonly observed linear relationship between entropy and enthalpy of adsorption, which can be interpreted taking into account that a greater binding energy of the molecule to the surface would restrict its vibrational and rotational degrees of freedom. This is not the case in our system, in which no compensation effect is observed for the adsorption. In fact, the heats of adsorption remained constant as a function of the alkyl chain length, but the entropy of adsorption did increase due to a greater number of degrees of freedom with increasing chain length. By contrast, the compensation effect was in fact

observed for the enthalpies and entropies of activation, when the transition state was involved, which gives us more information about the nature of this species and consequently, sheds light on the reaction mechanism.

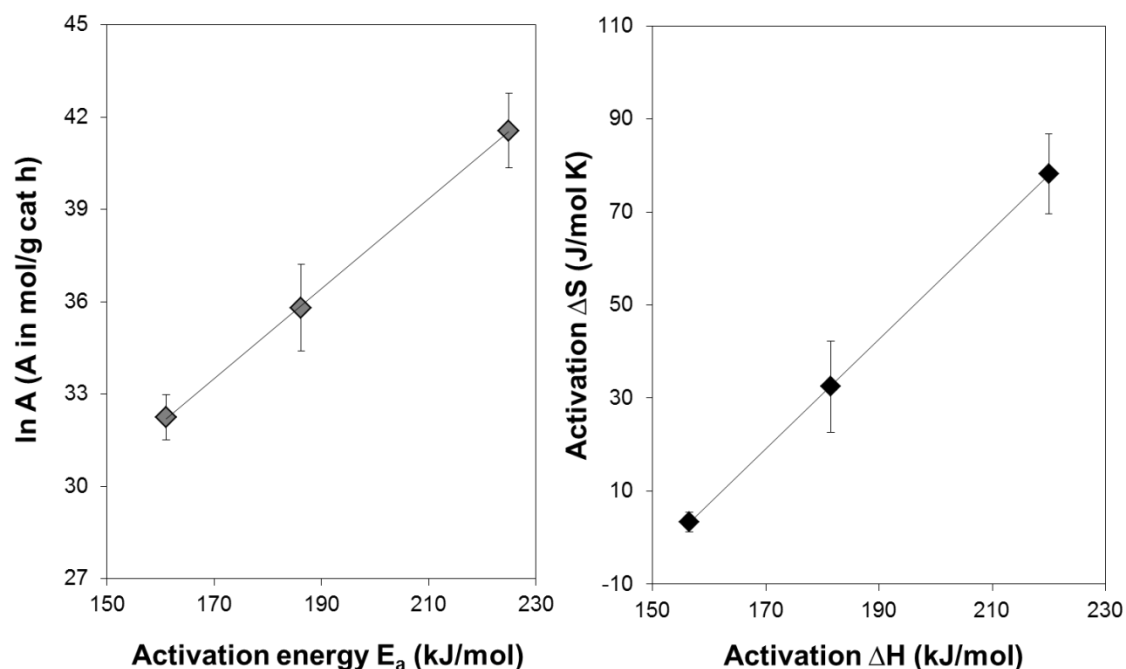


Figure 33. Compensation plots for ketonization of acetic, propionic and butyric acids over Ru/TiO₂ catalyst. Error bars indicate 95% confidence interval.

As mentioned above, the ketonization can either go through an early or a late transition state, depending on the position of the energy peak along the reaction coordinate. The early transition state involves the formation of the C-C bond between the two adsorbed carboxylates, leading to the formation of the β-ketoacid (RCO•••RCOO) intermediate. In contrast, the late transition state involves the decarboxylation of β-ketoacid (RCOR•••COO), as suggested by Renz et al. [45].

The observed trend in activation enthalpy is an increase in the following order, acetic < propionic < butyric. We believe that this trend supports the idea of an early transition state, since we can expect that increasing the alkyl chain length would

enhance the energy requirement to overcome the increasing steric repulsion of bulkier alkyl groups that make the formation of the C-C bond more difficult. In other words, larger molecules imply larger spatial hindrance to overcome to reach the appropriate coupling configuration, and therefore a higher energy requirement. In contrast, in the case of the late transition state, we would not expect a higher enthalpy barrier with increasing alkyl chain length. The decarboxylation of β -ketoacid only involves the redistribution of electrons within the ketone and acid functional group [46], which is not only a relatively simple process from an energy requirement point of view, but also independent of the alkyl chain length.

The positive activation entropy for all three acids with respect to the adsorbed state indicates that the bidentate carboxylates go through a transition state with an entropy gain. This is indicative of a structure for the activated complexes with more degrees of freedom than the sum of the two adsorbates.

During the catalytic cycle the transition state could undergo a transformation to a less restricted adsorption configuration such as monodentate linkage to the surface, but the increase in entropy is most probably related to intramolecular configurational contributions to the entropy. Configurational entropy is the portion of a system's entropy related to the position of its constituent particles or physically related to the number of ways of arranging all the particles of the system. Its partition function becomes larger upon inter-molecular coupling in comparison to changes that might occur in the translational, vibrational and rotational contributions. As a result, the longer the alkyl chain the greater would be the enhancement in configurational entropy, which would explain the observed trend, i.e., acetic < propionic < butyric. While one

expects the same trend in entropy increase for both, early and late transition state cases, the activation entropy trend supports the notion that the rate limiting step is the formation of a surface dimer with more possible configurations than the adsorbates. Correspondingly, the activation enthalpy trend indicates an early transition state (i.e. formation of the C-C bond).

B.5.5. Summary

In this study, we have conducted a comprehensive kinetics analysis of the ketonization of carboxylic acids with different alkyl chain lengths over a pre-reduced Ru/TiO₂ catalyst. A Langmuir Hinshelwood model that considers second order kinetics with respect to surface coverage of carboxylic acids and competitive adsorption of products can accurately describe the ketonization reaction over a wide range of reaction conditions (temperature, composition) for three different acids. Detailed analysis of the kinetics data revealed significant insights into the reaction.

- a) The carboxylic acids adsorb on the catalyst surface in a bidentate bridging mode via the carboxylic group with little or no interaction of the alkyl groups with the surface, as evidenced by the independence of the adsorption enthalpies of acids on carbon chain length and the decreased entropy change upon adsorption of increasingly longer chains.
- b) Both the enthalpy and entropy of activation for the ketonization reaction increase with increasing alkyl chain length of the acid. Transition state theory analysis suggests that the reaction path proceeds through an early transition state towards the formation of the β -ketoacid intermediate via bimolecular coupling of two

surface carboxylates in which the formation of C-C bonds is hindered when the alkyl groups are bulkier.

References

- [1] C. Friedel, *Ann.* 108 (1858) 125.
- [2] S. Sifniades, A. B. Levy, *Acetone in Ullmann's Encyclopedia of Industrial Chemistry*; Wiley-VCH: Weinheim, Germany (2005).
- [3] T.N. Pham, T. Sooknoi, S.P. Crossley, D.E. Resasco, *ACS Catal.* 3 (2013) 2456.
- [4] D.M. Alonso, J.Q. Bond, J.A. Dumesic, *Green Chem.* 12 (2010) 1493.
- [5] S.H. Hakim, B.H. Shanks, J.A. Dumesic, *Appl. Catal., B* 142 (2013) 368.
- [6] R.W. Snell, B.H. Shanks. *ACS Catal.* 4 (2014) 512
- [7] R. Aguado, M. Olazar, M.J. San Jose, G. Aguirre, J. Bilbao, *Ind. Eng. Chem. Res.* 39 (2000) 192.
- [8] J. Kijenski, M. Glinski, A. Jakubowski, *Appl. Catal., A* 128 (1995) 209
- [9] R. Pestman, R.M. Koster, A. van Duijne, J.A.Z. Pieterse, V. Ponec, *J. Catal.* 168 (1997) 265.
- [10] O. Nagashima, S. Sato, R. Takahashi, T.J. Sodesawa, *Mol. Catal A: Chem.* 227 (2005) 231.
- [11] A. Ignatchenko, E. Kozliak, *ACS Catal.* 2 (2012) 1555.
- [12] K. M. Dooley, A.K. Bhat, C.P. Plaisance, A.D. Roy, *Appl. Catal. A* 320 (2007) 122.
- [13] F. Gonzalez, G. Munuera, J.A. Prieto, *J. Chem. Soc. Faraday Trans.* 1(1978)1517.
- [14] S. Rajadurai, *Catal. Rev.* 36 (1994) 385.

-
- [15] J. A. Dumesic, D. F. Rudd, L. M. Aparicio, J. E. Rekoske, A. A. Treviño, *The microkinetics of heterogeneous catalysis*. ACS Professional Reference Book, American Chemical Society, Washington, DC, (1993).
- [16] D. W. Flaherty, E. Iglesia, *J. Am. Chem. Soc.* 135 (2013) 18586.
- [17] T. Komaya, A.T. Bell, Z. Weng-Sieh, R. Gronsky, F. Engelke, T.S. King, M. Pruski. *J. Catal.* 150 (1990) 400
- [18] H.S. Fogler. *Elements of Chemical Reaction Engineering*. 4th edition (2005). Prentice Hall Publisher. Chapter 10-12
- [19] M.A. Vannice. *Kinetics of Catalytic Reaction*. 1st edition (2005). Springer Publisher.
- [20] M.A. Vannice, S.H. Hyun, B. Kalpakci, W.C. Liauh, *J. Catal.* 56 (1979) 358.
- [21] S. Rajadurai, J.C. Kuriacose. *Mater. Chem. Phys.* 16 (1986) 17.
- [22] J.C. Kuriacose, S.S. Jewur, *J. Catal.* 56 (1977) 330.
- [23] A.V. Ignatchenko, *J. Phys. Chem. C* 115 (2011)16012.
- [24] S. Ricote, G. Jacobs, M. Milling, Y. Ji, P.M. Patterson, B.H. Davis, *Appl. Catal. A* 303 (2006) 35.
- [25] W. Curtis Conner, J.L. Falconer, *Chem. Rev.* 95 (1995) 759.
- [26] M.A. Henderson, *J Phys Chem B* 108 (2004) 18932.
- [27] A. Vittadini, A. Selloni, F.P. Rotzinger, M. Gratzel, *J. Phys. Chem. B* 104 (2000) 1300.
- [28] L.F.Liao, C.F. Lien, D. L. Shieh, M.T. Chen, J.L. Lin, *J. Phys. Chem. B* 10 (2002) 11240.
- [29] L.Deng, Y. Fu, Q.X. Guo, *Energy & Fuels* 23 (2009) 564.

-
- [30] C.A. Gaertner, J.C. Serrano-Ruiz, D.J. Braden, J.A. Dumesic, *J. Catal.* 266 (2009) 71.
- [31] Onishi, H.; Aruga, T.; Iwasawa, Y. *J. Am. Chem. Soc.* 1993, 115, 10460
- [32] S. P. Bates, G. Kresse, M.J. Gillan, *Surf. Sci.* 409 (1998) 336.
- [33] M. Bowker, P. Stone, R. Bennett. Perkins, N. *Surf. Sci.* 511 (2002) 35.
- [34] C.Y. Wang, H. Groenzing, M.J. Shultz., *J. Am. Chem. Soc.* 127 (2005) 9736.
- [35] J.M. R. Muir, H. Idriss, *Surf. Sci.* 607 (2013) 187.
- [36] P.R. McGill, H. Idriss, *Surf. Sci.* 602 (2008) 3688.
- [37] D. Brinkley, M. Dietrich, T. Engel, P. Farrall, G. Gantner, A. Schafer, A. Szuchmacher. *Surf. Sci.* 395 (1998), 292
- [38] A. Bhan, R. Gounder, J. Macht, E. Iglesia. *J. Catal.* 253 (2008) 223.
- [39] A.K. Galwey , *Adv. Catal.* 26 (1977) 247
- [40] L. Liu, Q-X. Guo. *Chem. Rev.* 101 (2001) 673
- [41] G.C. Bond, M.A. Keane, H. Kral, J.A. Lercher. *Catal. Rev. Sci. Eng.* 42 (2000) 323
- [42] G. C. Bond, *Catal. Today* 17 (1993) 399
- [43] G. C. Bond, A. D. Hooper, J. C. Slaat, A. O. Taylor, *J. Catal.* 163 (1996) 319
- [44] D. H. Everett, *Trans. Faraday Soc.* 46 (1950) 957
- [45] A. Pulido, B. Oliver-Tomas, M. Renz, M. Boronat, A. Corma, *ChemSusChem* 6 (2013) 141
- [46] F. A. Bettelheim, W. H. Brown, M. K. Campbell, S. O. Farrell, *Introduction to General, Organic and Biochemistry*, 9th edition, 2010

B.6. General Conclusions and Recommendations for Ketonization

With the ultimate goal of bio-oil upgrading to fungible transportation fuels, this work has focused primarily on the more fundamental chemistry of potentially important heterogeneously catalyzed ketonization reaction. Ketonization was investigated as an ideal reaction to eliminate acidity, enlarge carbon chain length and remove oxygen to improve the stability and energy content of bio-oil. However, the presence of aqueous environment and competing coke forming side reactions in biomass conversion reactions present challenges for utilization of conventional ketonization catalyst. Therefore, it would be crucial to develop more active and hot-water tolerant ketonization catalyst for the process. Unfortunately, very little was understood about the reaction including both detailed mechanism and desirable catalyst properties. With this in mind, the objective of this study was to gain a more fundamental understanding of the reaction to engineer a better catalyst for bio-oil upgrading application.

Our initial study started with the system of using simple TiO_2 catalyst to promote ketonization in the aqueous phase at moderate temperature using acetic acid as the model acid carboxylic compound present in the bio-oil. The results indicated that TiO_2 showed small activity for this reaction under the testing condition. Moreover, it was found that the incorporation of Ru and pre-reduction of TiO_2 significantly enhanced the catalytic activity. A detailed characterization investigation, including X-ray photoelectron spectroscopy, temperature programmed reduction and electron paramagnetic resonance clearly suggested that the addition of Ru on TiO_2 and pre-reduction of catalyst under H_2 facilitates the formation of coordinatively unsaturated Ti^{3+} as the catalytic active sites for ketonization.

In the next step, a kinetics study was performed on ketonization of carboxylic acids of varying alkyl chain lengths (acetic, propionic, and butyric) catalyzed by a pre-reduced Ru/TiO₂ catalyst as developed in the previous step. A thorough analysis built upon a Langmuir Hinshelwood model that considers second order kinetics with respect to surface coverage of carboxylic acids and competitive adsorption of products can accurately describe the ketonization reaction over a wide range of reaction conditions (temperature, composition) for three different acids. The kinetics analysis revealed significant insights into the reaction. The heats of adsorption were found to be very similar for the three different acids, independent of the carbon chain length, and significantly higher than those of the ketonization products, i.e. ketone, water and CO₂. At the same time, the change in adsorption entropy of the acids (in absolute value) with respect to the gas phase was found to decrease with increasing alkyl chain length. These results are consistent with a strongly adsorbed bidentate configuration, in which the main interaction with the surface is via the carboxylic group while the alkyl group moves rather freely. In addition, both the true activation energy and the activation entropy were found to increase with increasing carbon chain length of the acids, indicating that larger molecules imply larger spatial hindrance to overcome to reach the appropriate coupling configuration, and therefore a higher energy requirement. The positive activation entropy for all three acids with respect to the adsorbed state as well as the compensation effects indicate that the bidentate carboxylates go through that ketonization proceeds through a β -ketoacid intermediate with an early transition state, in which the C-C bond forms.

While much about the ketonization reactions and how they relate to the upgrading of bio-oil was learned in this study, there remains many different research directions that can be taken to further understanding.

Our kinetics investigation demonstrates that the self ketonization strongly depends on the molecular structure of acids. Thus it seems attractive to expand that study to the mixture of acids for cross ketonization. A project is envisioned in which ketonization activity is tested over a mixture of carboxylic acids with different carbon chain length. The results of this study could then allow comparing the activation energy of self and cross ketonization, and understanding the role of the acid structure in cross ketonization.

From bio-oil application stand point, one important issue that must be addressed is the investigation of catalyst stability for ketonization catalysts in the presence of other compounds in the liquid mixture, such as furanics. For example, Hakim *et al.* studied the catalytic upgrading of acetic acid in the presence of other common bio-oil compounds including furfural, acetol, p-cresol, and levoglucosan over a bed of CeZrO₂ to investigate the effects of these compounds on ketonization. Known as a highly active catalyst for carboxylic acid ketonization, CeZrO₂ showed high stability for ketonization of pure acetic acid for long time on stream. However, the conversion of acetic acid dramatically decreased by 90% when furfural was added to the feed. This result suggests that it is likely that the metal oxides will not be stable in the presence of highly prone to coke compounds such as furfural. A detailed study on the effects of other bio-oil compounds on Ru/TiO₂ catalyst is required. In addition, other alternatives must be examined and studied as well. For example, introducing a metal function into the

catalyst system, which is capable of converting strongly inhibiting species and cleaning the catalyst surface is particularly promising. Another potential approach is through oxidation step to completely convert all compounds into acids, which then undergo ketonization. This strategy could be highly advantageous with regard to catalyst performance. However, a detailed study of the mixed acid as aforementioned would be needed.

C. Catalytic Conversion of Bio-Ethanol to 1,3-Butadiene

(This study is in collaboration with Abengoa Research, Spain)

C.1. Motivation

Ethanol production from corn as well as lignocellulosic biomass feedstock has seen a fast and continuous increase in its production worldwide, from 13,123 million gallons in 2007 to 21,812 million gallons in 2012, and is projected to 24,000 million gallons by the end of 2014, vastly attributed to the technological advances in production process [1]. Most of the bio-derived ethanol is currently used as a partial gasoline replacement. However, its low energy content and high corrosion aggressiveness remain the major drawbacks for transportation purpose. In addition, since 2012, the entire ethanol industry has been experiencing tight margins due to faster increase in corn price in comparison with ethanol price [2]. A process that uses ethanol as the feed source and targets more valuable chemicals is potentially more economically beneficial, depending on the technological merit of the process.

One case in point is the conversion of ethanol to produce 1, 3-butadiene (or butadiene), an important industrial chemical widely used in the production of numerous valuable polymers, including polybutadiene and polystyrene-butadiene. Worldwide demand for butadiene is expected to grow steadily at about 3% per year [3,4]. Currently, over 95% of global butadiene production is by naphtha steam cracking of paraffinic hydrocarbons. In this process, butadiene is one of the co-products in the production of ethylene and is purified by a butadiene recovery process [4]. However, in recent years, the increase in shale gas production has triggered the proliferation of

ethane cracking in substitution of naphtha steam cracking, which has tightened butadiene supply [5].

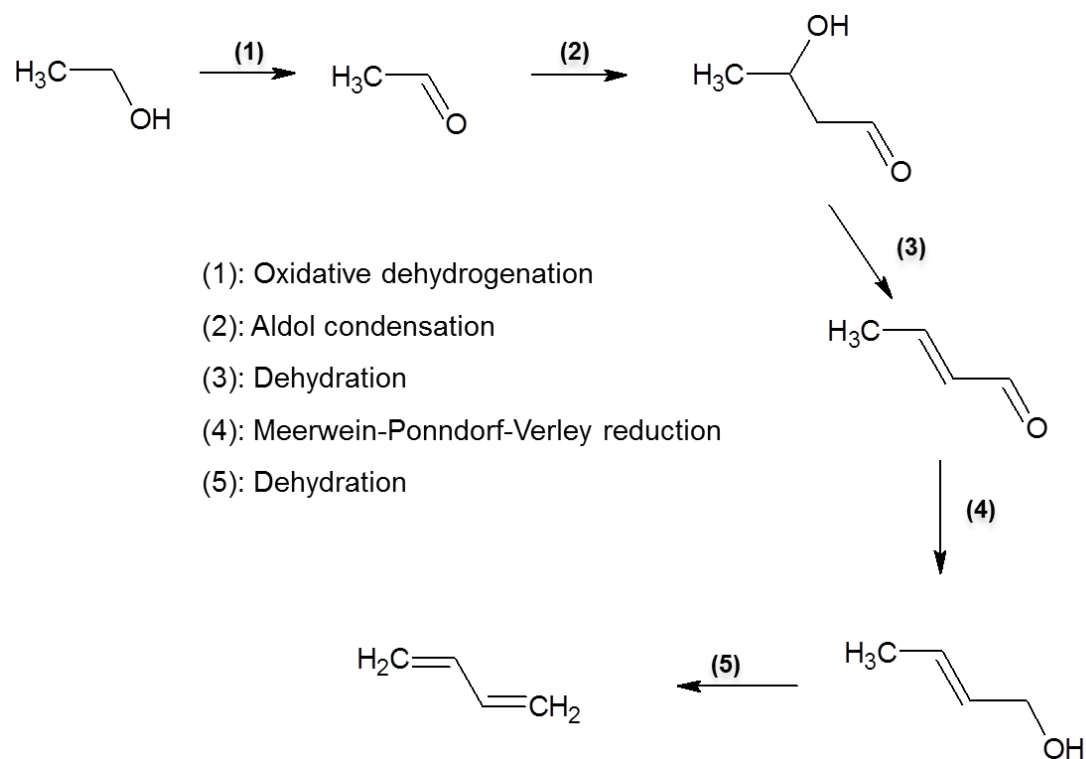


Figure 34. Reaction pathway to convert ethanol to butadiene

Conversion of ethanol to butadiene can be achieved through several reaction steps as proposed by Toussaint *et al.* [6] and schematically described in Figure 34. During World War II, butadiene was solely produced in the United States via the two-step, namely Ostromislensky process. In the first step, ethanol is dehydrogenated to form acetaldehyde. In the second step, acetaldehyde undergoes aldol condensation to produce hydroxybutanal, which is dehydrated into crotonaldehyde and then reduced to crotyl alcohol via Meerwein–Ponndorf–Verley (MPV) reduction by ethanol. Crotyl alcohol, once formed, can be rapidly dehydrated into butadiene. MPV reaction is hydrogen transfer reduction of aldehydes and ketones by using alcohols as hydrogen

donors [7,8]. It is noteworthy by itself for its advantages over hydrogenation in its high chemoselective reduction of carbonyl groups in the presence of other reducible functional groups such as unsaturated C=C bond in an α, β - unsaturated ketones, as well as the avoidance of the use of expensive noble metals and hydrogen.

In this process, the most challenging step is producing crotyl alcohol with high selectivity from ethanol and acetaldehyde mixture. Therefore, an effective catalyst for the process would be one that can efficiently catalyze aldol condensation and MPV, converting ethanol-acetaldehyde mixture into crotyl alcohol and minimize byproducts during the process that are usually formed in significant amounts.

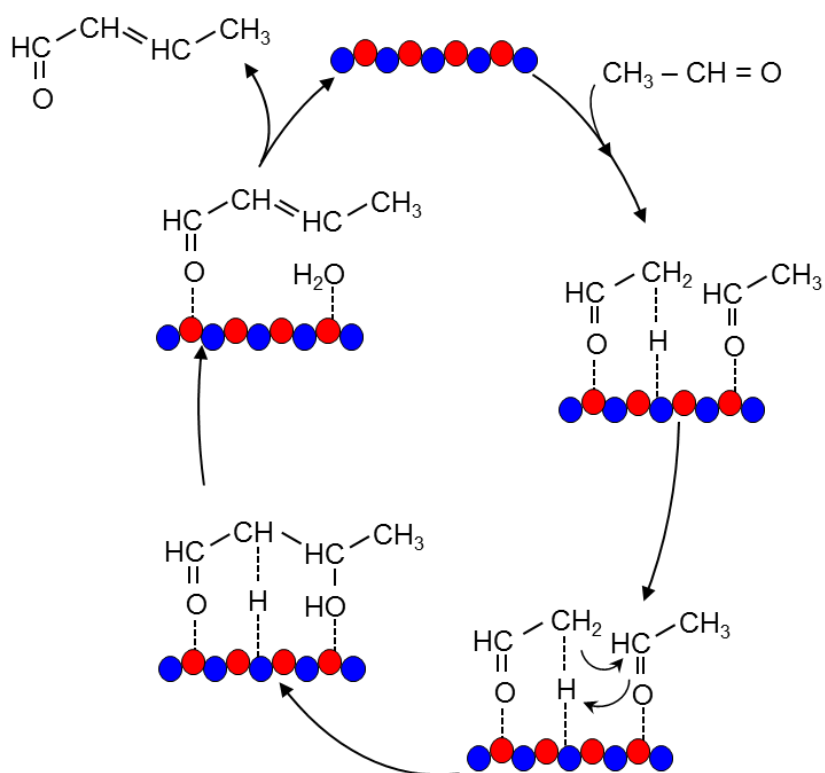


Figure 35. Base catalyzed mechanism for the aldol condensation of acetaldehyde followed by dehydration

Aldol condensation of aldehydes is a well-known reaction in organic chemistry. It has been known to be catalyzed by bases. As shown in Figure 35, reaction mechanism begins with a deprotonation of the α -carbon of one of the reactants to form an enolate anion. This enolate anion then acts as the nucleophile in an attack on the carbonyl of the other molecule involved to form an alkoxide anion. Protonation of this alkoxide reforms the catalyst and generates the product, which is quickly dehydrated to form larger aldehyde. It is noteworthy that achieving good selectivity with the aldol reaction is challenging as the product often continues to undergo further condensation to produce larger molecules.

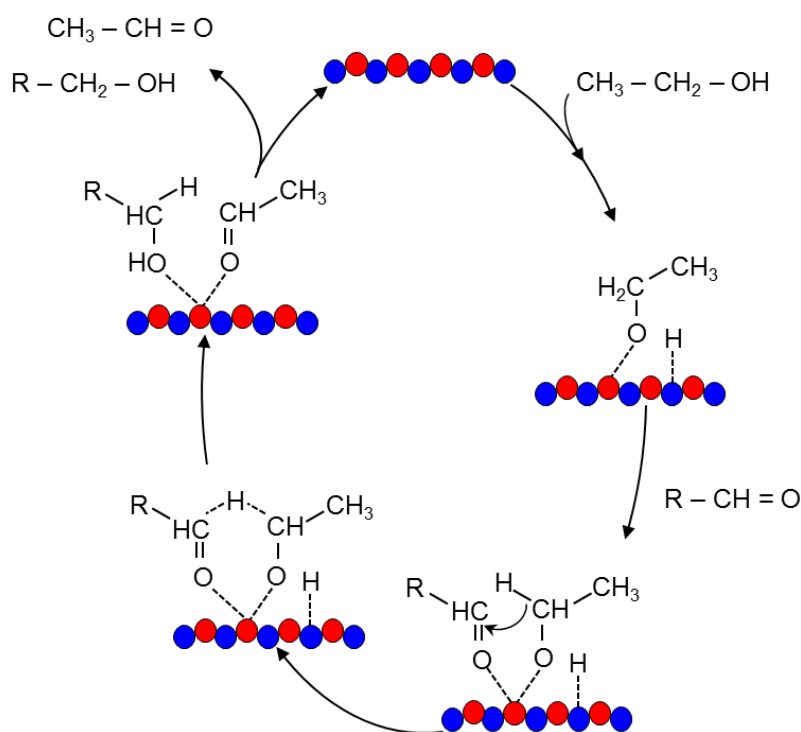


Figure 36. Meerwein-Ponndorf-Verley (MPV) reaction mechanism of acetaldehyde and ethanol

Traditionally, MPV reaction is conducted in the presence of a homogeneous metal alkoxide catalyst, e.g., aluminum or zirconium alkoxide [11-13]. It is widely

accepted that hydrogen transfer takes place from the dissociatively adsorbed alcohol (alkoxide) to the carbonyl compound coordinated to a Lewis acid site, through a six-membered ring, as depicted in Figure 36. Heterogeneous catalysts have been more explored for this process in the last three decades for their advantages over homogeneous catalysis such as easy separation and good reusability. Many solid catalysts have been developed and shown to possess high activity and selectivity for MPV reactions, including Beta zeolites [14-17] and various metal oxides [18-22].

In order to efficiently convert ethanol and acetaldehyde to crotyl alcohol, the catalyst is expected to be well balanced between acid and base properties, which are critical in achieving high selectivity and conversion. In this work, we have prepared mixed MgO and B₂O₃ with various B₂O₃ weight contents of 0%-15%. The effects of preparation method and catalyst composition on surface and catalytic properties have been investigated by combining characterization techniques and chemical reactions using ethanol and acetaldehyde as probe molecules. In addition, emphasis is placed on the high activity and selectivity of the catalyst toward MPV reactions, which, as a stand-alone reaction, has their own merit as mentioned above and therefore deserves special attention.

C.2. Experimental

C.2.1. Catalyst Preparation

Pure MgO and B₂O₃ were purchased from Alfa Aesar and used without further modification. Mixed MgO-B₂O₃ were prepared by thermal decomposition (citrate-nitrate combustion) method [23], using Mg(NO₃)₂ (Sigma-Aldrich, 99%) and B₂O₃ (Alfa Aesar, 99.999%) as precursors. Different ratios of Mg(NO₃)₂ and B₂O₃

corresponding to different final compositions were dissolved in deionized water. When the solution became clear, citric acid was added in a proportion of 1.2 mol acids per mol of metal atom. The mixture was then heated on a hot plate (at 140 °C) for 1 hour to evaporate the water. After that, it was quickly transferred and combusted inside an oven pre-heated to 550 °C. The grey ashes obtained after combustion were calcined at 550 °C for 12 hours in air to eliminate the carbonaceous residues. The resulting material was then grinded into a fine powder for use and labeled c-x-B-MgO with x as weight percent loading of Boron.

A 2 wt% loading of B₂O₃ on MgO catalyst was prepared by conventional incipient wetness impregnation of an aqueous solution of B₂O₃ (Alfa Aesar, 99.999%) onto MgO support (Alfa Aesar, 96%), at a liquid/solid ratio of 0.15 ml/g. After impregnation, the catalyst was dried overnight in an oven at 400°C.

C.2.2. Catalyst Characterization

The BET surface area of the catalyst was measured by N₂ physisorption at liquid nitrogen temperature on a Micromeritics ASAP 2010 unit. For these measurements, the sample was degassed for 12 h at 250°C prior to the analysis. X-ray diffraction (XRD) analysis was conducted on a Rigaku automatic diffractometer (Model D-MAX A), equipped with a curved crystal monochromator and system setting of 40kV and 35 mA. Data were collected over 5-40° angle range with a step size of 0.05 and a count time of 1.0 s.

The basic properties of the catalysts were characterized using temperature programmed desorption (TPD) of CO₂. A 100-mg sample was heated in the TPD system under a He flow of 30 mL/min to 200 °C with a heating rate of 10 °C /min and

held at this temperature for 3 h. The sample was then cooled down to room temperature and pure CO₂ at a flow-rate of 30 mL/min was then passed through the sample for 30 min. The sample was subsequently purged with He for 2 h to remove the physisorbed CO₂. The TPD was performed under the same He flow rate by heating from 0 to 600 °C with a heating rate of 10 °C /min.

X-ray Photoelectron spectroscopy (XPS) analysis was conducted on a Physical Electronics PHI 5800 ESCA system with standard non-monochromatic Al X-rays (1,486.6 eV) operated at 250W and 15 kV in a chamber pumped down to a pressure of approximately 1.0×10⁻⁸ Torr. A sealed transfer cell was used to transport the ex-situ dehydrated samples from a glove box to the analysis chamber without exposure to air. A 93.9 eV and 58.7 eV pass energy were typically used for survey and specific element analysis, respectively. The electron takeoff angle was 45° with respect to the sample surface. The binding energies were adjusted to the C signal at 284.6 eV as an internal reference.

¹¹B NMR experiments were performed on a Bruker AVIII HD NMR spectrometer operating at a magnetic field strength of 11.74 T with a 4 mm Bruker MAS probe. For the MAS experiments of ¹¹B (160.5299 MHz), a single pulse acquisition was applied with a spinning speed of 14 KHz and a short RF pulse (less than 15°) with a recycle delay of 15-20 s. Spectra were collected after 4096 scans and referenced to solid NaBH₄ at -42.16 ppm.

Scanning electron microscopy (SEM) imaging was carried out on a Zeiss NEON 40 EsB system equipped with a Schottky emitter electron source, and operated at an accelerating voltage of 2 kV using secondary electrons as the major signal source. High

angle annular dark-field scanning transmission electron microscopy (HAADF-STEM) characterization was carried out using a FEI Tecnai F30, operated at 300 kV equipped with a Gatan CCD camera, an EDS (EDAX) detector and a Gatan Tridiem Energy Filter. Aberration corrected STEM analyses were performed in a XFEG FEI Titan 60-300, operated at 300 kV, equipped with a monochromator, EDS detector and a Gatan Tridiem Energy Filter. The microscope possesses a CEOS spherical aberration corrector for the electron probe allowing a resolution of 0.8 Å.

C.2.3. Catalytic Activity Measurements

The liquid phase catalytic MPV reaction of acetaldehyde (99%, Sigma Aldrich) and ethanol (100%, Pharmco AAPER) was studied in a 50-mL stainless steel autoclave batch reactor (Parr Corporation), equipped with an impeller, temperature and pressure controllers. In a typical experiment, measured amounts of catalyst were mixed with 20 mL ethanol and 2 mL acetaldehyde and placed in the reactor vessel. After the reactor was sealed, it was purged and pressurized with N₂ to 300 psi and heated up to 250°C. High speed mechanical stirring kept the catalyst suspended to avoid external mass transfer limitations. After the reaction, products were filtered and analyzed using gas chromatography (GC). Product identification was done on GC-MS (Shimadzu QP2010S) equipped with a ZB-1701 column, 60.0 m long x 0.25 µm nominal. GC-FID (Agilent 7890B) with a capillary column of polyethylene glycol (ZB-WAX) of 60.0 m x 0.25 mm x 0.25 µm nominal was employed for quantification, using the corresponding chemical standards to obtain response factors.

C.3. Results

C.3.1. Catalyst Characterization

BET surface areas and pore volumes of commercial MgO, B₂O₃ and mixed c-B-MgO with different weight loading of Boron prepared by combustion method are shown in Table 13. MgO has relatively high surface area (225 m²/g), which is consistent with measurements reported in the literature [24]. B₂O₃, on the other hand, has much lower surface area (2 m²/g) in comparison with MgO. As expected, the effect of Boron incorporation on surface area and pore volume is found to be quite drastic with lower loading of Boron resulting in surface areas of 63-136 m²/g while higher loading materials has only 6-16 m²/g. This similar phenomenon has been seen elsewhere in literature for mixture of B₂O₃-MgO despite different preparation methods [25].

Table 13. BET surface area, pore volume and pore diameter of MgO, B₂O₃ and mixed c-B-MgO prepared by combustion method

Catalysts	BET surface area (m²/g)	Pore volume (cm³/g)	Pore diameter (nm)
MgO	223.5	0.179	3.21
c-2.5-B-MgO	136.4	0.150	4.39
c-5.0-B-MgO	110.7	0.145	5.24
c-7.5-B-MgO	62.5	0.141	9.35
c-10.0-B-MgO	16.0	0.019	4.78
c-15.0-B-MgO	6.7	0.005	2.73
B ₂ O ₃	2.0	0.004	0.31

Figure 37 shows the XRD diffractograms of pure MgO, B₂O₃ and c-B-MgO with various Boron content. For all mixed c-B-MgO oxides, the XRD patterns are identified as the periclase phase of MgO. As the Boron content in the mixed oxides increases, all the XRD peaks become broader, suggesting smaller crystallites or less ordered structures. In addition, the XRD patterns of c-B-MgO oxides display a small shift to smaller 2 Θ values as compared to MgO. This shift is associated with the lattice expansion possibly resulting from the introduction of Boron into the MgO lattice. No peaks corresponding to B₂O₃ were detected in all mixed oxides samples, indicating the absence of large B₂O₃ crystalline structures. More interestingly, the relative intensity of the peak corresponding to MgO (111) plane decreases with respect to those of the peaks corresponding to (200) and (220) planes with increasing Boron content as shown in Figure 38.

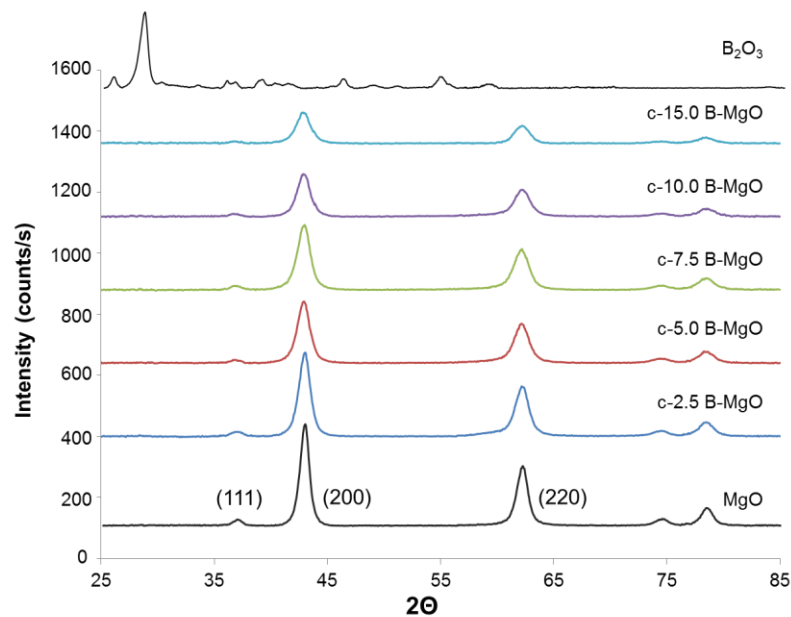


Figure 37. X-ray diffractograms of MgO, B₂O₃ and mixed B-MgO prepared by combustion method

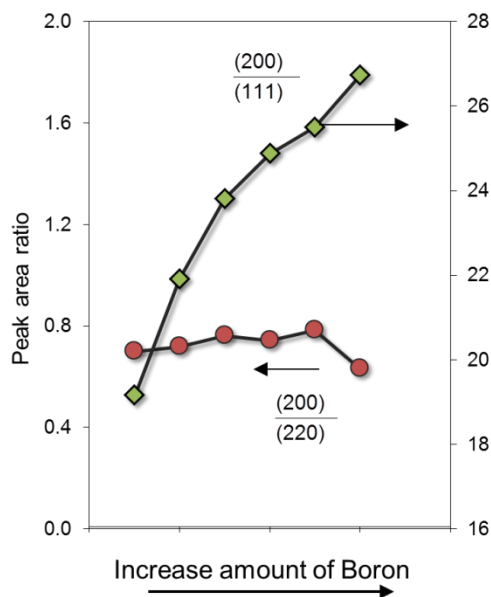


Figure 38. Effect of Boron loading on the XRD intensity of different MgO planes

To understand catalyst basicity and how it changes with the loading of Boron, CO₂ TPD-MS was performed and the results are presented in Figure 39. For MgO, the CO₂ TPD profile can be divided into three regions representing weak adsorption sites (80-150°C), medium adsorption sites (300-400°C), and strong adsorption sites (400-500°C), which appeared as the dominant peak. With increasing Boron content in c-B-MgO, the high temperature peak disappears, leaving the medium temperature peak as the major one, indicating the disappearance of strong basic sites, and the increasing dominance of medium strength sites. Detailed quantification result suggests that total basic sites and basic site density decrease considerably with increasing Boron content as shown in Table 14.

To characterize the difference in electronic states of different catalysts, O1s and B 1s XPS characterization was conducted and the results of catalysts are displayed in Figure 40. For the O 1s spectra, two peaks are observed with the lower binding energy one associated with the oxide phase whereas the higher binding energy one resulted

from the presence of some hydroxide present on the surface. The binding energy of O 1s core levels of MgO, appearing at 528.92 eV, agrees well with values reported in literature [26]. Interestingly, upon addition of Boron, significant shifts of O 1s binding energy to 529.34-530.23 eV is observed, giving clear evidence of the electron deficiency of oxygen due to electronic effect from Boron. Modification in electronic state of c-B-MgO catalysts is further evident from B 1s results. As being shown, the B 1s peak on pure B₂O₃ appears at 193.33 eV, which is consistent with the values in literature [27]. Incorporation of Boron into c-B-MgO catalysts leads to the lower binding energy of B 1s, indicating the enrichment of electron density on Boron.

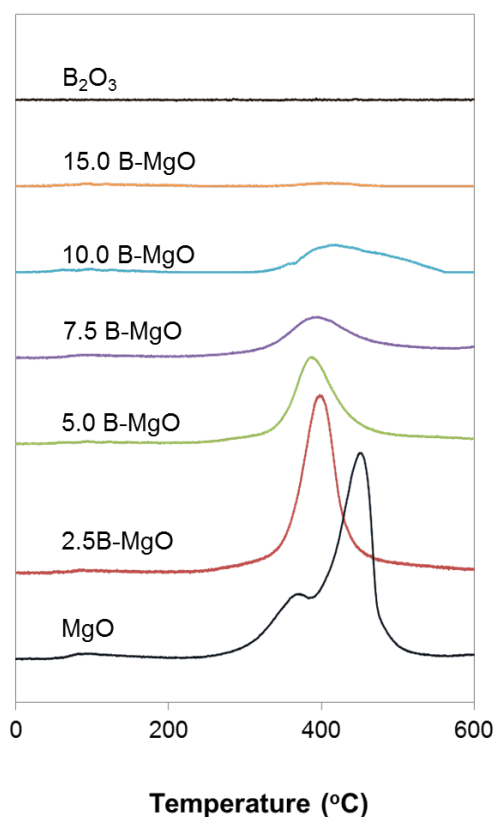


Figure 39. CO₂- TPD MS characterization of MgO, B₂O₃ and mixed B-MgO prepared by combustion method

Table 14. Basic site density of of MgO, B₂O₃ and mixed B-MgO prepared by combustion method obtained from CO₂-TPD analysis

Catalysts	Total basic density ($\mu\text{mol}/\text{m}^2$)	Total basic density ($\mu\text{mol}/\text{g}$)
MgO	1.88	419.27
c-2.5-B-MgO	2.34	318.62
c-5.0-B-MgO	1.61	177.21
c-7.5-B-MgO	1.18	71.04
c-10.0-B-MgO	1.31	21.08
c-15.0-B-MgO	1.05	7.01
B ₂ O ₃	0.00	0.00

Changes in Boron structure upon the incorporating into MgO is evidenced by the ¹¹B NMR spectra of B₂O₃ and c-B-MgO catalysts as shown in Figure 41. Pure B₂O₃ catalyst gives a sharp resonance peak, corresponding to trigonally coordinated BO₃ as previously reported in the literature [28]. Upon the loading of B₂O₃ into MgO, a new resonance peak appears, associated to four-coordinated tetrahedral BO₄. The relative intensity of the tetrahedral peak increases as the amount of Boron loading increases in MgO up to 10%.

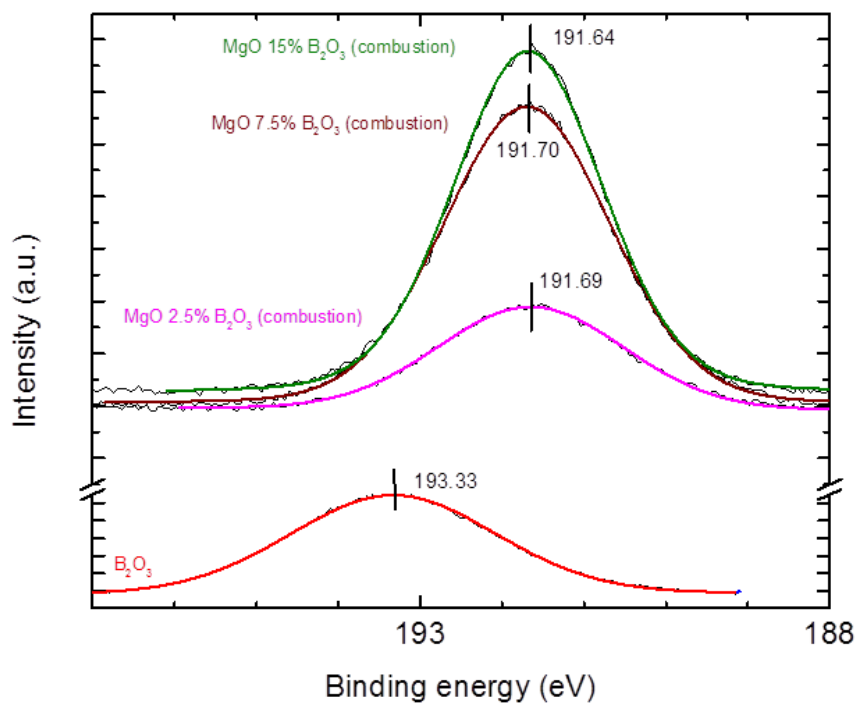
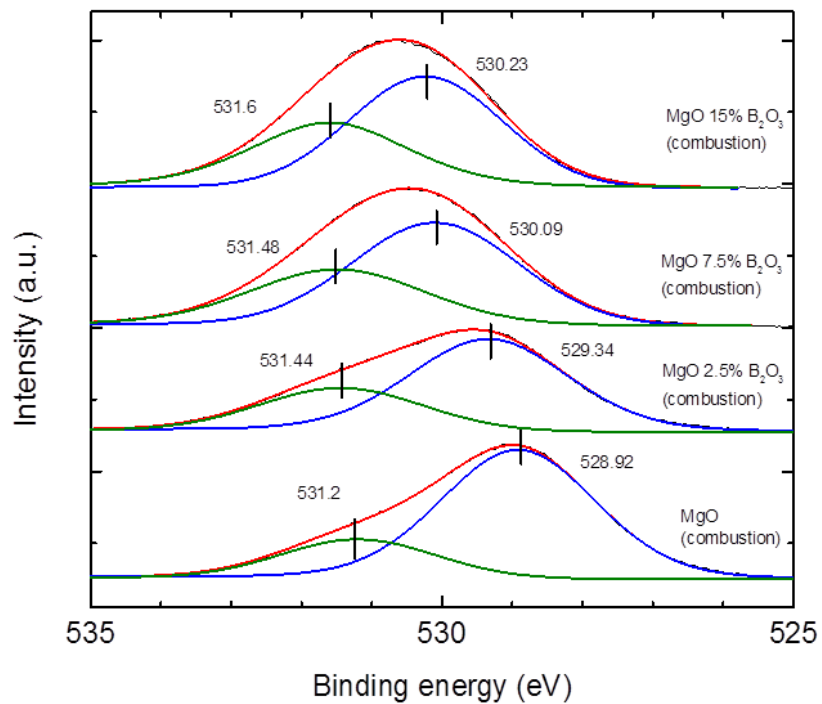


Figure 40. *O 1s* (top) and *B 1s* (bottom) X-ray photoelectron spectroscopy data of MgO, B₂O₃ and mixed B-MgO prepared by combustion method

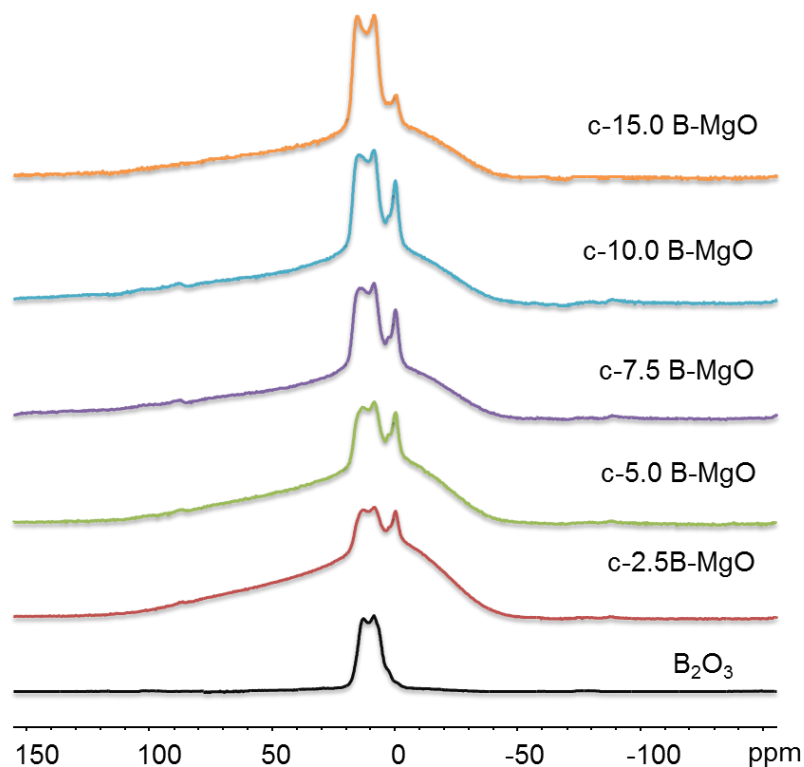


Figure 41. ^{11}B -NMR characterization of B_2O_3 and mixed B-MgO prepared by combustion method

SEM and TEM characterization was employed to examine the catalyst morphology. SEM images of MgO , B_2O_3 and c-B-MgO are shown in Figure 42. While MgO is clearly demonstrated to consist of whiskers and needle-like structure, B_2O_3 shows a more like platelet structure. Interestingly, c-B-MgO displays completely different morphology from MgO and B_2O_3 , showing tiny granules homogeneously distributed throughout the smooth surface of platelets. Detailed high resolution TEM combined with EDS reveals that these tiny clusters appears to be mainly Magnesium whereas the smooth surface contains both Boron and Magnesium, as displayed in Figure 43.

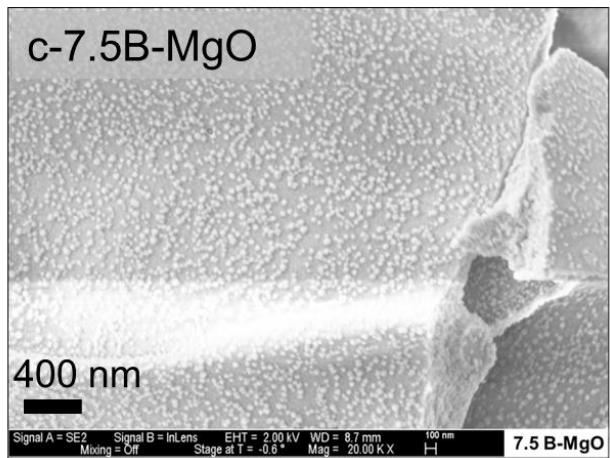
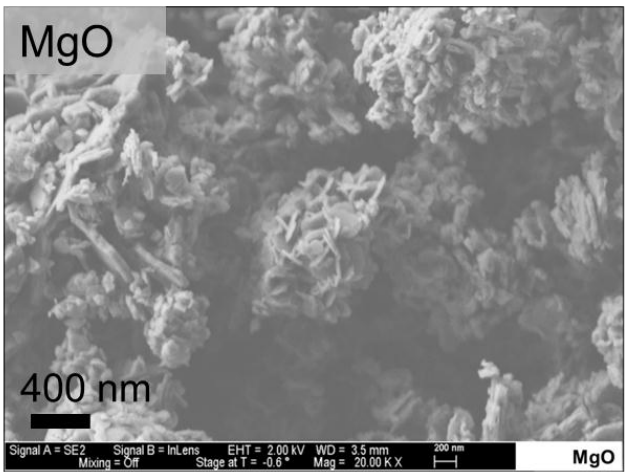
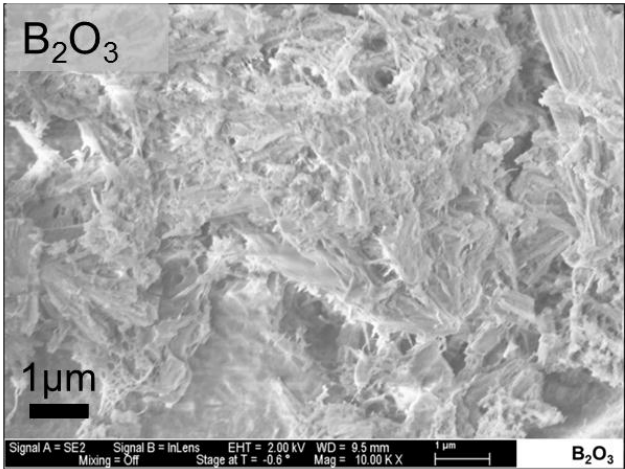


Figure 42. SEM images of MgO, B₂O₃ and mixed B-MgO with 7.5% weight loading of Boron prepared by combustion method

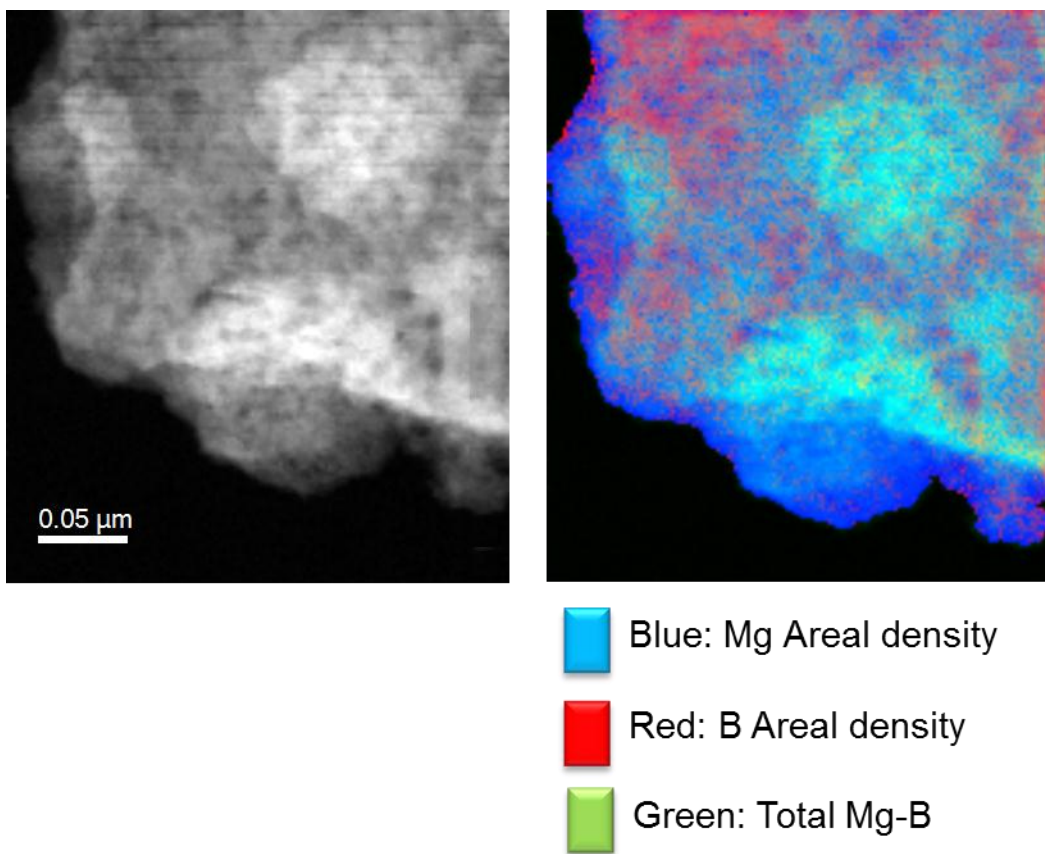


Figure 43. *TEM-EDS images of mixed B-MgO with 7.5% weight loading of Boron prepared by combustion method*

(Courtesy of Dr. Jimmy A. Faria, Abengoa Research Spain)

C.3.2. Reaction Network of Ethanol and Acetaldehyde

In this study, the conversion of acetaldehyde and ethanol over pure MgO, B₂O₃ and combination of B₂O₃ and MgO catalysts prepared by physical mixture, combustion or impregnation form many products via complex reaction pathways, involving both acidic and basic sites on the surface. The reaction network is presented in Figure 44 based on the observed products in all tested experiments.

The dominant products from acetaldehyde and ethanol are found to be crotonaldehyde and crotyl alcohol, as the dimer product of acetaldehyde aldol

condensation and MPV reduction. Additionally, coupling of crotonaldehyde and acetaldehyde led to the formation of ethylacetate, ethylhexanoate, 2,4-hexadienal, 2,4,6-octatrienal and tolualdehyde through Tischenko and aldol condensation combined with ring closing/dehydrogenation mechanisms. More interestingly, small amounts of butyraldehyde is also observed, as a result of hydrogen transfer to C=C double bond in crotonaldehyde, which will be discussed in more details below. Further hydrogenation of C=O of butyraldehyde or C=C of crotyl alcohol also yielded 1-butanol. Ethanol and acetaldehyde also undergo acetalization to yield 1, 1-diethoxyethane. In addition, condensation products also went through MPV reaction to produce corresponding alcohols. Other products, including diethylether and hydroxybutanal are also detected but in trace amounts.

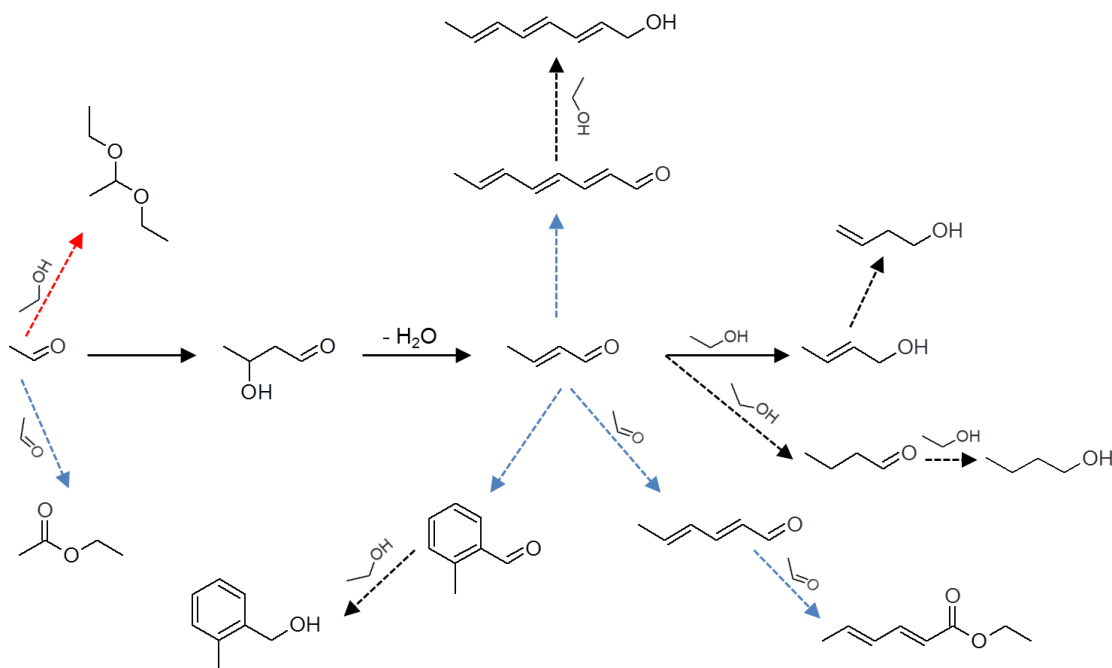


Figure 44. Reaction network for ethanol and acetaldehyde conversion in the presence of MgO, B₂O₃ or combination of B₂O₃ and MgO catalysts prepared by physical mixture, combustion or impregnation method

C.3.3. Reaction Data

Table 15 and Figure 45 display the product distribution and product yield ratios obtained on commercial MgO, impregnation B₂O₃/MgO and physical mixture of commercial MgO and B₂O₃ catalysts. All three catalysts showed similar conversion and comparable yield of crotonaldehyde and crotyl alcohol in comparison with >C₄ condensation products, i.e. mixed C₆ and C₈ products. In addition, in the presence of B₂O₃, either by impregnation or physical mixture, the yield toward 1,1-diethoxyethane formed via acetalization significantly increased. As illustrated in Figure 45, the introduction of Boron into MgO by impregnation method or physical mixture does not improve the selectivity toward the desirable products, i.e. crotonaldehyde and crotyl alcohol.

Table 15. Product yields for conversion of ethanol and acetaldehyde over MgO, physical mixture of B₂O₃ and MgO, and impregnation 2 wt% of B₂O₃/MgO. Reaction condition: T = 250°C, P= 300 psi N₂, t = 4 hours, catalyst mass: 200 mg, 20 mL ethanol, 2 mL acetaldehyde

Catalyst	Product Yield based on acetaldehyde feed (%)							
	Crotonaldehyde	Crotyl alcohol	Butanal	Butanol	1,1-Diethoxyethane	Ethyl acetate	Mixed C ₆	Mixed C ₈
MgO	1.05	23.76	0.78	1.38	0.71	6.20	31.51	12.53
B ₂ O ₃ – MgO (physical mixture)	2.68	27.03	0.43	0.58	4.65	5.32	17.56	9.68
2%B ₂ O ₃ – MgO (impregnation)	4.71	19.42	0.00	0.38	6.09	5.47	22.35	7.95

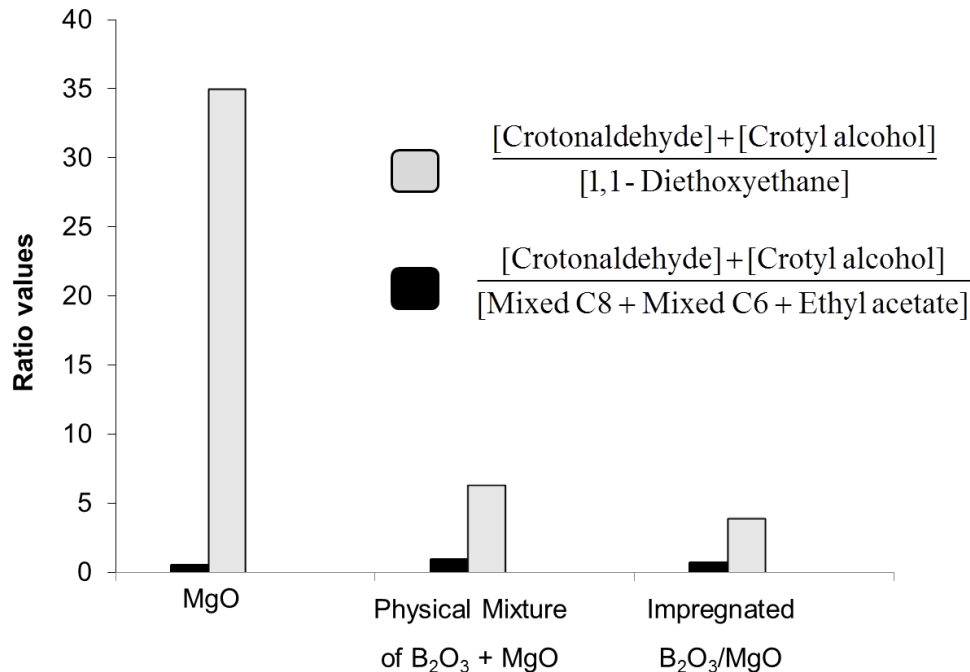


Figure 45. Product yield ratios obtained over the conversion of ethanol and acetaldehyde over MgO, physical mixture of B₂O₃ and MgO, and impregnation 2 wt% of B₂O₃/MgO. Reaction condition: T = 250°C, P = 300 psi N₂, t = 4 hours, catalyst mass: 200 mg, 20 mL ethanol, 2 mL acetaldehyde

Product distribution and product yields as a function of Boron loading in c-B-MgO prepared by combustion method are shown in Table 16. As can be seen, the product yield of crotonaldehyde and crotyl alcohol significantly increased with the increase in Boron content from 0 to 7.5 wt%. However, further increase in B₂O₃ content led to decrease in total product yield. In contrast, with increasing Boron content, the yield toward >C₄ products and ethylacetate drastically decreased. It is important to note that the butyraldehyde + 1-butanol yields increased on the composition of the catalyst. As being displayed, this yield reached the maximum at the 7.5 wt% Boron content following the same trend observed with MPV products. In addition, opposite with the impregnation or physical mixture of MgO and B₂O₃, the introduction of Boron in MgO

by combustion method did not increase the yield of acetalization product, i.e. 1,1-diethoxyethane. In summary, the introduction of Boron into MgO by combustion method up to 7.5 wt% enhances significantly the desirable crotonaldehyde and crotyl alcohol yields, improving the ratio of desirable/undesirable products.

Table 16. *Product yields for conversion of ethanol and acetaldehyde over c-B-MgO prepared by combustion method with different loadings of Boron. Reaction condition: $T = 250^{\circ}C$, $P = 300$ psi N_2 , $t = 4$ hours, catalyst mass: 200 mg, 20 mL ethanol, 2 mL acetaldehyde*

Wt.% of Boron	Product Yield calculated based on acetaldehyde feed (%)							
	Croton-aldehyde	Crotyl alcohol	Butanal	Butanol	1,1-Diethoxy Ethane	Ethyl acetate	Mixed C6	Mixed C8
0.0	1.05	23.76	0.78	1.38	0.71	6.20	31.51	12.53
2.5	3.67	19.51	0.92	2.75	0.95	6.44	11.59	10.96
5.0	8.16	35.93	3.35	4.56	0.85	7.33	7.33	9.04
7.5	8.55	63.47	4.45	5.95	0.93	6.31	1.45	5.80
10.0	6.95	48.38	2.51	3.71	1.75	4.37	0.96	5.40
15.0	8.39	20.35	0.96	0.35	5.36	3.01	0.65	3.21
100.0	5.03	1.35	0.12	0.02	6.42	0.08	0.06	0.05

To further study the product evolution, the product yield as function of reaction time over c-7.5-B-MgO was conducted and the results are shown in Table 17. Once crotonaldehyde is formed through aldol condensation, it is quickly converted to crotyl alcohol, resulting in the high yield of crotyl alcohol at short reaction time. As reaction time increases, crotyl alcohol and other product yields increases with the former at much higher rate.

Table 17. Product yields for conversion of ethanol and acetaldehyde over c-B-MgO prepared by combustion method with 7.5 wt% of Boron. Reaction condition: $T = 250^{\circ}C$, $P = 300$ psi N_2 , catalyst mass: 200 mg, 20 mL ethanol, 2 mL acetaldehyde

Reaction time (h)	Product Yield calculated based on acetaldehyde feed (%)							
	Crotonaldehyde	Crotyl alcohol	Butanal	Butanol	1,1-Diethoxy Ethane	Ethyl acetate	Mixed C6	Mixed C8
1.0	14.82	34.16	3.03	2.74	0.93	2.18	0.91	3.24
2.0	9.80	47.60	2.84	4.56	1.73	3.67	1.25	4.91
3.0	8.52	55.31	2.82	6.93	1.96	4.44	1.36	5.40
4.0	8.55	63.47	4.45	5.95	0.93	6.31	1.45	5.80

In order to test the stability and deactivation of the catalyst, experiments using recycled c-B-MgO 7.5 wt % catalyst were performed. As can be seen in Figure 46, the yield toward crotonaldehyde and crotyl alcohol decreased by about 20% for the recycle run but overall, it still maintains good selectivity (70%).

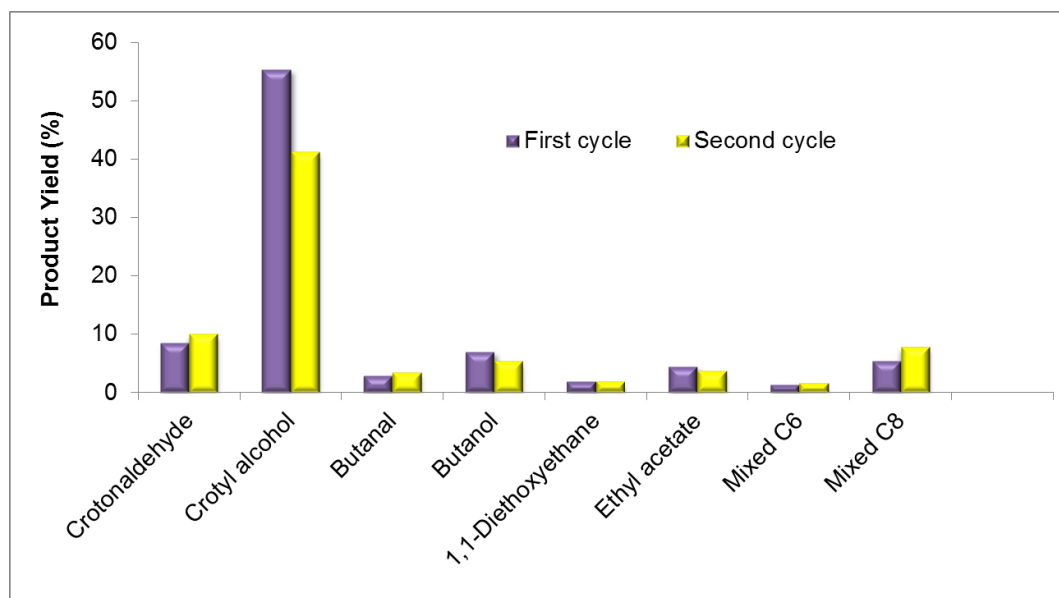


Figure 46. Product yields for conversion of ethanol and acetaldehyde over fresh and recycled *c*-B-MgO prepared by combustion method with 7.5 wt% of Boron. Reaction condition: $T = 250^{\circ}\text{C}$, $P = 300$ psi N_2 , $t = 3$ hours, catalyst mass: 200 mg, 20 mL ethanol, 2 mL acetaldehyde

Experimental results obtained at different ethanol: acetaldehyde feed ratios is shown in Figure 47, suggesting that the molar ratio of reactants plays a significant role in controlling the reaction selectivity. The presence of excess ethanol (ethanol: acetaldehyde molar ratio of 10:1) leads to the high selectivity of dimer condensation/MPV product, crotyl alcohol. As the ethanol: acetaldehyde ratio decreases, the selectivity for the formation of trimer and tetramers (C6 and C8) and ethyl acetate increases significantly.

Since H_2 is a concomitant product in the formation of tolualdehyde, it is not unreasonable to think that butyraldehyde might be formed from the reaction of crotonaldehyde and H_2 . To better understand the formation of butyraldehyde and 1-

butanol in the reaction, we carried out hydrogenation of crotonaldehyde under high H₂ pressure in the absence of an alcohol using in decahydronaphthalene (decalin) solvent over c-7.5-B-MgO catalysts. The results are shown in Figure 48. Over c-7.5-B-MgO catalyst, the formation rate of butyraldehyde were much faster in the presence of 1-propanol under the inert environment in comparison with that in the absence of alcohol and under H₂ environment and this rate further increases in the presence of isopropanol.

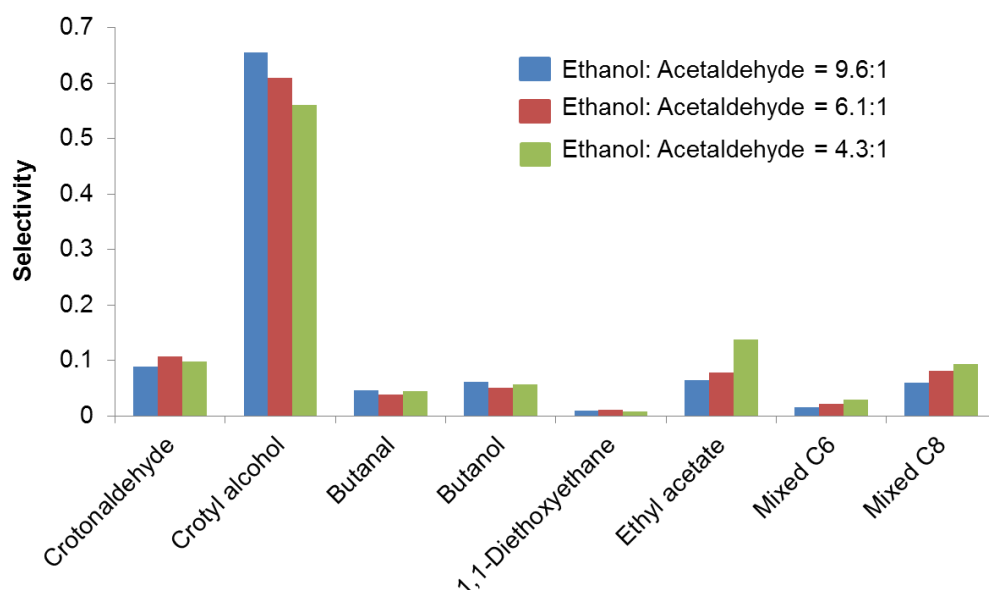


Figure 47. Comparison of product selectivity for conversion of ethanol and acetaldehyde over c-B-MgO prepared by combustion method with 7.5 wt% of Boron using different ethanol: acetaldehyde feed ratios. Reaction condition: $T = 250^{\circ}\text{C}$, $P = 300\text{ psi } N_2$, $t = 3\text{ hours}$, catalyst mass: 200 mg

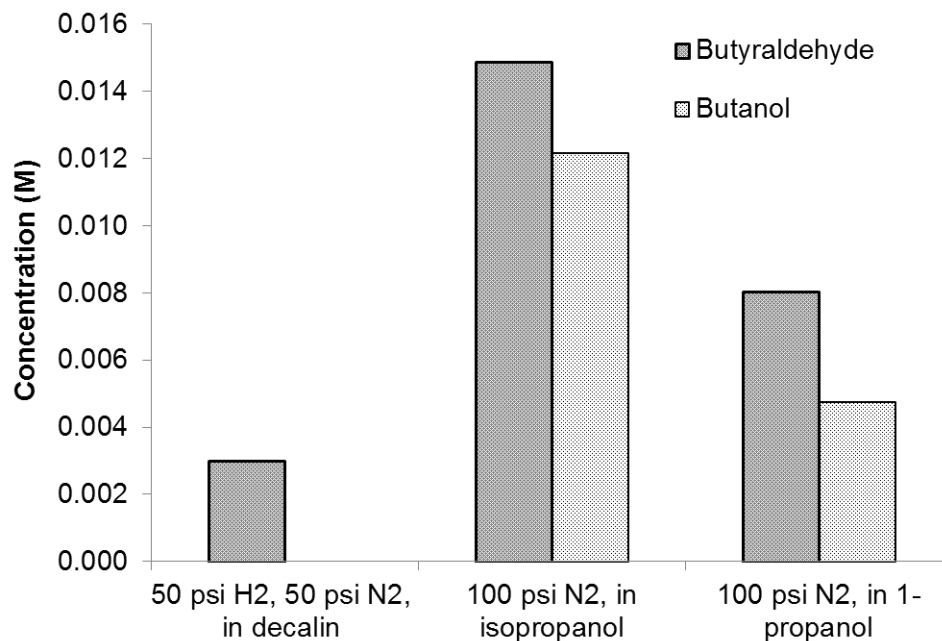


Figure 48. Product yields of butanal and butanol for the conversion of crotonaldehyde over c-B-MgO prepared by combustion method with 7.5 wt% of Boron using H₂, isopropanol and 1-propanol as the hydrogenation agent.

C.4. Discussion

C.4.1. Structural Characteristics and Properties of B-MgO catalysts prepared by combustion method

The structure of c-B-MgO catalysts is consistent with the MgO periclase structure, which resembles that of rock salt. This structure consists of a cubic close-packed array of O²⁻ anions providing regular octahedral coordination sites, all of which are occupied by Mg²⁺ cations [29]. The XRD results indicate that over the wide range of Boron loadings, no crystalline B₂O₃ phase is observed suggesting that Boron cations remain closely associated with the MgO structure, and/or B₂O₃ phase is finely distributed throughout the MgO bulk. Interestingly, the lattice parameter of c-B-MgO catalysts slightly increases as the Boron content increase, which is likely to be caused

by the diffusion of Boron within the periclase layer without modifying the crystalline structure. However, as suggested by XRD analysis, the incorporation of Boron affects the crystal growth of MgO, as supported by the decrease in XRD peak intensity, especially for that corresponding to (111) plane.

Another strong evidence for the diffusion of Boron into MgO structure is given by ^{11}B -NMR characterization, which indicates that Boron coordination partially changes from trigonal in pure B_2O_3 to tetrahedral upon incorporation into MgO. This finding suggests that Boron might locate in tetrahedral sites within the MgO lattice, resulting in slight increase in lattice constant of MgO as observed with XRD. More interestingly, as indicated above, the effect of Boron on (111) plane is more significant than on other planes, which can be explained by the fact that Boron preferentially locates along the (111) planes which is oxygen terminated and negatively charged.

The effect of Boron content on the properties of c-B-MgO was thoroughly studied by different characterization techniques. CO_2 TPD results demonstrate the monotonic decrease in both basic strength and density with increasing Boron loading. Di Cosimo *et al.* [30] have correlated TPD and FTIR studies of CO_2 adsorbed on hydrotalcites and have associated the CO_2 desorption temperature with different types of CO_2 binding sites. The weakly binding sites are associated with surface OH- groups and the formation of bicarbonate, the medium-strength sites are associated with the formation of bidentate carbonates, and the strong binding sites are associated with the formation of strongly bounded unidentate carbonates. In our case, the dominance of the strong CO_2 binding sites on MgO possibly results from the presence of electron rich O^{2-} on the surface, which can strongly bind CO_2 . The disappearance of the strong binding

sites and dominance of medium strength sites upon the addition of Boron is due to decreased electron density on O^{2-} , as clearly evidenced in XPS results.

SEM results demonstrate that the macroscopic morphology of c-B-MgO is vastly different from pure MgO or B_2O_3 . The co-presence of smooth surface consisting uniformly of Boron and Magnesium and tiny Magnesium-enriched granules possibly results from the disruption of Boron on the crystal growth of certain planes. It is reasonable to attribute the formation of MgO granules to the absence of Boron interference on the growth of (111) plane.

C.4.2. Compositional Effects on the Catalytic Activity.

Based on the reaction data, it is clear that there exist four types of reaction on the surface of the catalysts: (i) Condensation reaction involving self or cross-coupling of two aldehyde molecules; (ii) MPV reaction involving reduction of a carbonyl group to the corresponding alcohol; (iii) Acetalization of alcohol and aldehyde; and (iv) Hydrogenation of C=C double bond in unsaturated aldehyde. The data also indicate that the first two are dominant.

The product distribution in ethanol and acetaldehyde conversion reactions is strongly influenced by the surface acid-base properties because as aforementioned, each individual reaction requires different catalyst properties depending on its mechanism. MgO, physical mixture of MgO and B_2O_3 or impregnation B_2O_3/MgO showed high selectivity toward aldol condensation, i.e. crotonaldehyde, mixed C6 and C8 coupling compounds, whose formation is catalyzed by strong basic sites. These results are consistent with the predominant presence of strong basic O^{2-} ions on MgO surfaces as seen in CO_2 TPD and XPS characterization. It appears that the addition of Boron by

physical mixture or impregnation is unable to generate the acid-base pair on the surface which catalyzes the MPV reaction. On the other hand, the isolated acid sites from B_2O_3 enhance the formation of 1,1-diethoxyethane.

In contrast, the addition of Boron into MgO through the combustion method appears to drastically increase the surface density of active acid-base pair desirable for MPV reaction. As shown, the yield toward crotyl alcohol monotonically increases with the Boron content up to 7.5%. In addition, the yields of undesirable condensation products, including mixed C6, mixed C8 and ethyl acetate significantly decrease, owing to the disappearance of strong basic sites as evidenced in CO_2 TDP and XPS characterization results. In contrast with the results obtained over MgO- B_2O_3 mixture by impregnation or simple physical mixtures, we did not observe significant formation of 1,1-diethoxyethane, which can be explained by the good dispersion of Boron into MgO structure and the absence of isolated B_2O_3 sites. It is noteworthy that the overall activity of the combustion catalysts decreases significantly when the Boron loading goes beyond 7.5 wt%. This result can be explained by the drastic drop in surface area of catalyst as indicated in BET analysis.

While the mechanisms for MPV and condensation reaction are well understood in the literature, that for the hydrogenation of C=C bond of unsaturated aldehyde over metal oxides under hydrogen-lean environment is unclear. The formation of saturated aldehydes as side products of the MPV reaction was documented in the literature but detailed explanation is missing [31]. In this study, we find that on c-7.5-B-MgO catalyst, the product yields of butanal and butanol via hydrogen transfer to the C=C double bond of crotonaldehyde decreases in the order of isopropanol, 1-propanol and

hydrogen. This observation clearly suggests that the production of butanal happened through hydrogen transfer from alcohol to C=C double bond.

C.5. Conclusion and Recommendations for Ethanol Conversion

A new B-in-MgO material was prepared and its catalytic properties were investigated in the effort to maximize crotonaldehyde and crotyl alcohol production in the ethanol-to-butadiene process. The combustion method used in the catalyst preparation differentiates itself from other “milder” conditions, such as impregnation or physical mixing, in the extent to which the two participating components interact with each other. Multiple characterization techniques revealed that B was well incorporated into MgO “frame” and its coordination number was altered as well. This higher extent of interaction was reflected by its extraordinary selectivity in favor of the desirable products, whose formation requires well-balanced acid-base pair in both relative density and strength.

The significance of this study lies in two aspects. First and foremost, it proposed a practical catalyst for an industrially important process and therefore its application and economic benefit can be foreseen. Second, it opens up a new realm of catalyst preparation, in which the overall properties of the resulting catalyst is not a simple accumulation of each constituent, but rather a result of coordination and “neutralization”. Consequently, the catalyst and the method can be greatly extended to many other important reactions that require dual- or multi-functions. As with any pioneering work, this study still left a lot of room to explore. For example, a more comprehensive observation and therefore a shaper probe into the nature of this new material is desirable in revealing more detailed information of the c-B-MgO catalyst.

Toward that end, both experimental as well as computational tools can be useful in finalizing the picture of the material. In addition, techno-economic analyses for the processing of ethanol to butadiene will be valuable in assessing the merits of an overall process.

References

-
- [1] www.afdc.energy.gov/data/
- [2] Dakota Ethanol News Letter (2012)
- [3] N.L. Morrow. Environ. Health. Perspect. 1990 86 7
- [4] W.M. C. White. Chemico-Biological Interactions. 207 166 10
- [5] <http://processengineering.theengineer.co.uk/shale-gas-hits-us-butadiene-production/1014412.article>
- [6] W.J. Toussaint, J.T. Dunn, D.R. Jackson. Ind. Eng. Chem. 1947, 39 120
- [7] C.F. de Graauw, J.A. Peters, H. van Bekkum, J. Huskens. Synthesis 10 (1994), 1007
- [8] V.J. Shiner, D. Whittake. J. Am. Chem. Soc. 91 (1969), 394
- [9] P. Mäki-Arvela, J. Hájek, T. Salmi, D.Yu. Murzin. Appl. Catal. A: Gen. 292 (2005) 1
- [10] P. Kluson, L. Cerveny. Appl. Catal. A, 128 (1995), 13
- [11] E.J. Campbell, H. Zhou, S.T. Nguyen. Org. Lett. 3 (2001), 2391
- [12] Y. Ishii, T. Nakano, A. Inada, Y. Kishigami, K. Sakurai, M. Ogawa. J. Org. Chem. 51 (1986) 240
- [13] T. Ooi, T. Miura, Y. Itagaki, H. Ichikawa, K. Maruoka. Synthesis (2002) 279
- [14] A. Corma, M.E. Domine, S.J. Valencia. J. Catal. 215 (2003) 294
- [15] M. Boronat, A. Corma, M. Renz. J. Phys. Chem. B, 110 (2006), 21168
- [16] J.C. van der Waal, E.J. Croyghton, P.J. Kunkeler, K. Tan, H. van Bekkum. Top. Catal. 4 (1997), 261
- [17] O. Bortnovsky, Z. Sobalik, B. Wichterlova, Z. Bastl. J. Catal. 210 (2002) 171

-
- [18] J.F. Miñambres, A. Marinas, J.M. Marinas, F. J. Urbano. *Appl. Catal. B; Environ.* 140 (2013) 386
- [19] J.F. Miñambres, A. Marinas, J.M. Marinas, F. J. Urbano. *J. Catal.* 295 (2012) 242
- [20] M. A. Aramendía, V. Borau, C. Jiménez, J.M. Marinas, J. R. Ruiz, F. Urbano. *Appl. Catal A: General.* 249 (2003), 1
- [21] V.A. Ivanov, J. Bachelier, F. Audry, J.C. Lavalley. *J. Mol. Catal.* 91 (1994) 45
- [22] C. Angelici, B.M. Weckhuysen, P.C. A. Bruijninx. *Chemosuschem* 6 (2013) 1595
- [23] E. Flahaut, C. Laurent, A. Peigney. *Carbon.* 43 (2005), 375
- [24] T. Klicpera, M. Zdrzil. *Catal. Lett.* 58 (1999) 47
- [25] M. A. Aramendia, V. Borau, C. Jimenez, J. M. Marinas, A. Porras and F. J. Urbano. *J. Mater. Chem.* 9 (1999) 819
- [26] S. Ardizzone , C.L. Bianchi, B. Vercelli. *Appl. Surf. Sci.* 126 (1998) 169
- [27] D.J. Joyner, D.M. Hercules. *J. Chem. Phys.* 72 (1980) 1095
- [28] M.R. Hansen, G. K. H. Madsen, H. J. Jakobsen, J. Skibsted. *J. Phys. Chem. A* 109 (2005) 1989
- [29] S.D. Jackson, J.S.J. Hargreaves. *Metal oxide catalysis.* 1 (2009)
- [30] J. I. Di Cosimo, V. K. D'iez, M. Xu, y E. Iglesia, y and C. R. Apesteguía. *J. Catal.* 178 (1998) 499
- [31] S.H. Liu, S. Jaenicke, G.K. Chuah. *J. Catal.* 206 (2002) 321-330